2014

EXPERIMENTAL DEVELOPMENT OF ADVANCED AIR FILTRATION MEDIA BASED ON ELECTROSPUN POLYMER FIBERS

Negar Ghochaghi
VCU

EXPERIMENTAL DEVELOPMENT OF ADVANCED AIR FILTRATION MEDIA

BASED ON ELECTROSPUN POLYMER FIBERS

A Dissertation submitted in partial fulfillment of the requirements for the degree of Doctor of Philosophy at Virginia Commonwealth University.

by

NEGAR GHOCHAGHI
MS in Mechanical and Nuclear Engineering, Virginia Commonwealth University, 2012
BS in Material Engineering, Isfahan University of Technology, IR, 2010

Director: GARY C. TEPPER
PROFESSOR AND CHAIR, DEPARTMENT OF MECHANICAL AND NUCLEAR ENGINEERING

Virginia Commonwealth University
Richmond, Virginia
December 2014

Acknowledgement

First, I offer my deepest gratitude to my supervisor, Dr. Gary C. Tepper, who has supported me with his patience and knowledge. He is a pleasant person and a great human being who gave me his precious time and advice whenever I needed it. He has allowed me room to work in my own way.

I would like to thank my committee members, Dr. Hooman V. Tafreshi, Dr. Daren Chen, Dr. Karla M. Mossi, Dr. Dmitry Pestove, and Dr. Hu Yang. I also would like to thank Dr. Gary L. Bowlin and Dr. Gary Glaspell for their help in the experimental setup. Special thanks to all my lab mates and undergraduate interns in Dr. Tepper's research lab for their valuable help on this research project.

My heartfelt gratitude extends to Dr. Maryam Zarei who makes me proud to have such a loving and wonderful person for an aunt. I can't thank her enough for believing in me and making me believe in myself.

I want to acknowledge my lovely sister Niloufar Ghochaghi who has been making every day of my life such a joy. I love her and I owe her every bit of the pride I take in my degree today. Additionally, I want to thank my loving husband for his encouragement and insightful comments during this time, as well as my relatives and friends for their constant support.

I offer special thanks to my mother and my father, Farkhondeh and Hassan, who always took pride in my academic achievements. They were always there to soften the difficulties of life.

Finally, I am happy to devote this work to my mother, who most of all provided me a strong academic foundation. She is not in this world any more but I hope she knows that I couldn't be more proud to be her daughter. I love her as much as she loved me.

Table of Contents

Page

List of Tables

Page

List of Figures

Page

Abstract

EXPERIMENTAL DEVELOPMENT OF ADVANCED AIR FILTRATION MEDIA BASED ON ELECTROSPUN POLYMER FIBERS

By Negar Ghochaghi, M.Sc.

A Dissertation submitted in partial fulfillment of the requirements for the degree of Doctor of Philosophy at Virginia Commonwealth University.

Virginia Commonwealth University, 2014

Major Director: Dr. Gary C. Tepper
Professor and chair, Department of Mechanical and Nuclear Engineering

Electrospinning is a process by which polymer fibers can be produced using an electrostatically driven fluid jet. Electrospun fibers can be produced at the micro- or nano-scale and are, therefore, very promising for air filtration applications. However, because electrospun fibers are electrically charged, it is difficult to control the morphology of filtration media. Fiber size, alignment and uniformity are very important factors that affect filter performance. The focus of this project is to understand the relationship between filter

morphology and performance and to develop new methods to create filtration media with optimum morphology.

This study is divided into three focus areas: unimodal and bimodal microscale fibrous media with aligned, orthogonal and random fiber orientations; unimodal and bimodal nanoscale fibers in random orientations; bimodal micrometer and nanometer fiber media with orthogonally aligned orientations. The results indicate that the most efficient filters, which are those with the highest ratio of particle collection efficiency divided by pressure drop, can be obtained through fabricating filters in orthogonal layers of aligned fibers with two different fiber diameters. Moreover, our results show that increasing the number of layers increases the performance of orthogonally layered fibers. Also, controlling fiber spacing in orthogonally layered micrometer fiber media can be an alternative way to study the filtration performance. Finally, such coatings presented throughout this research study can be designed and placed up-stream, down-stream, and/or in between conventional filters.

CHAPTER 1 Background and Introduction

1.1 Filtration

In general terms, using physical differences to separate one or more phases of materials from another is called separation. These physical differences can be in size, density, or electric charge. Two major branches of physical separation are filtration and sedimentation. The density difference between the suspended particle and the suspending fluid causes sedimentation. In other words, the force of gravity or centrifugal force can cause separation by sedimentation. Filtration is one of the other physical techniques for separation, which operates entirely on the particle size and particle shape. Filtration and other forms of separation have been used for over 40 years in industry protocols. Specifically, a filter is a device for separating one or more substances from the others, which utilize physical differences in the phases. In order to trap the solid in a suspension, a filter should be placed in the path of fluid flow. Filtration functions entirely based on particle or droplet size, such that particles below a certain size will pass through the barrier while the barrier captures larger ones. Therefore, one of the characteristics of the barrier is the separating size. Selection of the appropriate filter types is based on mean particle size and particle size distribution. Filters are chosen to maximize filtration efficiency, cost effectiveness, and energy efficiency. Nowadays filtration is divided into four categories: macro-filtration, for separating particles in the approximate range of 1 mm down to 5 μm;

microfiltration, for separating particles from 5 μm down to 0.1 μm; ultrafiltration, for separating the finest distinct particles; and below ultrafiltration in term of particle size nanofilteration appear [1].

1.1.1 Filtration business:

Many human activities and industries are affected by filtration. Filters are widely used in kitchens, heating, ventilation and air conditioning (HVAC) systems, hospitals, manufacturing industries, and mineral processing systems. Table 1.1 is a sector shares of the 10 largest end-users for the year of 2007. There is an obvious need for a growing filtration process. It is well understood that there is a high demand for continued studies of filters and filtration performance [1, 2].

Table 1.1: Filter market share for the year of 2007 [2].

End-used sector	Market share (%)
Domestic, commercial and institutional	17.9
Transport equipment and systems	15.9
Fresh and wastewater treatment	10.3
Bulk chemicals	9.9
Food and beverage production	7.5
Fine chemical, pharmaceuticals and biochemicals	6.5
Power generation	6.3
Pulp and paper	5.1
Medical and health	4.8
Electrical and electronic materials and equipment	3.5

Most penetrated particle sizes are in the range of 100-500 nanometers. Filters with small pore sizes can be good candidates to clean out these particle sizes. Many places, such as hospitals, uranium mines, and nuclear industries require removal of airborne nanoscale particles. High Efficiency Particulate Air filters (HEPA) and Ultra Low Penetration Air

filters (ULPA) are the most commonly used air filters for cleaning the air of these particle sizes. Nanofibrous media are a suitable entrant to make HEPA and ULPA filters for removal of the nanosized particles [3-5].

1.1.2 History of filtration media:

The development of air filters begins two thousand years ago when Roman mines and industries recognized the dust problems caused by lead carbonate, a common cosmetic. For centuries workmen covered their nose and mouth with cloth to protect themselves against fumes. Leonardo da Vinci (1452-1518) wrote of the use of wet cloth for protection against fumes in warfare. A book called “De Re metallica” were published by Georg Bauer in 1556, explained many kinds of mining problems and prescribed protection against dust.

Charcoal was used in 1854 in hospitals to purify water. In 1868, it was discovered that coarse granules of charcoal were not able to filter out the fine airborne particles. This discovery led to the use of fibrous materials as filters. In 1871, Oakum and glass wool were used as filters. The first study on the principle of filtration by fibrous pad were done in Germany by Albrecht and Kaufmann. In the nineteenth century, the first filtering mask to protect firemen appeared. These filtering masks were also used to protect people against disease. In 1905, respirators were successfully tested against bacteria in the form of suspensions.

In World War I (1914-1918), gasmasks filters were made of a mixture of wool and asbestos fibers. It was found that mixtures of asbestos, an extremely fine fiber, with wool can be an excellent media for filtration. Also adding asbestos fibers to paper will result in

making effective paper filters. It was found that pleating the paper filter can increase the efficiency due to increase in filter area in the same volume. In 1930, Hansen's filters were replaced by the asbestos fibrous mats. Handen's filters were based on electric field, which arose from resin particles. Further developments in resin filter types continue to be widely used in industries.

High Efficiency Particulate Air filters (HEPA) were first developed as a standard during World War II. Capturing radioactive particles and agents of chemical and biological warfare was necessary at that time, which resulted in developing high efficiency filters. Ultra Low Penetration Air filters (ULPA) were developed more recently and are considered a newer filter media. Typically, HEPA and ULPA are filters with 99.97% and 99.999% efficiency for capturing the most penetrating particles (MPP), respectively. Most penetrating particles have a diameter of 0.3 μm. Nowadays efficiency is no longer a limiting factor, and improvements in new technology focus on prevention of leakage and minimizing the pressure drop [6].

1.1.3 Fibrous filters:

In general terms, filters are nonwoven or woven fibrous media. The fibers can be produced via different methods such as drawing [7], self-assembly [8], phase separation [9], template synthesis [10], and electrospinning [11]. Each process will be described briefly.

The drawing process is similar to dry spinning for commercial fiber production. In this method, a very high stress is induced to the visco-elastic material, which results in producing a long single fiber. The disadvantage of this process is the limitation of raw

materials. The materials should have very strong visco-elastic properties, which exhibit cohesion during the elongation.

In the self-assembly process, a defined structure will be made from assembly of its nano-scale components. The disadvantages of this process are that it is time consuming and cannot produce continuous fiber.

The phase separation process makes very short nanofibers. In this process, the foam-like products are extracted from a solution, which is made by dissolving a polymer into a solvent, that is within the same or a different solvent. The solution should be in form of a gelatin. This procedure is time consuming and it cannot be used for long fiber fabrication.

The template synthesize process fabricates nanoporous membranes to make nanofibers. The nanoporous membrane is considered as a template by the desired polymer solution, which synthesizes the formation of the fibers within its pores. This method is not effective for mass production.

Electrospinning produces continuous fine fibers using electric charges, which are produced on the surface of the polymer solution. Fibers can be fabricated from polymer solutions or polymer melts.

Among these methods, the electrospinning process is popular method due to its low cost, formation of continuous fibers using a simple setups. Also, the electrospinning method is used to produce fibers from a large variety of bulk starting materials without additional purification. The electrospun fibers possess properties which are not found in other fiber making processes. They have high surface to volume ratios, high aspect ratios, controlled

pore sizes, and superior mechanical and optical properties. The ability to make fibers with different diameter sizes, from nanometer to millimeter, is an additional feature that makes electrospun fibers valuable [12].

1.2 Electrospinning:

Electrospinning, an electrohydrodynamical phenomena, is used to produce fibers in nanometer and micrometer ranges from polymer solutions or melts. It is a low cost, easy applicable process, which serves a broad range of materials.

The handiness of the electrospinning process to produce inexpensive fibers from many kinds of polymers is a huge improvement in nano- or micro-scale technology. The resultant fibers have diameters that range from 2 nm to several micrometers. This technique offers a unique capability to produce novel structures with controllable pore characteristics and mat morphology. This technique has been known for more than 60 years in the textile industry. Electrospinning got more attention in the last decade due to its capability to spin a wide range of polymers and an ability to produce fibers consistently. The nanofibers and fabrics can be used in many applications, such as drug delivery, tissue engineering, artificial organs, reagents and catalysts, superhydrophobic materials, and filtration technology [12-16].

Filtration technology is improved by using electrospun fibers as they have smaller pores and a higher surface area than regular fibers. Also, producing nanofibers using this simple technique offer several advantages, such as high surface to volume ratio, tunable porosity, malleability to conform to a wide range of shapes, and ability to control the composition.

With all the advantages with the electrospinning method and producing nanometer and micrometer fibers, there are still challenges in using the electrospun mats for applications, which requires additional considerations. One of these challenges is controlling the pore size distribution, which will affect the non-uniformity of electrospun filter mats [17].

The following of this section is organized into four sub-sections. The first gives a review on the history of electrospinning. The second provides a brief introduction to electrospinning theory. The third discusses the principle related to the assembly of electrospun fibers and strategies to control the structure and morphology of the products. The fourth summarizes recent developments related to the alignment and controlling the deposition of electrospun fibers.

1.2.1 Electrospinning history:

The formation of an electrostatically driven jet first occurred back in 1745 with Bose's patent [18]. The parameters of this process was explained later in 1882 by Lord Rayleigh. The formation of the jet and relationship between the surface tension and surface charges were describe in 1917 in Zeleny's work [19]. These works can be considered as the fundamental principle of electrospinning and electrospraying, whereas the actual process of electrospinning and experimental setup date back to the 1930's, when Formhals patented his work. It was the first attempt for developing an experimental process for producing polymer filaments [16].

Formhals' first patent was on the electrospinning of cellulose acetate dissolved in acetone. Two electrodes were used, one was place in the solution while the other was placed on the

collector. Applying the electric field between two electrodes resulted in the formation of polymer filaments. Figure 1.1 is the schematic of his setup. The process was named electrostatic spinning, which today is known as electrospinning. The disadvantages of his method was the difficulty of drying the collected fibers as well as the difficulty in removing the fibers. Later on, in 1940, he patented another method, which was based on moving the substrate [20]. The difficulty in removing the fibers for further application was still a major drawback for his apparatus.

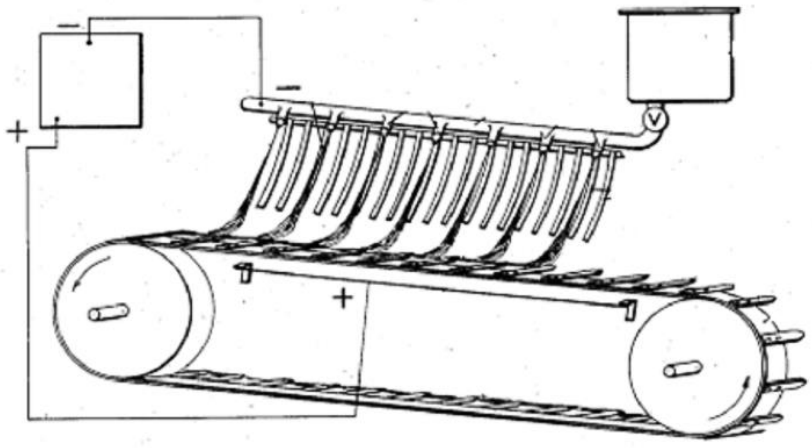

Figure 1.1: Schematic diagram of Formhals' electrostatic spinning setup [16].

In 1952, uniform droplets 0.1mm in diameter were produced via a glass tube attached to a capillary with a high voltage introduced. Three years later, Drozin used the same apparatus to convert liquids into aerosols. He found that liquid type and setup conditions played an important role to production of droplets with uniform size.

In the 1960s, Taylor studied the process of forming the polymer jet. He studied the solution droplet before initiating the jet. He observed that by applying the electric field on

the solution, a cone will form and the jet is ejected from the vertices of the cone. This cone shape is called the "Taylor cone" [21, 22].

In 1966, Simons patented his setup for the production of non-woven fabrics, which eliminated the disadvantage of the Formhals' setup. His apparatus used a smooth belt with a negative electrode attached to it as a collection belt, which allowed easier removal of the fibers. He also studied the relationship of solution viscosity and fiber characteristics. Solutions with low viscosity tend to produce fine and shorter fibers while high viscosity solutions will give continuous fibers [19].

In 1971, acrylic fibers were produced with diameters from 0.05 to 1.1 microns. Fibers of polyethylene and polypropylene were spun from their melts and compared with the solution spun fibers. Since the 1980s electrospinning has gotten more attention due to the fabrication of nanofibers and nanoparticles. Figure 1.2 is another electrospinning setup which has two traveling belts. One belt used as the polymer source and the other is as the collector. The advantage of this setup was to collect a continuous layer of non-woven electrospun fibers by placing a stripping plate at the end of the collection belt [23, 24]..

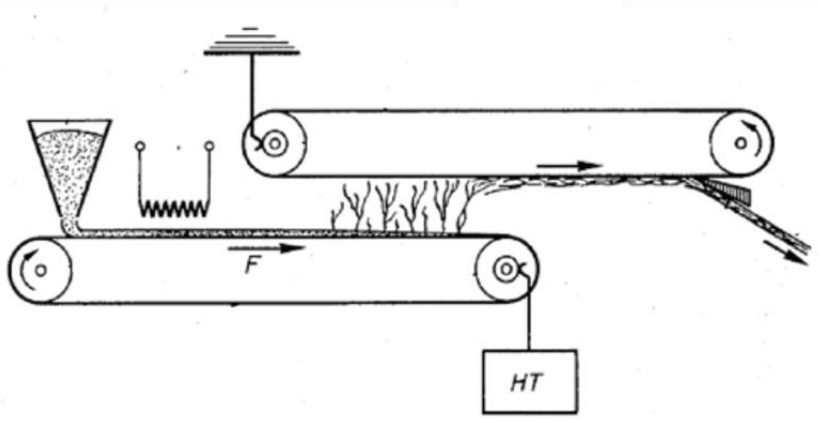

Figure 1.2: Schematic diagram of electrospinning setup with two traveling collector [23].

In 1982, the electrospinning setup was modified such that the fibers were collected on a rotating drum [25]. Figure 1.3 is a schematic of electrospinning set up with a rotating drum and several syringes in series. In 1987, the jet stability and some experimental conditions were studied. Reneker and Doshi from Akron University studied different aspects of the spinning process [26]. Many other polymers were also studied by other research groups.

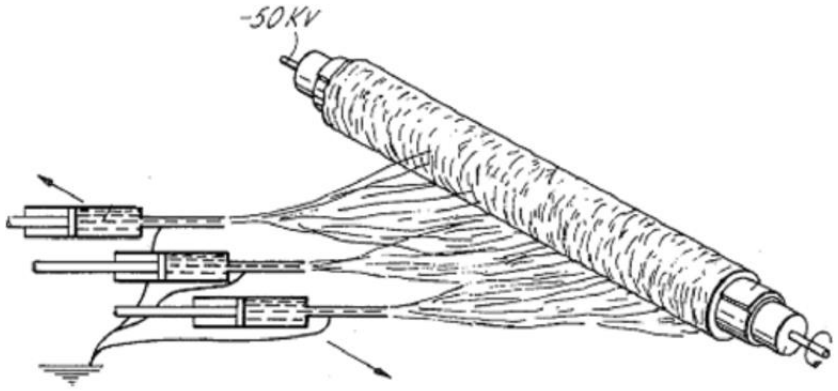

Figure 1.3: Schematic diagram of electrospinning setup with a rotating drum [25].

Due to the high demand for nanotechnology, in recent years, over 200 universities and research centers all over the world are studying the different aspects of this process. The devices, such as Scanning Electron Microscope (SEM), Transmission Electron Microscope (TEM), Wide Angle X-ray Diffraction (WAXRD), Atomic Force Microscope (AFM), and etc., are used to characterize the electrospun nanofibers. Some companies such as the Donaldson Company have been using the electrospinning process to fabricate their products, e.g. air filters [17].

1.2.2 Electrospinning theory:

Electrospinning is a process that involves an interaction between two forces: liquid surface tension and repulsion of charged ions. In this process, the polymer solution or polymer melt receives electrical charges. The charge is carried by ions through the fluid. The ions in the liquid will cause a Coulomb repulsion force when they become charged. On the other hand, the surface tension of the fluid favors a spherical shape with a smaller surface area. If the repulsive force between the charged ions overcomes the fluid surface tension, an electrified liquid jet may be formed and elongate [11].

An electrospinning solution is usually an ionic solution that contains charged ions or molecules. The number of positive and negative charged particles is equal; therefore, the solution is electrically neutral. By applying an electrical potential to the solution, the electrons will move. The direction of these electrons depend on the electric potential. For example, by applying a negative potential, the electrons from the electrical source will move toward and create excess negative ions in the solution. The excess ions will cause elongation in the liquid and form the fluid jet. Generally, the fiber formation from droplets can be divided into three stages: the first stage is the jet initiation, the second stage is the elongation, thinning and whipping instability of the jet, and the third stage is the jet solidification [11, 27-29]. A description of these three stages follows.

1.2.2.1 Initiation of the jet:

Typically, the electrospinning solution is placed into a syringe or a capillary. There are two electrodes in the electrospinning system where one is attached to the polymer solution and one is applied to the collector target. By increasing the applied electrical potential to the

electrospinning solution, the ions in the solution aggregate around the electrode of opposite polarity. The cumulative ions at the tip of the capillary will lead to a charge build up. These excess charges at the surface of the solution droplet causes the fluid meniscus to become conical from its original planar position. The surface tension of the polymer will hold the solution at the end of capillary. When the electric field is increased, surface tension can no longer balance the electric force at the tip. At this point, the jet will be ejected from the vertices of this cone. The jet will travel until it gets collected at the nearest collector with a lower electric potential. In 1969, Taylor determined that an angle of 49.3 degrees is needed to balance the surface tension and the electrostatic force. Later on the exact Taylor angle were suggested. Figure 1.4 shows the picture of the Taylor cone and its required angle [22, 30].

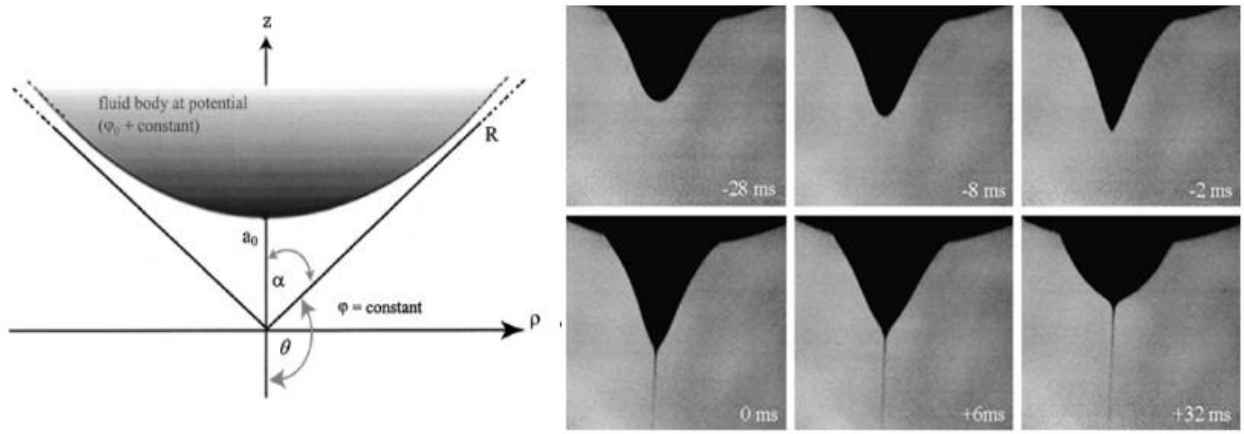

Figure 1.4: Formation of the Taylor cone [22, 30].

1.2.2.2 Elongation, thinning and whipping instability of the jet:

The jet will start bending, winding, spiraling and looping in three dimensions after two to three centimeters of traveling. This is a result of an electrically driven instability caused by the lateral position and lateral velocity of the jet.

Typically, instability occurs during the formation of the jet. Many researchers have studied jet instability. Taylor evaluated the critical voltage required for maximum instability of the jet [21]. It is given as:

$$V_c^2 = 4\frac{H^2}{L^2}\left(\ln\frac{2L}{R} - 1.5\right)(0.117\pi R\gamma) \quad (1.1),$$

where H is the distance between the nozzle and collector, L is the length of capillary tube, R is the radius of the tube, and γ is the liquid surface tension.

High speed photographs were taken to understand jet instability during its travel distance. It is observed that the jet followed a series of loops in which the loops diameters get larger and their circumferences increase. The jet becomes longer and thinner in each loop. The jet segment develops a new instability on a smaller scale in each curved loop after it gets smooth. These observations were made by different groups, including Reneker et al., Yarin et al., and Rutledge et al., using high speed photography experiments. Whipping jet is the term used for the bending instability of this rapidly moving jet. Figure 1.5 shows the schematic diagram of bending instability. Due to this whipping periodicity, it would appear that the jet splays into multiple jets when observing with the naked eye. This hypothesis was rejected after characterizing the jet using high speed photography [29, 31-33].

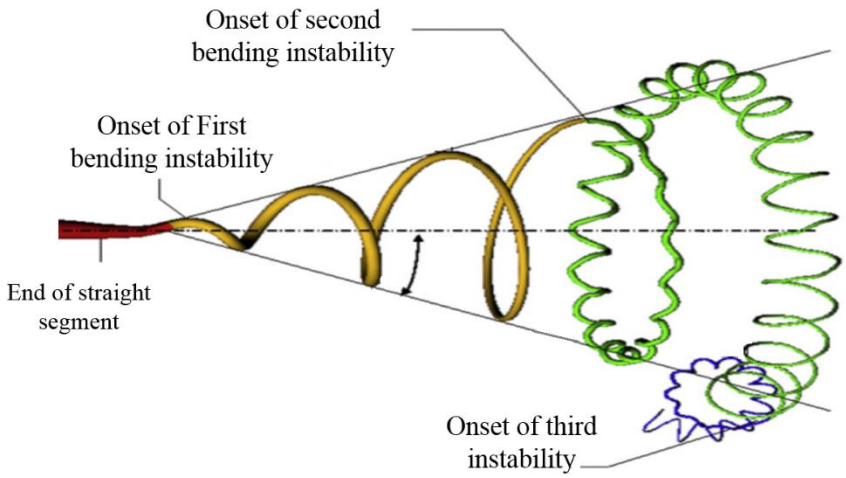

Figure 1.5: Schematic diagram of bending instability of the polymer jet during electrospinning [30].

While the jet is traveling, the electric field inside the conductive fluid must be zero. Therefore, the repulsive Coulomb force between the excess charged ions moves them toward the surface. The repulsive forces between the jet segments will elongate the jet in the direction of its axis [30].

In summary, the fluid instability such as Rayleigh instability, electric field induced instability and whipping instability will occur in this stage. The first two instabilities are axisymmetric to the jet centerline. The jet thinning and jet branching mainly occurs due to whipping instability. The radial charge repulsion may cause the primary jet to split into multiple jets.

1.2.2.3 Solidification of the jet:

As the jet moves toward the collector, it continue to expand by passing through the loops. Jet solidification is based on the traveling distance of the fibers. The distance between the collector and the capillary tip has a direct effect on the jet solidification and fiber diameter.

If the nozzle-to-collector distance is long enough or the whipping instability is high, there is more time for fibers to dry before being collected [22, 29]. In fact, there are many parameters that influence the electrospinning process. In the next section these parameters are explained in detail [26, 34].

1.2.3 Electrospinning principle:

In the electrospinning process, the polymer solution or melt is placed in a syringe, which is located in an infusion pump. A high voltage power supply is connected to the needle of the syringe as shown in the Figure 1.6. By applying the voltage, the solution will get charged. At a certain threshold voltage, the repulsive force between the charged particles in the solution will overcome the surface tension. Therefore, a Taylor cone will be formed. Then the fluid jet is ejected out of the cone. Based on the molecular weight and viscosity of the solution, electrospinning or electrospraying can occur.

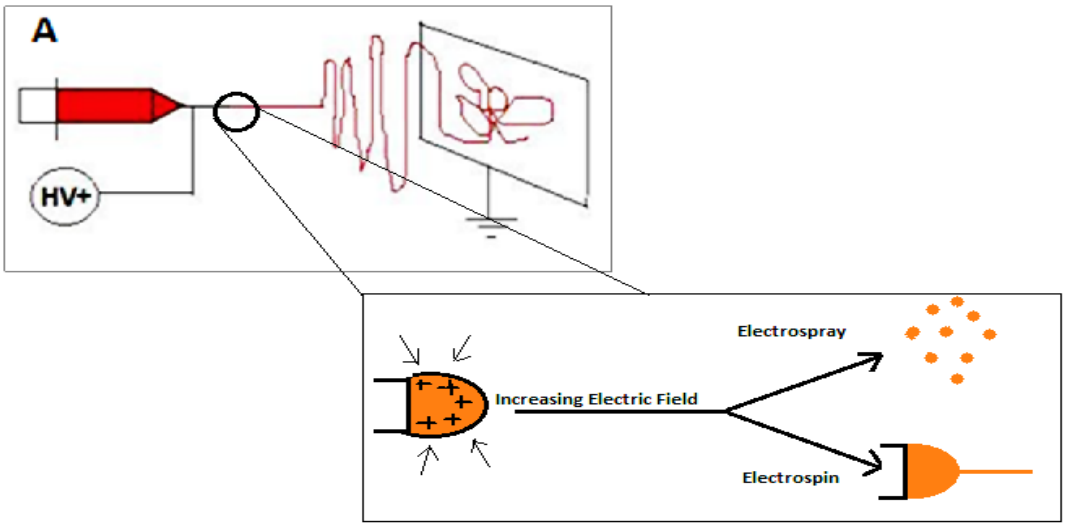

Figure 1.6: Electrospinning setup.

For example, if the viscosity of the solution is high enough, the breakup will not occur in the jet, which results in electrospinning. For the case of low viscosity, various breakups will occur, which results in droplets, and is called electrospraying. The jet will travel from its initiation point to the collector. Further details on the effect of viscosities and charge densities of polymer solutions on electrospinning were described by Hohmann et al. They expressed a formula to describe the electrospinning process as a function of viscosity and charge density of the solution [35].

The results of this process are based on the operating conditions. The distance between the nozzle and the collector is varied between 5 and 30 cm. The internal diameter of the capillary tip is usually 0.1 to 2 mm. The solution infusion rate and the applied potential are normally from 0.1 to 100 µl/min and 5 to 20 kV, respectively. These are just some of the typical operating conditions.

During the normal operation of electrospinning, the jet gets stretched on the way to the collector. The jet can undergo a series of electrically induced bending instabilities, which also can exhibit a whipping motion. The electrospun fibers are smaller than ones produced via conventional techniques. The process can be carried out at room temperature, in heated environments, or in vacuum chambers. The actual electrospinning setup used in this study is shown in Figure 1.7.

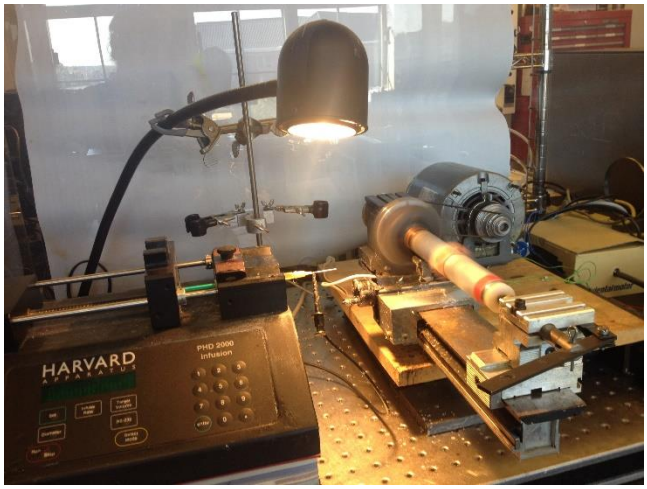

Figure 1.7: Actual electrospinning setup.

In general, fiber morphology can be controlled by manipulating electrospinning parameters. These parameters can be classified into three categories: 1) solution parameters, such as viscosity, surface tension, electrical conductivity, and solution concentration, 2) governing parameters, such as electric potential, nozzle-to-collector distance, and hydrostatic pressure in the syringe, and 3) ambient parameters, such as temperature and humidity [36].

1.2.4 Recent developments:

Controlling the electrospinning process and parameters result in producing various structures, such as: different cross-sectional shapes, beads, branches, buckling, zigzags, and aligned fibers [30]. Nonwoven and randomly arranged electrospun fibers, which are due to the whipping instability of the electrospinning jet, are the forms that usually are collected with conventional electrospinning setups [17, 37]. In order to get other forms of

fibers, additional efforts may needed. For instance, some studies are focused on controlling fiber orientation, such as fiber alignment. Different procedures and determinations were consider to produce aligned fibers, including bubble electrospinning, using a high speed rotating drum, biased AC electrospinning, using a gap method, etc. [38-47]. A few methods are shown in Figure 1.8.

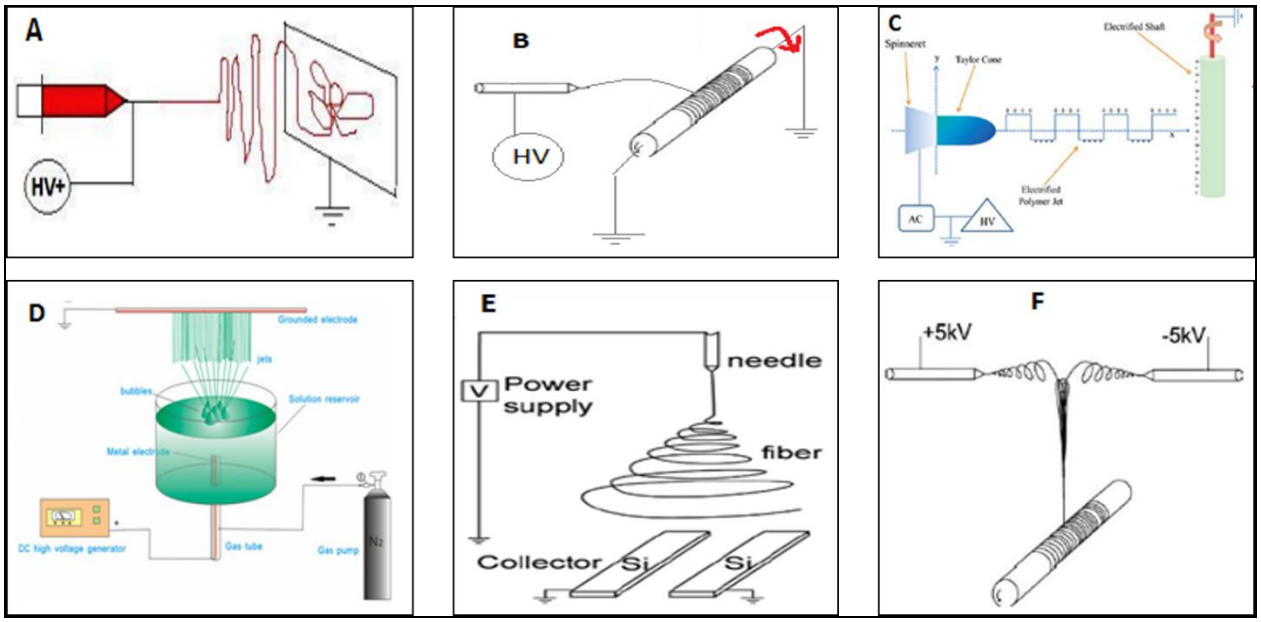

Figure 1.8: Schematic diagram of A) Conventional electrospinning setup, B) High speed rotated drum, C) AC electrospinning, D) Bubble electrospinning, E) Gap method, and F) Modified electrospinning [38, 41, 44, 46].

In bubble electrospinning, the aligned nanofibers are made by producing bubbles at the surface of the solution that has been placed in the reservoir. The high voltage is applied to the solution and the jets form at the surface of the bubbles. The fibers are collected on a single thin cylindrical metal electrode. In biased AC electrospinning, a combination of DC and AC potential are used. The fiber instability is eliminated by using the AC potential. The negative half cycle of the AC voltage will introduce a negative charge on the fiber,

which will contrast with DC bias voltage. This results in highly aligned fibers. In this method the frequency range for producing stable fibers is based on the polymer system. When using a high speed rotating drum, the collector rotates at a high speed (1.8 m/s), and fibers will align along the rotating axis due to their inertia. While using the gap method, the alignment of the fibers will be achieved by manipulating the electric field. Two spilt conductive copper plates are used to manipulate the electric field. In this study, the high speed rotating drum and gap method are the two methods used to collect aligned fibers.

1.3 Filtration performance:

Many efforts are devoted to studying the performance of filtration media. In order to evaluate filter performance, basic definitions for fiber diameter and length, fiber orientation, thickness, solid volume fraction, and face velocity have to be explained. Other scientific terms such as single fiber efficiency, mechanism of particle capturing, total fiber efficiency, pressure drop, and figure of merit (FOM) are also explained in detail. The term aerodynamic slip condition in fluid dynamics is described as well. The filter life time and filter loading will be considered in this chapter.

1.3.1 Fiber characteristics:

1.3.1.1 Diameter and length:

The length and diameter of fibers will affect the filter performance. Thinner fibers will remove MPP from the aerosol more efficiently. Therefore, filtration efficiency will increase when using ultrafine fibers [48, 49]. The thicker fibers will contribute to the

mechanical characteristics of the filters as well as help capture particles with inertial impaction. In general, the fibers in a filter would not have the exact same size distribution. The fiber diameter is usually given as a range, where the equivalent fiber diameter will be calculated using equations. For the filters with two different fiber diameter (called bimodal filters), several ways to evaluate the equivalent diameter were suggested, such as area-weighted average diameter by Brown and Thrope [50], volume-weighted resistivity model by Clague and Phillips [51], and the cube root relation by Tafreshi et al. [52, 53]. These equations are listed below:

$$d_{eq}^{awa} = 2\frac{n_c r_c^2 + n_f r_f^2}{n_c r_c + n_f r_f} \quad (1.2),$$

$$d_{eq}^{vwr} = 2\sqrt{n_c r_c^2 + n_f r_f^2} \quad (1.3),$$

$$d_{eq}^{CRT} = 2\sqrt[3]{n_c r_c^3 + n_f r_f^3} \quad (1.4).$$

In these equations, n_c, n_f, r_c, and r_f are the number fraction and radius of coarse and fine fibers, respectively. These equations offer the best prediction for the filter with the number fractions between 0 to 1 and solid volume fraction from 0.05 to 0.15. Also, the fiber diameter ratio in the bimodal filter should be between 1 and 5 in order to be compatible with these equations.

Some filters are made from short fibers, which results in filters with irregular structure. This filters are suitable for use in capsules or other containers. When using filters in sheet form, the fibers should have an ideal length, which requires longer fibers [49].

1.3.1.2 Orientation:

The orientation of fibers in a filter media has a great effect on the filtration performance. Many previous studies were based on the simplified 2-D geometries of fibers placed in square arrangement perpendicular to the air flow. To reduce the errors, which are introduced to the model by such a simplifications, empirical correction factors were used. Later on, some studies investigated the effect of fiber orientation on filter efficiency and pressure drop. In general, the fibrous media can be classified in three major categories based on their fibrous microstructures: unidirectional, random layered, and 3-D isotropic structures. For unidirectional structures, all fibers are parallel to each other. Fibers are randomly oriented in a parallel plane perpendicular to the air flow for random layered structures. In 3-D isotropic structures, fibers are randomly oriented in any direction in space. Also, the structure of fibers can be classified based on the orientation of them relative to their plane direction, i.e. in-plane orientations and through-plane orientation. There are some studies on influence of in-plane and through-plane orientation of fibers on filter performance [54-57]. Banks et al. were the first to study the effect of through-plane fiber orientation on filter performance using a single fiber model. The effect of in-plane fiber orientation on filter performance based on the fiber diameter was studied by Fotovati et al. It was predicted that for filters with a fiber diameter comparable with particle diameters, decreasing the in-plane orientation of fibers will increase the performance of the filter [57]. To our knowledge, none of these studies have been tested experimentally.

1.3.2 Filter characteristics:

1.3.2.1 Thickness:

It is obvious that increasing the filter thickness will decrease the particle penetration and increase the pressure drop. In a filter media, increasing the number of layers will increase the probability of capturing particles. The penetration of particles through a filter can be calculated based on the filter thickness using the following equation:

$$P = e^{(\frac{-K}{t})} \quad (1.5).$$

In the previous equation, P is the penetration, K is the filtration constant, and t is the filter thickness [58, 59].

1.3.2.2 Solid Volume Fraction:

Solid volume fraction (SVF) is the ratio of the actual volume of solid fibers to the total volume of the filter [48, 54]. It is also called the solidity of a filter (α). The following equation is the expression for calculating the SVF:

$$\alpha = \frac{W}{\rho t} \quad (1.6).$$

In the previous equation, W is the basis mass, ρ is the fiber density, and t is the filter thickness. SVF is an important parameter of the fibrous mats. For a filter mats, increasing the SVF will result in increasing the filter efficiency and the resistance to the flow. Commonly, SVF for air filters have ranged from 0.001 to 0.2.

Kuwabara hydrodynamic factor (Ku) is dependent only on SVF, which is related to the individual streamline of a fiber. This factor deals with the flow around a fiber. It is given by

$$Ku = -0.5ln\alpha - 0.75 + \alpha - 0.25\alpha^2 \quad (1.7).$$

Ku is a dimensionless factor that includes the effect of distortion of flow field around a fiber. The distortion of the flow is usually due to the closeness of an individual fiber to the other fibers. For the cases where the fiber diameter are smaller than the mean free path of the gas ($d_f < \lambda$), the effect of slip at the fiber surface must be included for calculating the Ku. In such case, more complicated expressions should be used [60-62].

1.3.2.3 Face Velocity:

Face velocity (U) is the velocity of the flow when it enters the fibrous media. It can be defined by following equation:

$$U = \frac{Q}{A} \qquad (1.8).$$

In the above equation, Q is the air volume and A is the filter face area. Particle capture mechanisms are dependent on face velocity. Therefore, the efficiency of a fibrous mat is proportional to the face velocity. The pressure drop over a filter mat is also proportional to the face velocity [62, 63].

1.3.3 Aerosol:

Dispersing solid or liquid particles with a diameter ranging from 0.001 µm to 100 µm into a gas medium described as an aerosol [64]. The particles can be from natural sources such as soil, rock debris, sea salt, volcanic dust, and viruses, or from human activities such as particles from transportation, industrial processes, and power generation [62]. Aerosols are formed by one of these means: conversion of gases, disintegration of liquids or solids, resuspension of powdered materials, or the break-up of agglomerates [49]. Table 1.2 lists the several types of particulate suspensions. All the aerosols are two-component systems,

which have special properties. Aerosol properties depend on the particle size and particle concentrations in the suspending medium. Solid aerosol particles usually have complex shapes, however in developmental theory the particles are considered to be spherical and their shapes can usually be ignored. Therefore, particle diameter, which is considered as the particle size, is one of the parameters in characterizing aerosols [62]. There are four categories of particles based on their size: micrometer, submicrometer, ultrafine particles, and nanoparticles. The micrometer particles are the ones with a diameter between 1 to 10 μm, submicrometer particles have a diameter smaller than 1 μm, ultrafine particles have a diameter about 100 nm, and nanometer particles have a diameter less than 50 nm.

Aerosols are classified in different groups based on their particles sizes and shapes: bioaerosol, cloud, fume, haze, dust, mist, fog, spray, and smoke. For example, dust refers to the particles which are produced by disintegration of solid particles, smoke and fume are smaller particles that form the gas phase, and mists are composed of liquid droplets. Particles which are introduced directly to the atmosphere are called primary aerosol whereas those formed in the atmosphere are called secondary aerosol. Aerosols with the same particle size are called monodisperse whereas aerosols with a range of particle sizes are called polydisperse aerosols. Monodisperse aerosols are made only in the laboratory [49, 62, 65].

Aerosol concentrations can be measured based on their mass, called mass concentrations, or their number of particles, called number concentrations. The most common type of

measurement is number concentrations, which is the number of particles per unit volume of aerosol. The common units for number concentrations is number/cm^3 [62].

Table 1.2: Types of Particulate Suspension [62].

Suspending Medium	Type of Suspended Particles		
	Gas	Liquid	Solid
Gas	—	Fog, Mist, Spray	Fume, Dust
Liquid	Foam	Emulsion	Suspension, Slurry
Solid	Sponge	Gel	Alloy

For aerosols consisting of a solid or liquid particles suspending in a gas phase, the gas phase interacts directly with the particles and has a great effect on aerosol behavior. The gas phase should be considered as a collection of molecules which rapidly move and collide with the suspended particles. This is necessary to introduced two important gas properties due to the varied interaction between the particle and surrounding gas. This two characteristics are aerosol mean free path and Reynolds number, which are explained in details.

1.3.3.1 Aerosol Mean Free Path:

In this case, the approach depends on the particle size relative to the spacing of the gas molecules. The average distance that a gas molecule travels between each collision is called the mean free path. This term can be used instead of the average spacing between molecules. The mean free path of a gas can be defined by following equation:

$$\lambda = \frac{1}{\sqrt{2}\, n\pi d_m^2} \qquad (1.9).$$

In the previous equation, d_m is the collision diameter of a molecule and n is the number of collisions. The distance between the centers of two molecules at the instant of the collision is defined as the collision diameter. The mean free path of air at 1 atm and 20°C is 0.06 µm. The ratio of mean free path to particle radius is called the Knudsen number, $Kn = \frac{2\lambda}{d}$, which is a dimensionless number [66].

1.3.3.2 Reynolds Number:

To understand the aerodynamic properties of aerosols, a dimensionless number, which describes fluid flow around an obstacle can be used. This number is known as the Reynolds number. It is the ratio of inertial forces to frictional forces acting on each element of the fluid, which determines whether the flow is laminar or turbulent. The Reynolds number can be expressed by the following equation:

$$Re = \frac{\rho V d}{\eta} \qquad (1.10).$$

In the previous equation, V is the relative velocity between the fluid and an object, d is the characteristic linear dimension such as the diameter of an obstacle, η is the fluid viscosity, and ρ is the fluid density. The Reynolds number depends only on relative velocity between the gas and an obstacle. For Reynolds numbers smaller than unity (Re < 1), the viscous forces are greater than inertial forces. This will result in laminar flow around a particle, which is characterized by a smooth pattern of streamlines that are symmetrical on the upstream and downstream sides of the obstacle. As the Reynolds number increases above 1, eddies will form at the downstream of the particle, which results in a turbulent flow. Figure 1.9 a and b show a laminar flow around a sphere (Re < 1) and a turbulent flow

around a sphere (Re > 10,000), respectively [62]. The 1 < Re < 10,000 is for the transition region form laminar flow to turbulent flow.

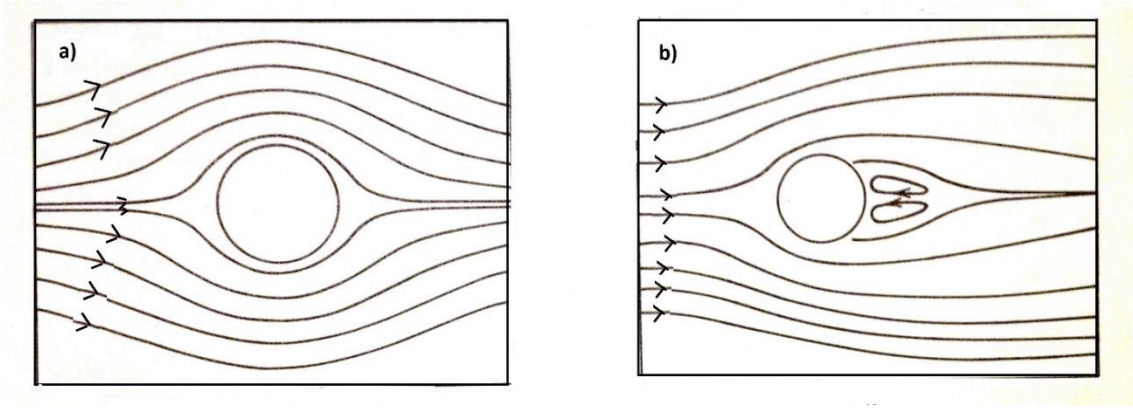

Figure 1.9: Flow around a sphere a) Laminar flow (Re < 1), b) Turbulent Flow (Re > 10,000) [62].

1.3.3.3 Impurities in air:

Particles in the air are likely in range from 0.01 µm to 100 µm size. Even smaller particles than 0.01 µm may be present in the air, such as; smallest particles of metallurgical industries, fumes, and viruses. Typically, particles with the size range from 0.1 to 10 µm are form the 90% of air impurities. Table 1.3 is the size range of typical contaminant in the airborne. Particles with 40 to 70µm are visible to the naked eye, particle with 0.2 to 40 µm can be seen with aid of conventional microscope. For atmospheric impurities, settling velocity should be considered. The settling velocity for very small particles are low, which make them permanently suspended in the fluid. In general, particles size of 1 µm and smaller are considered permanently suspended in the immobile air. Whereas particles up to 10 µm in size are suspended in air with gentle movement. The larger particles, such as 100 µm in size, may be suspended in air with strong velocities i.e. 0.3 m/s [67].

Table 1.3: Size range of typical contaminant [67].

Contaminant	Size Range (µm)	Contaminant	Size Range (µm)
Viruses	0.003-0.05	Fog	2-70
Bacteria	0.3-30	Dry ash	0.1-100
Dust in building	0.01-20	Oil mist	0.01-10
Fumes	0.001-0.1	Welding fumes	0.01-1
Industrial gases	0.2-4	Cement dust	4-100
Lint	10-100	Carbon black	0.01-0.5
Metallurgical fumes and dust	0.001-100	Insecticide dust	1-10
Cupola dust	0.002-100	Ground talc	0.4-50
Smog	0.01-2	Pollen	10-100

1.4 Filtration parameters

1.4.1 Single Fiber Efficiency:

Considering a single fiber, perpendicular to the air flow, is one of the basic means to analyze fibrous filtration. At this level, the fibrous filtration is based on the influence of parameters such as particle diameter (d_p), particle velocity (U_0), Solid volume fraction (α), and fiber diameter (d_f). Single fiber theory will predict collection efficiency for the fibrous structures [49, 68]. Single fiber efficiency is stated as a dimensionless particle deposition rate on the unit length of fiber. The collection efficiency for a single fiber is defined as:

$$E_{SFE} = \frac{2Y}{d_f} \qquad (1.11).$$

In the previous equation, d_f is the fiber diameter and Y is the distance between a trajectory and the axis passing the fiber center. In other word, the ratio of the collected particles compare to all particles that approach the projected area of the fiber is considered as the single fiber efficiency [62, 69].

1.4.2 Mechanisms of Particle Capture:

Particles in the air flow can be captured due to the different mechanisms. The next is a brief introduction of some of the major capture mechanisms, such as inertial impaction, direct interception, Brownian diffusion, gravitational settling, and electrostatic force.

1.4.2.1 Inertial Impaction:

The particles would not follow the streamline perfectly in some conditions, such as in accelerated air flow, which can include convergence, divergence, or any sharp curvature of the streamline. These particles are unable to change their path fast enough to adapt to the change in streamline and therefore collide with the fibers and get captured [70].

The stopping time and distance for particles due to the inertial impaction are based on the particle diameter. The inertial impaction is observed for particles with a diameter of 600nm and above. The Stokes number, a dimensionless parameter which is the ratio between particles' stoppage distance and fiber diameter, is the parameter that governs this mechanism. In this condition, Stokes drag, over the particle and the particle mass should be considered. The Stokes number (Stk) is represented by the following equation:

$$Stk = \frac{\rho^2 d_p^2 C_c V}{18\mu\, d_f} \qquad (1.12),$$

where ρ is the particle density, d_p is the particle, d_f is fiber diameter, μ and v is air viscosity and velocity, respectively, and C_c is particle concentrations [48, 71].

Different formulas were suggested to calculate the single fiber efficiency due to the inertial impaction (E_I). Table 1.4 is giving some of the common equations for calculating the single fiber efficiency due to inertial impaction, which depends on the Stokes numbers. Figure 1.10 shows a single fiber collection by impaction.

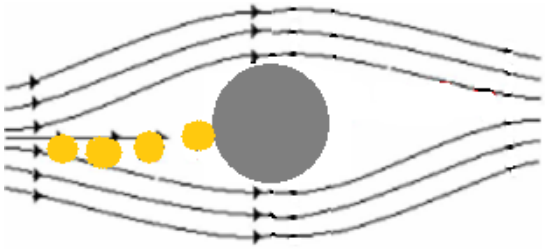

Figure 1.10: Particle capture due to impaction.

Table 1.4: Single fiber efficiency due to the inertial impaction.

Investigator(s)	**Regime/** **Equation Number**	**Single Fiber Efficiency Due to Inertial Impaction**
Brown (1993)	High Stokes number/ (1.13)	$E_I = 1 - \frac{0.805}{Stk}$
Brown (1993)	Moderate Stokes number/ (1.14)	$E_I = \frac{Stk^3}{Stk^3 + 0.77Stk^2 + 0.22}$
Stechkina et al. (1969)	Low Stokes number/ (1.15)	$E_I = \frac{(StK)J}{(2Ku)^2}$

For low Stokes number, J is defined as:

$$J = (29.6 - 28\alpha^{0.62})R^2 - 27.5R^{2.8} \quad (1.16),$$

for R < 0.4. R is a dimensionless parameter, $R = \frac{d_p}{d_f}$, where d_p is the particle diameter and d_f is the fiber diameter. J is approximately 2.0 for R > 0.4 because there is no simple equation for J when R is that high. Impaction is the most important mechanism for large particles [49, 62].

As it was shown in the above equations, single fiber efficiency due to the impaction is a function of Stokes number. Increasing stokes number results in increasing the single fiber efficiency due to the greater particle inertia, greater particle velocity, or more unexpected curvature of streamlines caused by smaller fiber size.

1.4.2.2 Brownian Diffusion:

Small particles have diffusion motion, which affect their capturing efficiency. At the equilibrium condition, gas molecules have thermal energy. Suspended particles inside the gas will reach equilibrium with the gas. The energy exchange between the particles and gas molecules will cause the Brownian motion. The average kinetic energy for small particles is higher than the large ones, therefore the average velocity for the small particles should be greater than the large ones. Brownian motion is a kind of random motion, which may lead to the collision of particles and also capturing particles close to the fibers. Brownian motion and particle capture with Brownian diffusion is more effective for particles sized from 50 nm to 200 nm. The single fiber efficiency due to diffusion, E_D, is a function of the Peclet number (Pe). Pe is a dimensionless number which is defined by following equation.

$$Pe = \frac{V d_f}{D} \qquad (1.17),$$

where V is the air velocity and D is the particle diffusion coefficient [24]. D can be defined with the following equation:

$$D = \frac{k_b C_c T}{3\pi\mu d_p} \quad (1.18),$$

where k_b is the Boltzmann constant, T is temperature, μ is air viscosity, and C_c is the Cunningham factor [56]. The Cunningham factor can be further defined as:

$$C_c = 1 + K_n\left[1.207 + 0.44exp\left(\frac{-0.78}{K_n}\right)\right] \quad (1.19).$$

Single fiber efficiency increases as the Peclet number and the particle size decrease. The single fiber efficiency due to the diffusion does not depends on Ku, therefore is not a function of α. Table 1.5 gives some common expression for single fiber efficiency due to Brownian diffusion. Figure 1.11 shows a single fiber collection by diffusion.

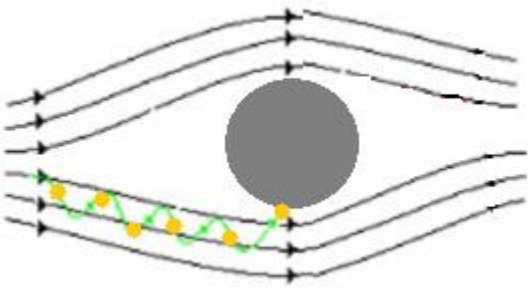

Figure 1.11: Particle capture due to Brownian diffusion.

Table 1.5: Single fiber efficiency due to the Brownian diffusion.

Investigator(s)/ Equation Number	**Single Fiber Efficiency Due to Brownian Diffusion**
Pich (1965)/ (1.20)	With Considering Aerodynamic Slip Effect: $E_D = 2.27(Ku^{-1/3})\left(Pe^{-2/3}\right)(1 + 0.62Kn(Pe^{1/3})(Ku^{-1/3}))$
	Without Considering Aerodynamic Slip Effect: $E_D = 2.7Pe^{\frac{-2}{3}}$
Stechkina (1966)/	$E_D = 2.9Ku^{-1/3}Pe^{-2/3} + 0.62Pe^{-1}$

(1.21)	
Lee and Liu (1982)/ (1.22)	$E_D = 1.6\left(\frac{1-\alpha}{Ku}\right)^{1/3} Pe^{-2/3}$
Liu and Rubow (1990)/ (1.23)	$E_D = 1.6\left(\frac{1-\alpha}{Ku}\right)^{1/3} Pe^{-2/3} C_d$ Where: $C_d = 1 + 0.388 Kn_f \left(\frac{(1-\alpha)Pe}{Ku}\right)^{1/3}$

1.4.2.3 Direct Interception:

When a particle in the gas streamline approaches a fiber within one particle radius, the fiber captures it. In this case, particles are not under the influence of the other capture modes. Interception capture is independent of the air viscosity and velocity, as the particles do not move relative to the air. The particles are entirely in a passive mode. This capture mode generally applies to the particles with a range size of minimum efficiency, such as particles with diameters equal to 400nm. Figure 1.12 shows the trajectory of one such particle that follows the gas streamline and intercepts with the fiber. The single fiber efficiency due to direct interception, E_R, is a function of Ku and a dimensionless parameter (R), which is the ratio of particle diameter to the fiber diameter.

$$R = \frac{d_p}{d_f} \qquad (1.24).$$

E_R increases with increasing R. The limit for E_R is the theoretical value of 1+R. For particles with negligible inertia or Brownian motion, the collection mechanism is usually

assumed to be pure interception [62]. These particles follow the streamline perfectly. Table 1.6 gives some common expressions for single fiber efficiency due to direct interception.

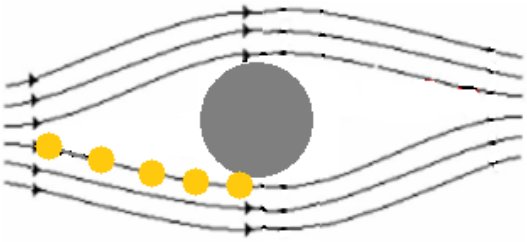

Figure 1.12: Particle capture due to direct interception.

Table 1.6: Single fiber efficiency due to the Direct Interception.

Investigator(s)/ Equation Number	**Single Fiber Efficiency Due to Interception**
Pich (1966)/ (1.25)	$E_R = \frac{(1+R)^{-1} - (1+R) + 2(1+1.996Kn)(1+R)\ln(1+R)}{2(-0.75 - 0.5ln\alpha) + 1.996Kn(-0.5 - ln\alpha)}$
Lee and Gieske (1980)/ (1.26)	$E_R = \frac{1-\alpha}{Ku}\frac{R^2}{(1+R)^m}$ where: $m = \frac{2}{(3(1-\alpha))}$
Lee and Liu (1982)/ (1.27)	$E_R = 0.6\frac{1-\alpha}{Ku}\frac{R^2}{(1+R)}$
Liu and Rubow (1990)/ (1.28)	$E_R = o.6\left(\frac{1-\alpha}{Ku}\right)\frac{R^2}{(1+R)}C_r$ where: $C_r = 1 + \frac{1.996\ Kn_f}{R}$

In summary, capturing particles due to interception is because of the particle finite size. There are certain streamlines, which result in particle capturing due to the particle size.

Pure interception takes place when the particles follow the streamline perfectly with negligible inertia or Brownian motion [62, 72].

1.4.2.4 Gravitational Settling:

Particle velocity has two terms, settling velocity and convective velocity. Settling velocity is the influence of gravity on the particle and may result in particle capturing. Gravitational settling depends on a dimensionless number (G) that controls the particle deposition. The following equation is for calculating G:

$$G = \frac{V_{TS}}{U_0} = \frac{\rho_p d_p^2 C_c g}{18\eta U_0} \quad (1.29).$$

In the above equation, U_0 and V_{TS} can be in the same direction or in opposite directions. The single fiber efficiency for gravitational settling (E_G) can be calculated using the following equations:

$$E_G \simeq G(1+R) \quad (1.30),$$

$$E_G \simeq -G(1+R) \quad (1.31).$$

Where equation 1.30 is when the U_0 and V_{TS} are in the same direction, and equation 1.31 is when the U_0 and V_{TS} are in opposite directions.

The effect of gravitational settling depends on the airflow direction and particle size. For a large particle and small U_0, the E_G has an effect in overall efficiency. For example impaction is more important than settling when the U_0 is greater than 10 cm/s. In general, E_G is not as effective as other capturing mechanisms [48, 62].

1.4.2.5 Electrostatic Force:

This mechanism is based on the attractive force between charged fibers and particles. Charged particles are attracted to oppositely charged fibers by Coulombic attraction. In the cases of charged fibers, the electric field, which induces a dipole on the particles, will be created. Therefore, the attraction force on the side of particle nearer to the fiber is slightly greater than the repulsive force on its farther side. This will tend to cause the attraction of particle to the fiber. Increasing the charge of particles or fibers will result in higher capturing due to the electrostatic force. It is difficult to classify the electrical charge on the particle and the fiber unless the particles or fibers have been charged in a quantifiable way. Therefore, it is difficult to quantify this deposition mechanism [54, 55, 57, 62].

1.4.3 Filter Efficiency:

The total fiber efficiency for any kind of filter can be described by using the percentage of penetration. In this case, the capturing efficiency is:

$$\eta=1-P \tag{1.32}$$

In the above equation, P is penetration of the particles through the filter. It is defined by the following ratio:

$$p = \frac{n_{out}}{n_{in}} \tag{1.33}$$

In this ratio, n_{out} is the number concentration of particles leaving the filter (downstream) and $n_{in}$is the number concentration of particles entering the filter (upstream). This is the main method to calculate the filtration efficiency in the experimental work.

However, calculating the efficiency of a filter as a whole unit is a complex process. But, analyzing this process on an elementary level is one way to approach this problem. Calculating the single fiber efficiency for each particle capturing mechanism would be an accurate way to approach the total fiber efficiency.

Capturing particles using a single fiber is influenced by many parameters, such as d_p, d_f, U_0, α, and etc. For example, for a filter with a thickness of 1 mm, a solidity of 0.05, a fiber diameter of 2 µm, and an operating face velocity of 10 cm/s, Interception and impaction are dominating mechanisms for particle larger than 0.5 µm and diffusion is only an important mechanism for particles below 0.2 µm. For all particles, the gravitational mechanism is small compared to other types of mechanisms.

Also, changing the fiber diameter will affect the filtration efficiency. For a filter with constant solidity and thickness, as the fiber size decreases, the minimum efficiency size decreases and the minimum efficiency increases [62].

By considering all the effects of different parameters, the total efficiency can be calculated by using the total single fiber efficiency [48, 56, 73-75]:

$$E_t = 1 - (1 - E_D)(1 - E_I)(1 - E_R)(1 - E_G) \quad (1.34),$$

$$\eta = 1 - exp\left[-\frac{4\alpha E_t t}{\pi(1-\alpha)d_f}\right] \quad (1.35).$$

In the above equations, E_t is the total single fiber efficiency. One can think that the E_t should be the summation of all the capturing mechanisms. However, since different particle capturing mechanisms are competing to capture the same particle, it is incorrect to add all the single fiber mechanisms for calculating E_t, because in this case the particle

capture could be counted at least twice. Generally, for calculating the total efficiency by using the modern theory of single fiber efficiency, the effect of neighboring fibers should be considered. Also, it is often one mechanism that serves as the primary mechanism in capturing particles, therefore the total efficiency is only calculated based on that mechanism.

Comparing the theoretical values for filtration efficiency are found to be greater than the experimental values. This is a result of imperfect dispersion of the fibers in a real filter, clumping the fibers together, and the chance for fibers to screening one another. Also in real filters, there are fibers that might not lie transverse to the airflow [6, 76, 77].

1.4.4 Pressure Drop:

In a fibrous filter, each individual fiber resist the air flow passing it, which causes filter resistance, or pressure drop. The amount of pressure drop after the air passes through the filter is called filter pressure drop. It represents the amount of energy needed to allow air to pass through the filter media.

Many expressions can be found in literature to calculate the pressure drop. One of the most important expressions for total filter pressure drop according to Darcy's law is as follows:

$$\Delta P = f(\alpha)\frac{\mu V t}{d_f^2} \qquad (1.36).$$

In this equation, μ is air viscosity, V is air velocity, t is filter thickness, d_f is fiber diameter, and f(α) is the correlation for dimensionless pressure drop. This equation is based on the total drag force of all the fibers. There are several studies on the calculation of f(α). One of

them, shown below, is proposed by Davis (1973), and holds for randomly oriented fibers and the solid volume fractions in the range of 0.006 to 0.3 [52, 56, 75, 78]:

$$f(\alpha) = 64\alpha^{1.5}(1 + 56\alpha^3) \quad (1.37).$$

From the above equations, it can be seen that the pressure drop is directly proportional to the filter thickness and face velocity and it is inversely proportional to the fiber diameter squared. Equation 1.36 is based on the empirical correlation, which includes filter parameters that are not ideal, such as fibers that are not perpendicular to the air flow.

It is worth mentioning, depending on their fiber diameters, that the predicted value for pressure drop for a filter should be considered with a correction factor due to the slip flow at the surface of the fibers. In the empirical correlation of Davies, it is assumed that there is continuous flow around the fiber with a no-slip condition. This assumption holds true for relatively large fibers. The Knudsen number can be used to describe the flow condition which will be explained in following section.

1.4.5 Flow Regimes:

In general, there are four different types of flow regimes; continuum flow, slip flow, transition regime, and free molecule regime.

The aerodynamics slip factor is dependent on the Knudsen Number [54, 68], which can be used to describe the importance of molecular movement of air molecules at the surface of the fiber in relation to the flow. This number is given by:

$$Kn = \frac{2\lambda}{d_f} \quad (1.38),$$

where λ is mean free path of the fluid molecules and d_f is the fiber diameter.

Table 1.7: Flow regime and Knudsen number range.

Knudsen Number Range	Flow Regime
$Kn < 0.001$	Continuum Flow
$0.001 < Kn < 0.25$	Slip Flow
$0.25 < Kn < 10$	Transition Regime
$Kn > 10$	Free Molecule Regime

In fluid dynamics, depending on the fiber size and mean free path of gas molecules, the fluid velocity around the fibers is varied. The no-slip condition is when the velocity of the flow around the obstacle is zero. This takes effect in fibers of 10 micron and above in diameter. For the fibers of smaller size, no-slip condition is no longer valid. The drag force acting on the fibers is reduced [79][6]. In this case, the slip factor correction is applicable. The slip factor correction suggested by Hosseini et al. is defined as:

$$C_r = \frac{\Delta P_{ns}}{\Delta P_s} \quad (1.39),$$

where ΔP_s and ΔP_{ns} are the pressure drop across a fibrous media with the slip boundary condition and no-slip boundary condition. By considering suggesting equation to obtain the pressure drop, one expression for C_r is in the following [54]:

$$C_r = \frac{K_u + 1.996 K_{nf}\left(-0.5\ln(\alpha) - 0.25 + 0.25\alpha^2\right)}{K_u\left(1 + 1.996 K_{nf}\right)} \quad (1.40).$$

1.4.6 Figure of Merit (FOM):

Figure of merit or quality factor is a measure of filter performance due to the energy expended. It can be expressed as a function of pressure drop and filtration efficiency. In a

filter media, increasing the solid volume fraction or decreasing the fiber diameter will improve the particle capturing efficiency. However, increasing SVF or decreasing fiber diameter will cause to an increase in filter's pressure drop. Therefore, filtration efficiency or pressure drop by themselves, cannot be the only evidence to judge the filters performance and it is preferred to use the quality factor.

FOM can be calculated by the ratio of the logarithm of the penetration over the pressure drop.

$$Q = \frac{-\ln(p)}{\Delta P} \qquad (1.41).$$

The performance of the filter is based on the FOM, higher values for FOM indicate the better performance of the filters. A filter with high efficiency and low pressure drop is consider as a good filter, this can be seen from the equation of FOM [72, 80-81].

1.4.7 Filter Clogging:

The filtration theory are based on the clean fibrous media, the study of air flow around a perfectly clean fibers. However, passing the air through the filter for some time will cause particle to deposit on the fibers. The deposited particle will change the fiber morphology, which will affect the flow field around a fiber as well as the particle capturing mechanism. There are some study on the filtration clogging based on modeling and experiments. Both efficiency and pressure drop of a fibrous filters will increasing by accumulation of collected particles. Initially it is beneficial to the filter performance due to the increase in filtration efficiency but eventually the filter is called to be clogged due to a very high

pressure drop. Filters with low value of solidity (α) can tolerate the great dust loading without clogging. However, in some cases with liquid droplets as aerosols, both the filtration efficiency and pressure drop will decreases by time. The liquid droplets which are deposited on the fibers, will wet the fibers and result them to draw together due to the capillary effects. This leads to the increase in pore size.

In general, While the particle deposition are taking place in the filter, important changes, such as change in morphology, build up chain aggregates, and filter weight, may occur which will change the filtration characteristics. Therefore, the time variation of pressure drop and penetration of a filter during its performance depends on the structure, material of the filter and the nature of aerosol. In general most of the experiments for evaluating the filter performance are usually carried out on the clean filters with negligible amount of particle loadings [6, 49, 62].

1.5 Conclusion:

In the above chapter a brief introduction to the fundamental theory of filtration and aerosol specifications were provided. In addition, a literature review of the filters and filtration was presented. The method of producing fibers for fibrous media were presented briefly and among those, electrospinning was chosen as the best available method to produce fibers for our experimental aims. In addition, fundamental principle of electrospinning and the properties of electrospun fibers were discussed. The empirical and theoretical studies to evaluate the filters performance were explained and the equations were presented.

The following chapters will present the research efforts in producing fiber mats with controlling morphology of fibers using electrospinning. It is also focused on the uniformity of fiber mats and controlling the fiber orientation. New experimental study on the performance of the fiber mats based on the fiber counts in each layer were also conducted and the results will be presented. These thin fiber mats made of controlled fiber position can be applied to an existed filter to improve its filtration performance. Our experimental research introduce a fiber mats as a coating that can improve the filtration efficiency of the filters that were applied to without adding significant pressure drop.

1.6 Purpose of Research Study:

Certain methods of configuring fibrous material in filtration media have the potential to provide high efficiency filters while minimizing pressure drop. A filter's air resistance and efficiency have a strong correlation to the thickness of fibrous mats. Controlling the pore size and the structural elements of a filter can be a good contribution to control the filter performance. Most fibrous research has been done with only one fiber diameter distribution which are randomly oriented. Electrospinning is a unique technique which provides aligned and random fibers with controlled fiber diameter. This study deals with the performance of nonwoven aligned and random electrospun fiber mats. The unimodal and bimodal fibers are two configurations which were studied in this research. Additionally, fibers can be oriented in orthogonal and random fashions. The purpose of the study was to compare the performance of unimodal and bimodal mats as well as the effect of fiber orientations. In bimodal fiber mats, the fine fibers are effecting the collection

efficiency while the coarse fibers help in reducing the pressure drop and provide mechanical support. In orthogonal fiber mats, where the aligned fibers are collecting perpendicularly on top of each other, the performance of the fiber mats will improve due to reducing the filter mats thickness as well as increasing the entropy of the system. This study can be the first experimental study that approach making and evaluating the orthogonal fiber mats with unimodal and bimodal fiber configurations.

CHAPTER 2 Experimental Setup

2.1 Introduction

Fiber mats were produced using micro- and nano-scale electrospun fibers with Polystyrene and Nylon 4,6 solutions. Different solution concentrations, electrospinning parameters, and various setups were considered to produce a variety of fiber diameters and orientations. Different morphologies were made, including layering aligned and random fibers. The samples were analyzed using optical and electron microscopes to evaluate their morphologies. The samples were tested based on their filtration performance such as: pressure drop, filtration efficiency and FOM. In order to validate experimental values with theory, the samples' masses and thicknesses were measured to use in calculating the empirical equations.

In this chapter, the electrospinning methods and setups, material specifications, analysis techniques and instruments, and filter test rig are explained in detail. More details on certain condition of electrospinning results in different filter morphologies will be outlined in Chapter 3.

2.2 Electrospinning Setup

The main setup for electrospinning used in this study is illustrated in Figure 2.1. As it is shown in Figure 2.1, the setup includes a DC power supply, infusion pump, rotating

collector, and positioning system. The deposition of electrospun fibers was done on the substrate attached to the collector.

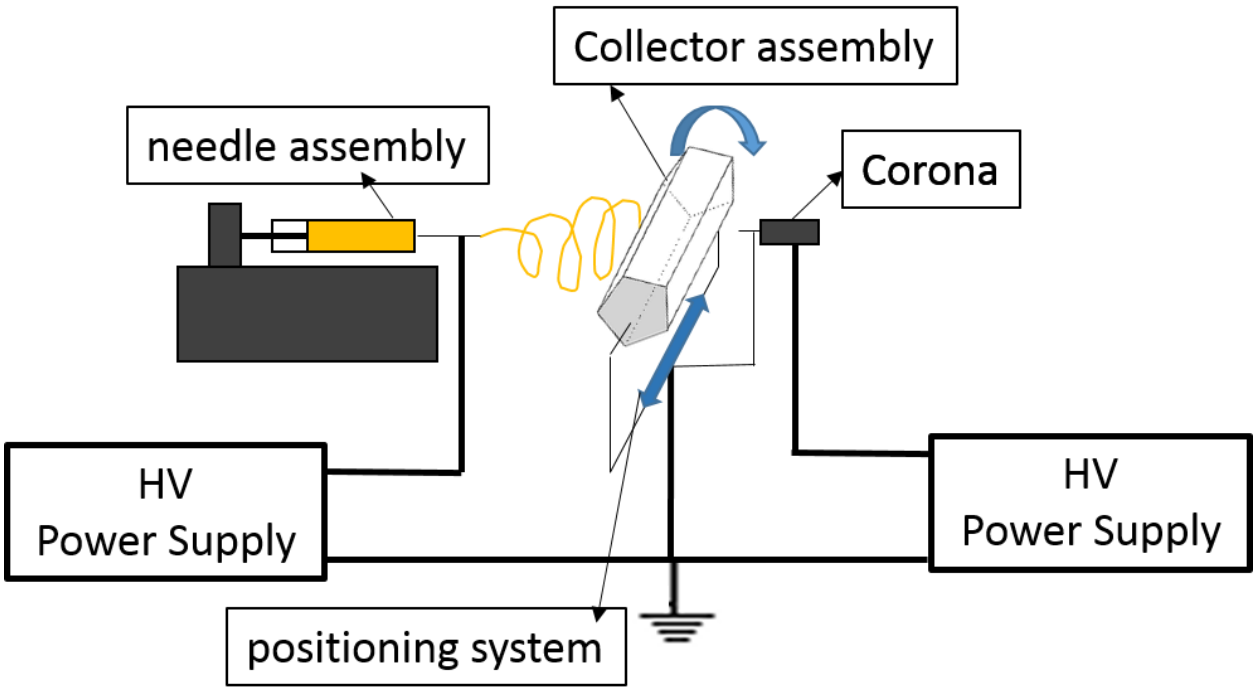

Figure 2.1: Electrospinning aparatus setup.

Polymer solutions were placed in the electrospinning needle assembly, which is a 1 ml syringe (National Scientific Company) with a flat tip stainless steel 27 G needle of length 1.27 cm (Becton- Dickinson, Precision Glide TM). The syringe was placed in an infusion pump (Harvard Apparatus PHD2000), where the solution flow rate could be controlled. The rotational collector consisted of a 17.5 cm long hexagonal cylindrical drum, each face having a width of 1.5 cm. The collector drum was electrically grounded and attached to the AC motor (Marathon Electric, Cat No. S102) via belt. Changing the belt position would cause a change in the rotational speed. The drum was rotated at a speed of 1200 rpm. A two-phase Vexta stepping motor (Model PK268-02A) was used as the positioning system,

where the sliding table attached to it. An Immediate Motion Creator (IMC) software was used to control the back and forth motion of the sliding table. The collector was mounted on the sliding table. All the setup, including needle assembly, collector, and sliding table, were placed on a vibration isolation table. The distance between the needle tip and the drum was kept at 7cm for most of the electrospinning. A high voltage was applied to the needle by a Matsusada Precision Inc. power supply (Model AMT-10810-LCS).

The corona apparatus was used on the opposite side of the collector to neutralize the surface charges. Needle assembly and corona assembly were placed on either side of the drum. The corona consists of a needle, which was connected to the high voltage. The needle was then shielded using a copper plate [82][83].

In the case of gap method, a stationary collector was used. Two copper strips 12 mm wide and 27 mm long were placed 2cm apart on the collector, facing the needle. The surface of the collector was insulated except for the two copper strips, which were grounded. Samples were individually placed in the middle of the two strips. Figure 2.2 is schematic of the gap stationary collector.

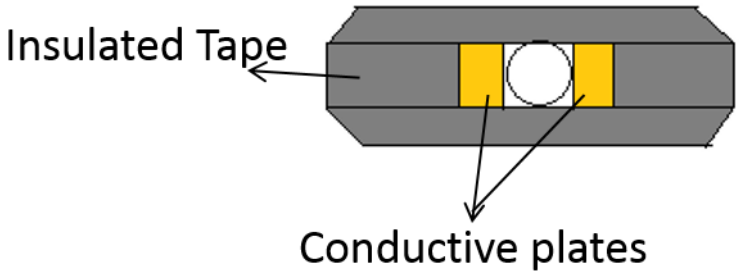

Figure 2.2: Schematic of the stationary collector used in gap method.

All of the current and voltage measurements were recorded from the power supplies directly or by using an Agilent 34401A digital multimeter with a Fluke 80k-40 HV probe. Ambient temperature and humidity was measured before each experiment by using a Vaisala HM 34 meter.

2.3 Electrospinning solutions:

In this study, Nylon 4,6 and Polystyrene were chosen as the focus materials to produce filter mats. These two polymers are relatively cheap and known to be easy to electrospin. Also, there are many studies on the physical properties and processing parameters of these two polymers. As an example, Nylon, an engineering plastic, is one of three major synthetic polymer in fiber industry [84]. Polystyrene is a synthetic aromatic polymer, which is considered the most inexpensive of hydrophobic polymers.

Nylon solutions were prepared by dissolving Nylon 4,6 (442992; CAS=50327-22-5, Sigma-Aldrich, USA) in Formic acid (98%, Fluka, USA). Nylon 4,6 was used without additional purification in the following concentrations, 10%, 15%, 18%, and 20% wt. Nylon in Formic acid. Additionally, 0.2 Wt. % Pyridine was added to the 10% Nylon 4,6 solutions exclusively as explained in Chapter 3 [85]. Polystyrene solutions were prepared by dissolving Polystyrene (331651 Aldrich**,** average M_w 350,000) in Toluene (244511, anhydrous, 99.8%, Sigma-Aldrich) and Tetrahydrofuran (THF) (anhydrous, ≥99.9%, inhibitor-free, Sigma-Aldrich) with various concentrations at 18%, 20%, 25%, and 30% wt. Polystyrene. Table 2.1 summarizes some of the specifications of the Polymers and other chemicals which were used in this study.

Table 2.1: Properties of polymers/chemicals used in this study [86][87].

Polymer/ Solvent	Molecular Formula	Molecular weight (g/mol)	Density (g/cm^3)	Solubility Parameter ($MPa^{1/2}$)	Dielectric Constant
Polystyrene	(C8H8)n	~350,000	1.05[a]	15.2	2.5 – 2.6[a]
Nylon 4, 6	(C10H22N2O4)n	~10,000	1.18	27.8[a]	3.2 – 3.5[a]
Toluene	C6H5CH3	92.14	0.87[b]	18.2	2.4[b]
THF	C4H8O	72.11	0.89[b]	18.6	7.5[b]
Formic acid	CH2O2	46.02	0.98	24.7	58.8[b]
Pyridine	C5H5N	79.1	1.22	21.9	12.4[b]

[a] Value reported for 25 °C.
[b] Value reported for 20 °C.

During the electrospinning, polymer solution properties; including solution concentration, polymer molecular weight, solution conductivity, solution viscosity, surface tension, and solvent dielectric constant, will strongly affect the morphology and diameter of the electrospun fibers.

It is worth mentioning that a large difference between the solubility parameters of the polymer and its solvent will result in the formation of beads on the electrospun fibers, which is due to the poor interaction between polymer and solvent molecules. In this study, Polystyrene was dissolved in Toluene/THF and Nylon 4,6 was dissolved in Formic acid. Both Solutions, Polystyrene in Toluene/THF and Nylon in Formic acid, were electrospun very easily at room temperature. The dielectric constant of the solution is related to the charges in solution, which effects the electrospinning process and the resultant fiber morphology [88-90]. As an example, the high dielectric constant of the solvent will reduce

the bead formation and improve the productivity of the fibers via electrospinning. Also, adding Pyridine to the 10% wt. Nylon 4,6 solution will eliminate the bead formation during electrospinning. Pyridine is a base and will react with formic acid to produce an organic salt. This reaction will hypothetically increase the electrical conductivity of solution [15]. For Polystyrene, 30% of the solvent is THF because of its high dielectric constant. This helps to increase the amount of electrical charge in the solution.

2.4 Electrospinning Parameters:

As it was explained in Chapter 1 Section 1.2.3, different electrospinning setups and polymer solution properties will results in different fiber diameters and orientations. Figure 2.3 illustrates different electrospinning setups, which were used in this study. Below is a detailed explanation of these setups.

Figure 2.3A is the schematic of a conventional electrospinning setup which consists of a high voltage source, an infusion pump and a rotation drum. Samples were placed on the drum, which acted as collector. A flat tip stainless steel 27G needle was connected to a plastic syringe containing the polymer solution, and placed in the infusion pump.

Figure 2.3B is the schematic of an electrospinning setup with negative ion deposition using a corona (high voltage on a sharp point). A negative voltage of 3.5-4.0 kV was given to the corona via a power supply. The corona was placed as close as possible to the drum surface with its tip coaxial to that of the needle.

Figure 2.3C is the schematic diagram of an electrospinning setup on stationary substrate and Figure 2.3D shows an electrospinning setup with a collector consisting of two copper

strips separated by a gap. In this case, substrate was placed in the gap between two the copper strips.

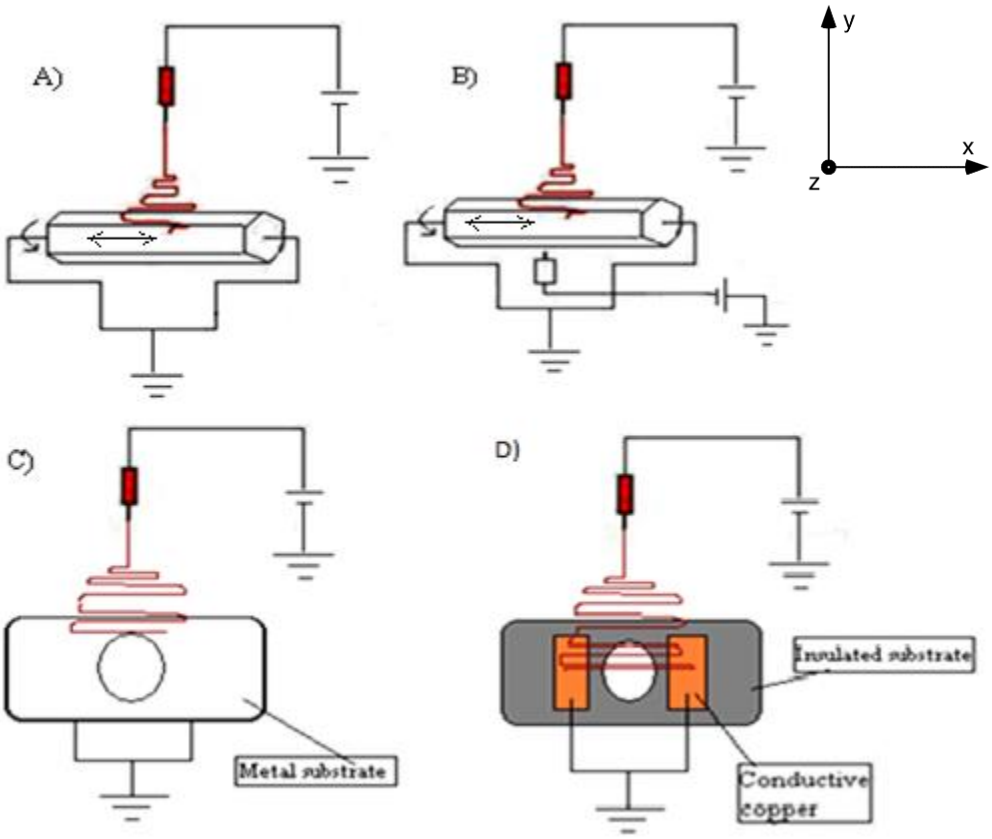

Figure 2.3: Schematic diagram of electrospinning setup, A) conventional electrospinning with rotational collector involved translational motion in x-direction, B) setup with corona for negatively charged ion deposition and rotational collector involved translational motion x-direction, C) conventional electrospinning setup with a stationary metal collector D) electrospinning with gap, using two conductive electrodes placed on insulated substrate as collectors.

Setups for fabricating aligned and random micrometer and nanometer fibers are as followed:

- The rotating collector was used to enhance the alignment of micrometer Polystyrene fibers, also the collector motion in the x-direction will help control fiber depositions (Figure 2.3 A),

- The stationary grounded collector was used to produce random micrometer Polystyrene fibers (Figure 2.3 C),
- The rotating collector was used to produce random nanometer Nylon 4, 6, using a corona and setting the collector motion in the x-direction will enhance fiber mats uniformity (Figure 2.3 B),
- The stationary collector, with two conductive plates in the form of strips, was used to produce aligned nanometer Nylon 4,6 fibers (Figure 2.3 D).

Table 2.2 summarizes the experimental conditions for electrospinning used in this study.

Polymer	Solvent	Concentration (wt. %)	Voltage (kV)	Needle to collector distance (cm)	Infusion Rate (μl/min)
Polystyrene	Toluene/THF <7:3>	18%, 20%, 25%, 30%	5.5	8 – 10	1 – 2.5
Nylon 4, 6	Formic acid	10%, 15%, 18%, 20%	7 – 7.5	7 – 8	0.5 – 0.8

2.5 Substrate:

The electrospun fibers were deposited onto a Nylon 6 mesh (McMaster, 9318Txx). The wet electrospun fibers deposited on the substrate strongly adhered to the substrate. Especially for the case of Nylon 4,6 solutions, the presence of Formic acid in the wet fibers reaching the substrate allowed the fibers to adhere to any material soluble in Formic acid [82]. Substrates were cut into circles with a 12 mm diameter using a cutting punch. Table 2.3 summarizes the substrate specifications used in this study. Figure 2.4 shows a substrate with and without fiber deposition.

Table 2.3: substrate specifications used in this study.

Material	Thread Diameter [a] (μm)	Opening width [a] (μm)	% Open Area [a]	Thickness [b] (μm)	Weight (mg)
Nylon 6	120	255	36	210	7.5 – 8

[a] The thread diameter, opening width, and % open area were obtained from measurements taken on SEM images. [b] Substrate thicknesses are determined using a Surface Contact Measurement Technique (Dektak Profilometer).

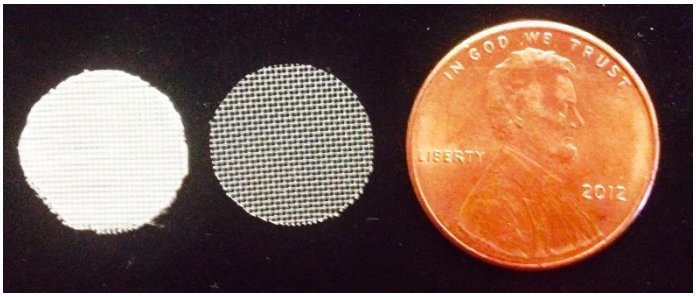

Figure 2.4: Mesh substrate left) with fiber deposition and right) without fiber deposition.

2.6 Characterizing Solution Properties

As it was previously mentioned, the electrospinning solution properties such as electrical conductivity, surface tension, viscosity, and density need to be measured and maintained at required values to produce the desirable electrospun fibers. In this study, three solution properties were measured. Electrical conductivity of the polymer solutions was measured using a conductivity meter (YSI Model 3200). Surface tension of the polymer solutions were measured using standard Goniometer/Tensionmeter with drop image advanced software (Rame-hart Model 250). The device takes measurements of solution droplet surface tension by a software package, DROPimage Advanced. Viscosity of the polymer solutions was also measured using a ball drop viscometer (Gilmont Falling Ball

Viscometer). The tube of size 3 and steel ball were used. All the measurements were taken at room temperature.

2.7 Characterizing Filtration Performance

2.7.1 Filter Test Assembly:

Figure 2.2 is a schematic diagram of the filter test setup. It consists of a vertical steel column with conical inlets, two pressure ports (upper and lower part), a differential pressure monometer (EXTECH Instruments Model HD 700), an optical particle counter (AeroTrak Model 8220), and a flowmeter (Cole-Parmer, model PMR1-010477) attached to a High Efficiency Particulate Air (HEPA) filter (controlling the face velocity). For evaluation of filter performance, filters were placed between the upper and lower parts. The optical particle counter was fixed at a volumetric flow rate of 2.8 LPM which is called Q3 in Figure 2.5. The rotameter has a maximum flow of 4.4 LPM which is called Q2 in Figure 2.5. The actual flow passing through the filter, Q1 in Figure 2.5, can be controlled by fixing the rotameter at a desired flow. The HEPA filter attached to the rotameter ensures that the Q2 is clean of any particles. Therefore, the particle counts from the optical particle counter are only from the flow passing through the filter (Q1). Face velocity was kept at ~5 cm/sec for filters containing nanometer electrospun fibers and at ~12 cm/sec for all other samples. The pressure drop is read directly from the digital pressure meter, which is connected to the two ports.

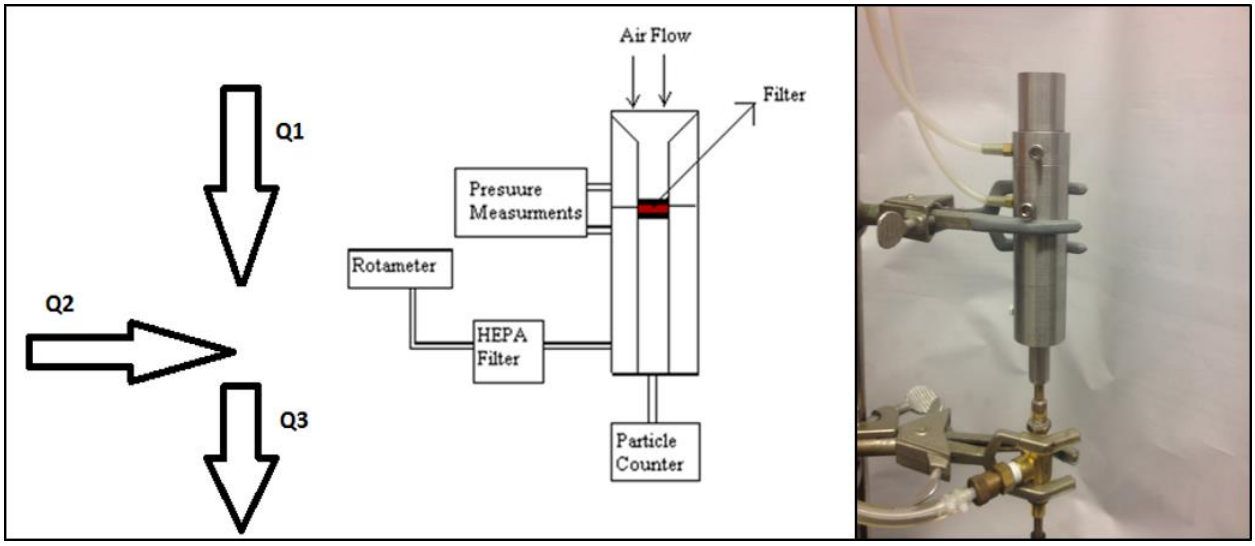

Figure 2.5: Filter test setup.

As it shown in Figure 2.5, two pressure ports are placed at the upper and lower pieces of a vertical orifice column. The upper piece has a length of 40 mm and a center tapped bore of 9.4 mm diameter. The inlet part of the upper piece is conical with length of 1 cm and diameters of 22.00 and 9.4 for its top and bottom, respectively. The lower piece has same center tapped bore to the entire length (9.4 mm in diameter). It is 50 mm long and conical opening at the end, which has a 12.6 mm diameter. The upper pressure port is placed at 38 mm from the top and the lower pressure port is placed 80 mm from the bottom. The optical particle counter is connected to the vertical column with a rubber tube having outer diameter of 9 mm and inner diameter of 6 mm. The upper piece of the assembly is fitted coaxially to the lower piece after the filter is placed between the upper and lower pieces. To ensure that all air is forced through the filter, two O-rings are placed on either side of the filter. The O-rings provide compressive force to the filter.

2.7.2 Particle Counting:

Filtration efficiency was measured using an AeroTrak Handheld Optical Particle Counter, Model 8220. The particle counter has a size range of 0.3 to 10 micrometers, with six defined bean sizes of 0.3-0.4, 0.4-0.5, 0.5-0.6, 0.6-0.7, 0.7-1, and >1. Measurements were done for 3-minute durations with a 10 second delay for each set. The bean size of 0.3-0.4 was considered for calculating the filter efficiency of most penetration particles.

2.7.3 Calibration of Instruments:

As previously mentioned, the filter test setup is made up of four parts; rotameter, optical particle counter, pressure meter and filter holder column. This system has been evaluated with other systems to check for the accuracy of the results and also to calibrate each of the four sections.

- Calibration of the rotameter:

The rotameter consists of a Brooks Tubes, 1110 and 1140 series flow meter. The filter test rig is attached to the Brooks tubes. The maximum air flow out of this rotameter is 4.4 LPM. The actual flow rate that passes through the filter is controlled by the position of the ball as it moves through the rotameter. In this section it is ensured that the ball position is in agreement with the expected flow meter reading. To achieve this, a Gilibrator Bubble Flow Meter was used to test the actual flow meter values for each ball position. The bubble cell with airflow ranging from 0.02 to 6 LPM was used. The wet cell generated perfect bubble films by the touch of a button. The bubble flies in the cell column and an infrared

sensor reads the bubble flow rate. There are two sensors at the button and top of the cell that detect the bubble at each position. The flow rate is calculated by knowing the distance between the two sensor points and the time it takes the bubble to pass from one point to the other.

The results from using the airflow calibrator agreed with previous lab group experimental results. Note that these preceding experiments were done using a manually operated bubble meter in contrast to the Gilibrator Air Flow Meter used in this study. Here, the rotameter flow rate is controlled based on the desired face velocity. The optical particle counter attached to the end of the filter test column is fixed at a volumetric flow rate of 2.82 LPM. Both results are compared in the following graph (Figure 2.6).

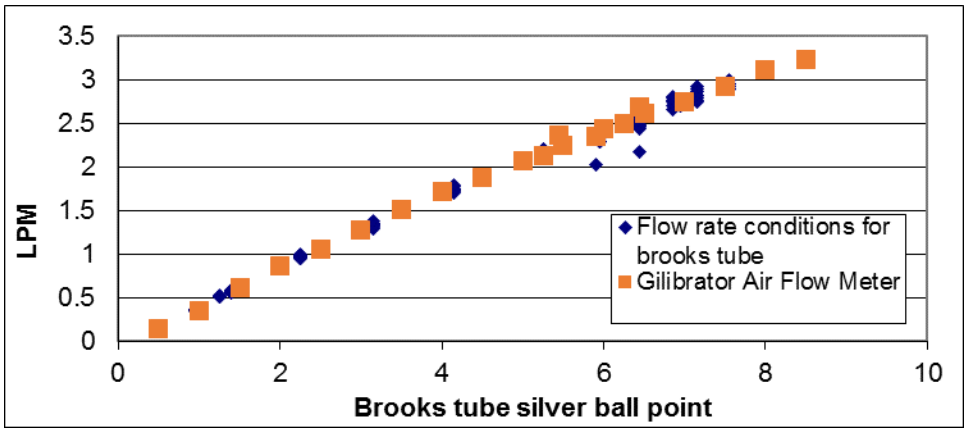

Figure 2.6: Plot comparing the results from Gilibrator Air Flow Meter with those from the previous studies.

- Calibration of the optical particle counter:

In order to calibrate the optical particle counter, a uniform air stream is passed through two different particle counters and the number of particles were compared. To accomplish this goal, the Condensation Particle Counter (CPC) model 3772 was used. CPC is an

instrument that detects airborne particles as small as 10 nm at an aerosol flow rate of 1.0 LPM, over a concentration range from 0 to 10^4 particles/cm^3.

Three different particle sizes were generated using three different solution concentrations. The solutions were made by dissolving Polystyrene Latex (PSL) granules in distilled water. After making the solutions, an atomizer was used to generate the particles in the air. The solution concentrations were picked such that three different particle sizes of 0.3μm, 0.5μm, and 2μm were obtained in the air stream. In order to check the particle size, a Differential Mobility Analyzer (DMA) was used. The stream containing these particles were sent to both the CPC and optical particle counter. The resulting number of particles from both instruments were closely matching.

- Calibration of the pressure meter:

As it was mentioned in Section 2.7.1, the pressure meter is connected to the test column through two connection points. The upper and lower air pressure were considered and readings of the differential pressure were taken directly from the pressure meter. In order to calibrate this digital pressure meter, a Dwyer Magnehelic differential pressure gauge was used. The results from the two pressure meters for the same filter sample with the same face velocity were obtained. The results indicate that the pressure meter is fully reliable.

- Calibration of the filter holder column:

In this section an attempt was made to check whether leakage occurred through the test rig. To achieve this goal, manufactured filter holders (13 mm Plastic Swinney Filter Holder, part number 4317) purchased from Pall Corporation were used.

Filters were tested with both the test rig in the lab and the Pall filter holder. Pressure drop values were measured for each filter using the two different filter holders at the same face velocity. The results indicate a very good matching between the two setups.

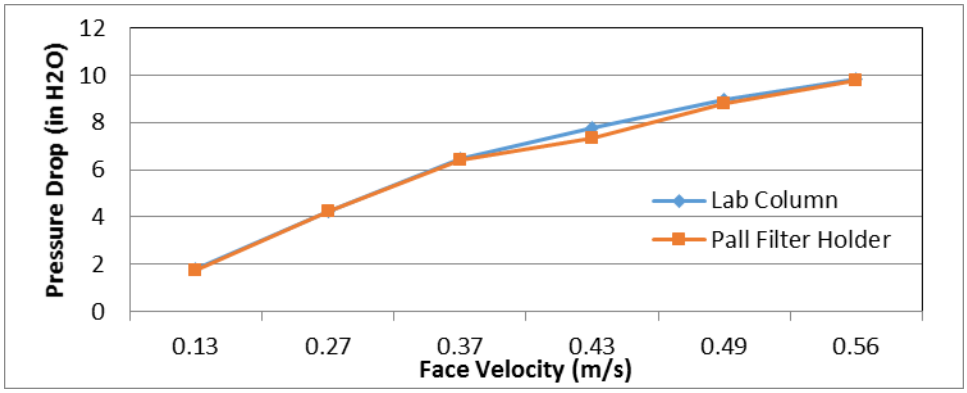

Figure 2.7: Testing pressure meter of a filter with two different filter holders.

The results from the Figure 2.7 indicate that the filter test rig has a very low chance of leakage and the pressure drop values equate to the pressure drop of each filter.

In this experiment the filter efficiency from the same filter in two different holders were also calculated by counting the number of penetrating particles through the filter using the optical particle counter. The plotted data indicates a very good agreement between the values coming from two different filter holders.

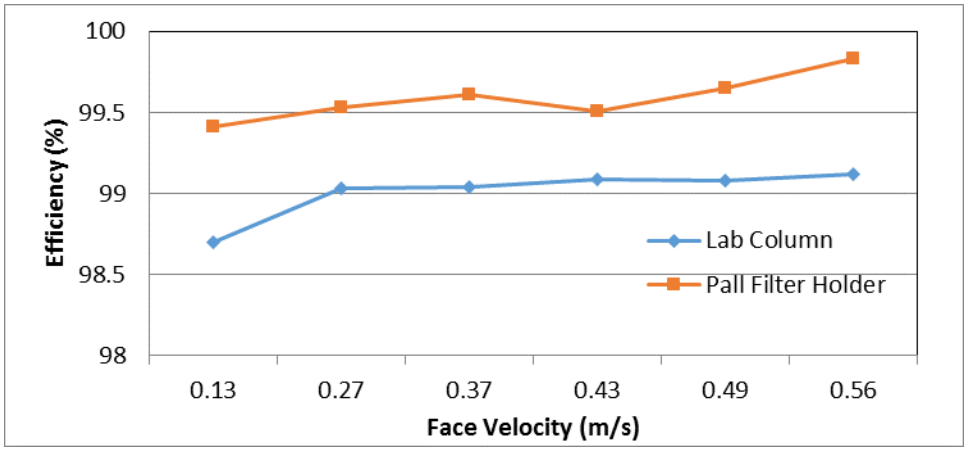

Figure 2.8: Testing the efficiency of a filter with two different filter holders.

From the calibration of the four different sections, the results from the experimental setup are with minimal experimental error.

2.8 Characterizing Filter Morphologies:

2.8.1 Scanning Electron Microscopy:

Scanning Electron Microscopy (SEM) is a vital tool for producing high-resolution images of sample surfaces. In this study, the morphology of samples was analyzed using a Ultra-High-Resolution Scanning Electron Microscope (Hitachi SU-70 FE-SEM). The electron beam voltage was at 5 kV with working distance of 15mm. The sample was placed on the stainless steel SEM holder with 15 mm in diameter using conductive tape (usually carbon tape). All samples were sputter coated with platinum metal for 60 to 90 seconds.

2.8.2 Optical Microscopy:

Another method used to obtain fibers is optical microscopy (OP). A Nikon Eclipse optical microscope (model LV100D-U) was used for all optical imaging. Images were taken at different magnifications (maximum of 100X) with top lighting.

2.8.3 Thickness Measurement:

Filter thicknesses were measured using a profilometer, Veeco Dektak 150 Stylus Profilometer. The Dektak is a profilometer for measuring step heights or trench depths on a surface. This is a surface contact measurement technique where a very low force stylus is dragged across a surface. The display range of the data is 200 Å to 20 mm. A video camera with variable magnification allows for manual placement of the stylus and the system is programmed to scan length and speed. In this study, the profile was kept at the hill position with a resolution of ~0.667 μm/sec and measurement range of ~524 μm. The stylus was dragged with the force of 5 mg. The thickness was measured three times for each sample by scanning the surface through its three individual diameters. For each set, the recorded thickness is the average value thickness of 2 samples each measured 3 times.

2.8.4 Weight Measurement:

A high precision analytical balance with the readability of 0.01 mg was used to weigh fabricated samples. The actual mass of the coated polymers was considered. Therefore, the samples were weighed before and after electrospinning and the difference between the two weights was considered as the mass of electrospun layer.

2.9 Analysis method:

For each set of samples, at least six samples were made and tested for pressure drop and filtration efficiency. Pressure drop values were recoded from the pressure meter readings and converted to Pascals. The ratio between particle counts with filter and without filter is defined as the particle penetration through a filter. The filtration efficiency was obtained by calculating particle penetration through the filter which was 1- penetration. Particle counts

were taken from the optical particle counter using the same flow rates for upstream and downstream. FOM was calculated by using those values and equation 1.41. Other specifications, such as fiber diameter, filter uniformity, and fiber spacing were investigated by SEM images. All SEM images were analyzed using ImageJ software.

All the readings and calculations were recorded and the corresponding plots were made using Microsoft Excel 2013. The standard deviation value for each case was calculated using "student-t distribution" at a minimum 90% confidence interval [91].

CHAPTER 3 Electrospun Fiber Mats

3.1 Introduction:

Fibers of Polystyrene and Nylon 4,6 were electrospun at polymer weight concentrations from 18% to 30% and 10% to 18% solutions, respectively. Different polymer concentrations will form fibers with different diameters. The fibers were collected on a nylon substrate by controlling the deposition mode, in order to achieve different filter structures. The resulting fibers were investigated based on their physical characteristics such as fiber diameter, formation of beads, and formation of nanowebs. The resulting fibers, with beads eliminated and controlling nanoweb formation, were deposited onto a nylon substrate with random and aligned configurations. For each deposition, certain conditions were considered in order to obtain a uniform fiber mat. Resulting fiber mats were tested based on their uniformity. Fiber deposition was much more controllable in micrometer fibers than nanometer fibers. In this chapter, the results from a study on the uniformity of fiber mats produced with nanometer fibers are presented. The following sections are focused on characteristics of the fibers and the resulting fiber mats used in this study.

3.2 Fiber Morphology:

3.2.1 Random and aligned fibers:

Different electrospinning methods yielded different fiber orientations and distributions. Random and aligned orientations of fiber were used in this study. The electrospinning method to produce aligned and random fibers both for micrometer and nanometer fiber diameters were explained in chapter 2. Random fiber mats were made by random configuration of fibers using a stationary collector. Whereas, orthogonal fiber mats were made by arranging the aligned fiber layers perpendicular to one another with a rotational collector. SEM images of random and aligned Polystyrene fibers and Nylon 4,6 fibers are shown in the Figure 3.1 and 3.2, respectively.

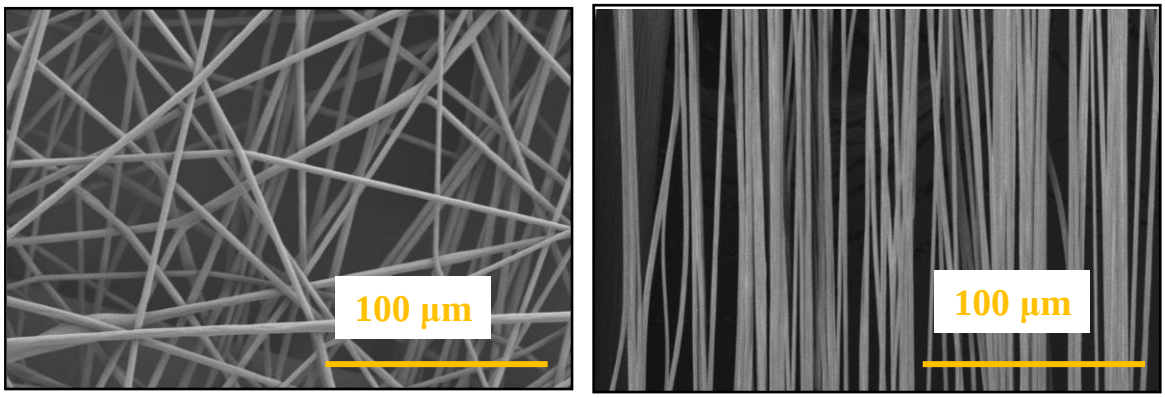

Figure 3.1: SEM images, a) random 30% Polystyrene fibers and b) aligned 30% Polystyrene fibers.

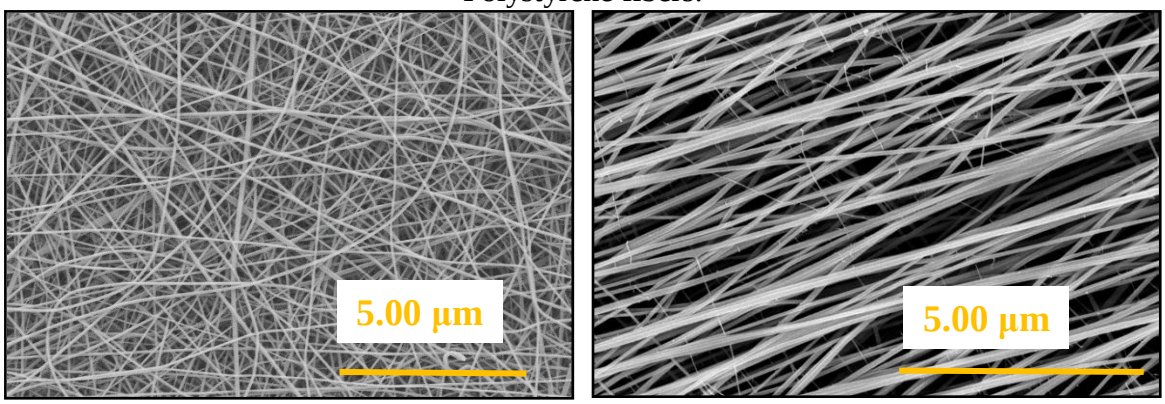

Figure 3.2: SEM images, a) random 15% Nylon 4,6 fibers and b) aligned 15% Nylon 4,6 fibers.

3.2.2 Fiber diameter:

The fiber diameters were measured from multiple SEM images, analyzing 20 fibers per experiment. To obtain a valid diameter of each fiber, two diameter measurements were taken on different ends of the fiber. The mean diameters and standard deviations were calculated.

With micrometer fibers, controlling the electrospinning parameters and setup as well as the polymer solution concentrations will result in controlling the fiber diameter. Figure 3.3 and 3.4 give a distribution of aligned and random fiber diameters for different Polystyrene solution concentrations as well as the corresponding SEM images.

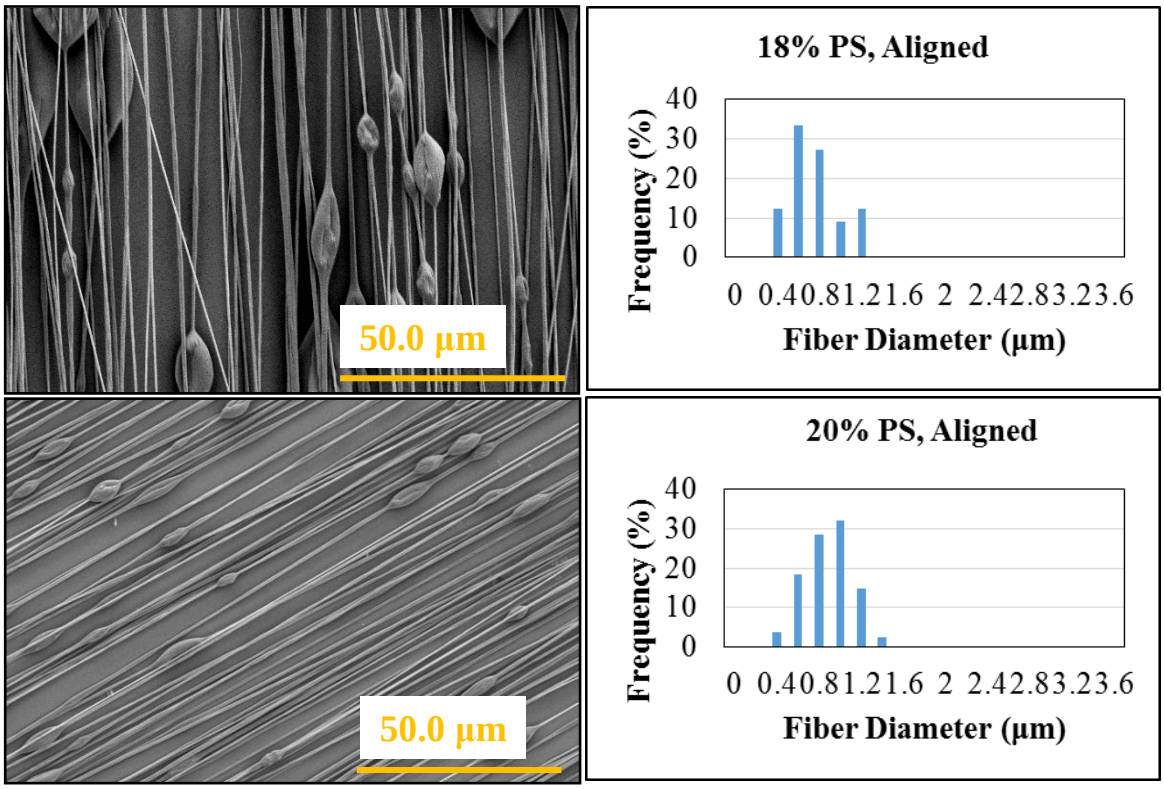

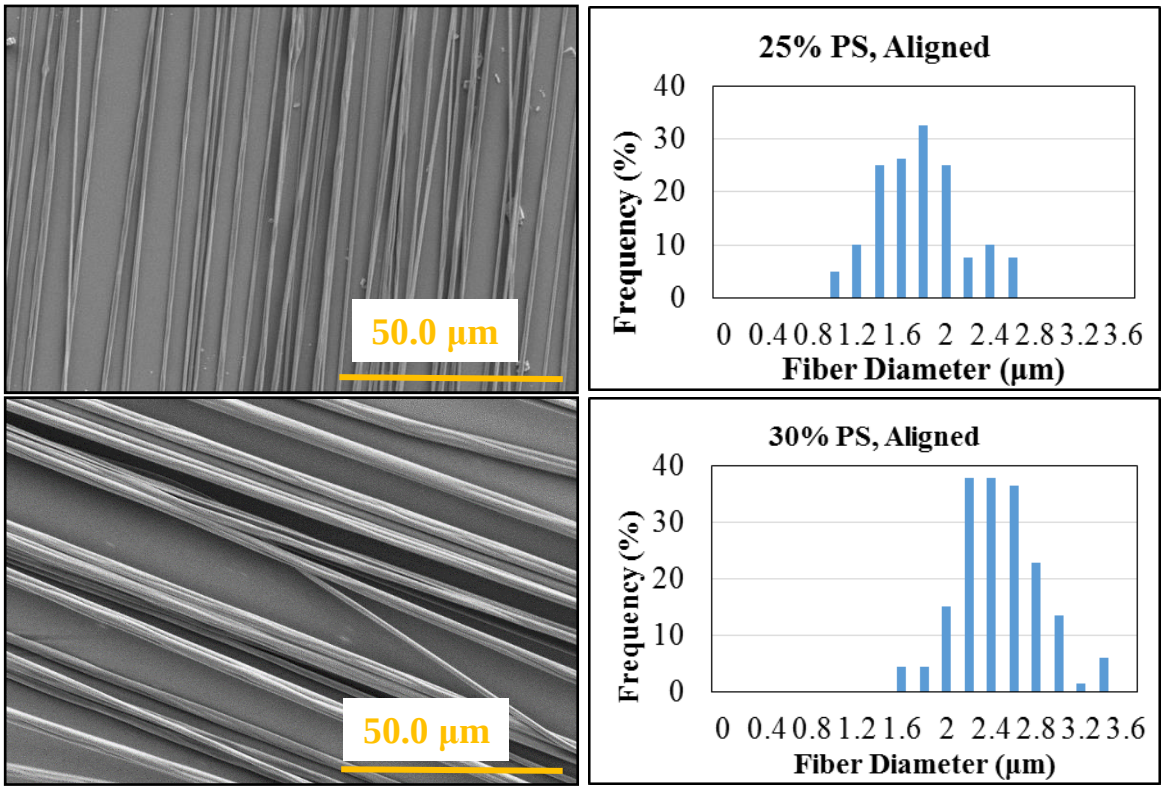

Figure 3.3: SEM images and histograms representing the aligned Polystyrene fiber diameter distribution.

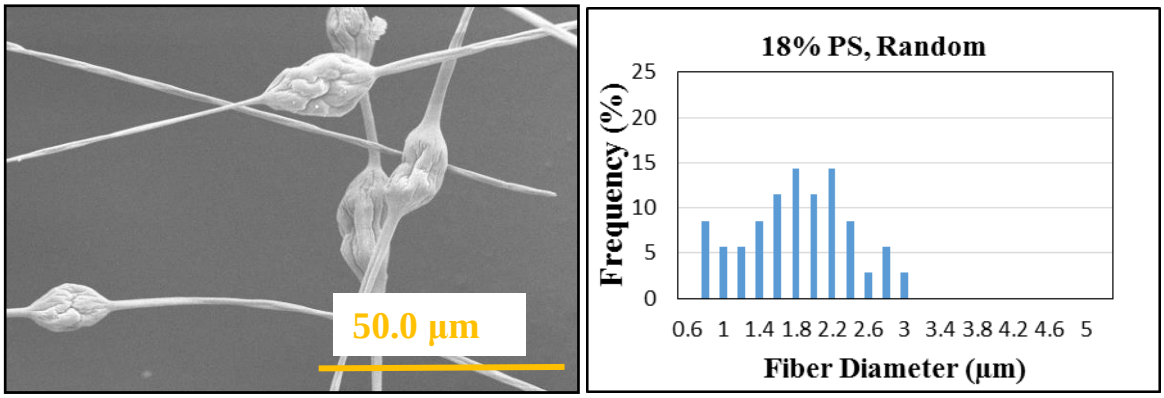

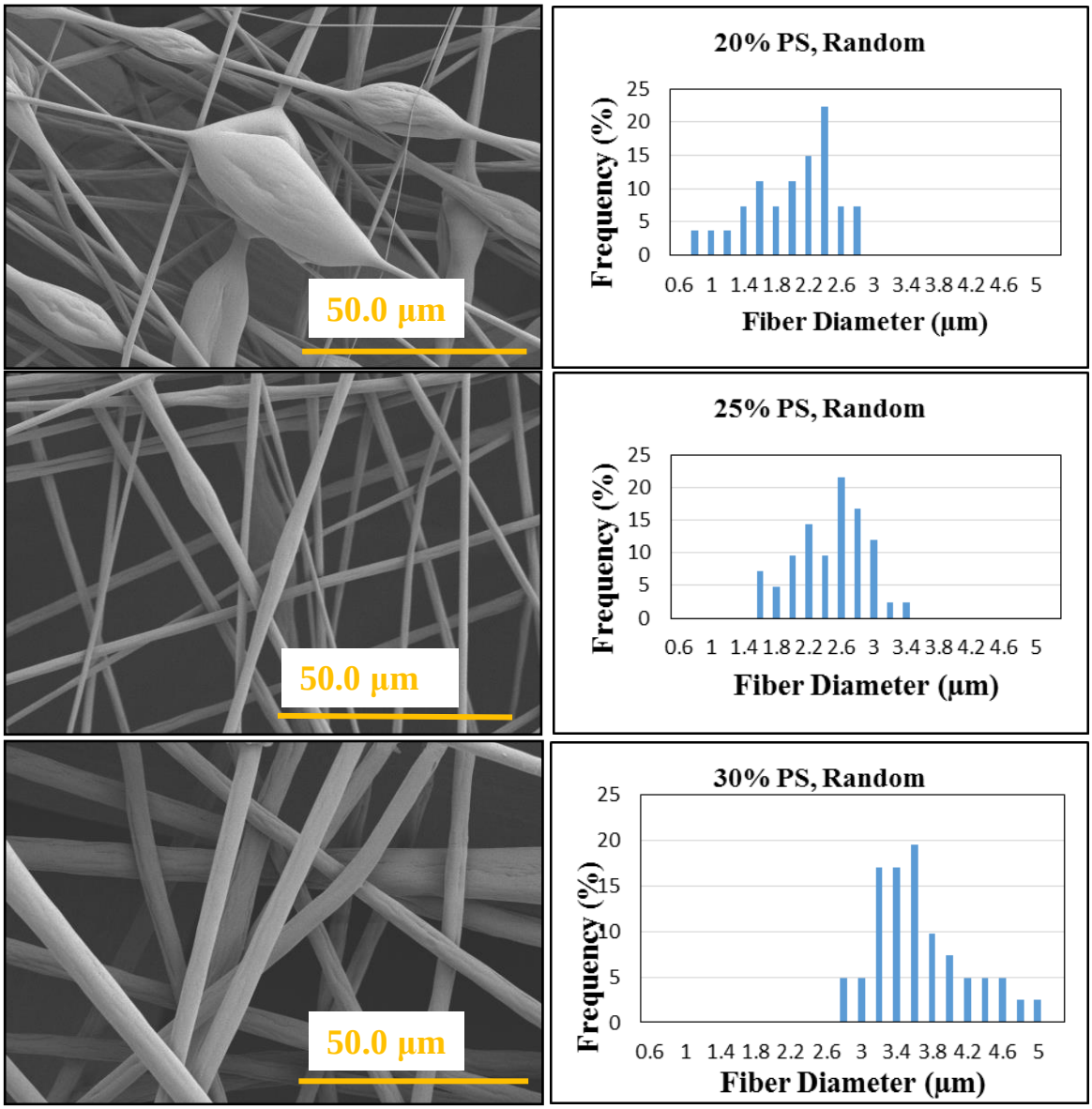

Figure 3.4: SEM images and histograms representing the random Polystyrene fiber diameter distribution.

Two methods resulted in fiber diameter decreases: lower solution concentrations and the rotational collection method. Fiber elongation as a result of the rotational collection method produced thinner fibers. Therefore, the average fiber diameter of Polystyrene, with the same polymer concentrations, is higher for random fibers due to the electrospinning

procedure. Table 3.1 lists all of the Polystyrene concentrations with corresponding fiber diameters.

Table 3.1: Table showing results for changes in fiber diameter due to the polymer concentration and fiber orientation.

Polystyrene Concentration (%)	Fiber Diameter (μm)	
	Random Fiber	Aligned Fiber
18%	1.8±0.6	0.7±0.2
20%	2.0±0.5	0.9±0.2
25%	2.5±0.4	1.8±0.4
30%	3.7±0.5	2.5±0.4

Nanometer fibers made of Nylon 4,6 concentrations and their corresponding electrospun fiber diameters are listed in Table 3.2, using a stationary collector for producing aligned fibers and a rotational collector for producing random fibers. Figure 3.5 and 3.6 give a distribution of aligned and random fiber diameters for different Nylon 4,6 solution concentrations as well as their corresponding SEM images.

Table 3.2: Table showing results for changes in fiber diameter due to the polymer concentration and fiber orientation.

Nylon 4,6 Concentration (%)	Fiber Diameter (nm)	
	Random Fiber	Aligned Fiber
10%	100±10	75.5±22.6
15%	—	110±15.9
18%	—	117±18.5
20%	190±10	227±52.2

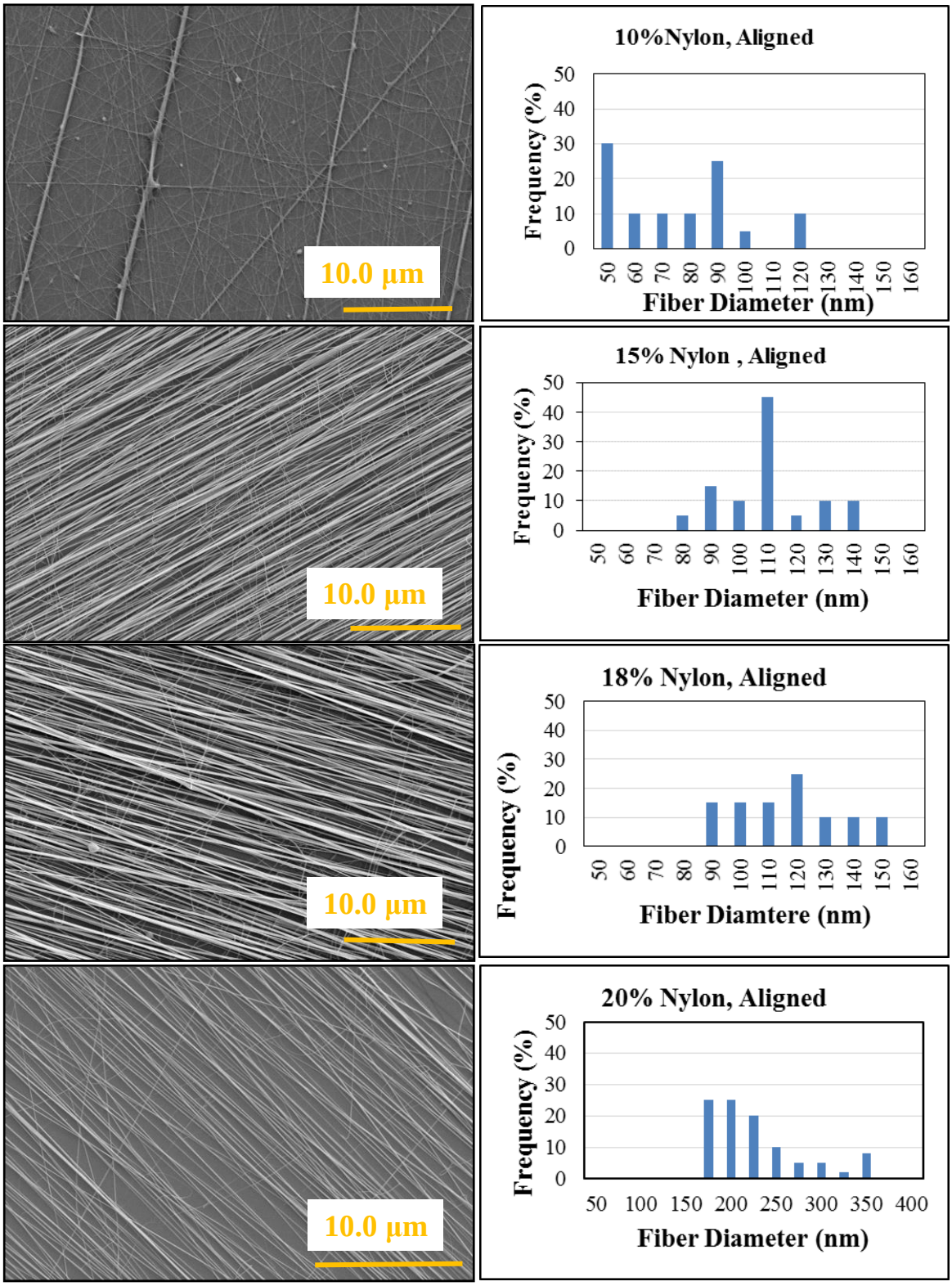
10.0 µm
10%Nylon, Aligned
Frequency (%)
Fiber Diameter (nm)
10.0 µm
15% Nylon , Aligned
Frequency (%)
Fiber Diameter (nm)
10.0 µm
18% Nylon, Aligned
Frequency (%)
Fiber Diamtere (nm)
10.0 µm
20% Nylon, Aligned
Frequency (%)
Fiber Diameter (nm)

Figure 3.5: SEM images and histograms representing the aligned Nylon 4,6 fiber diameter distribution.

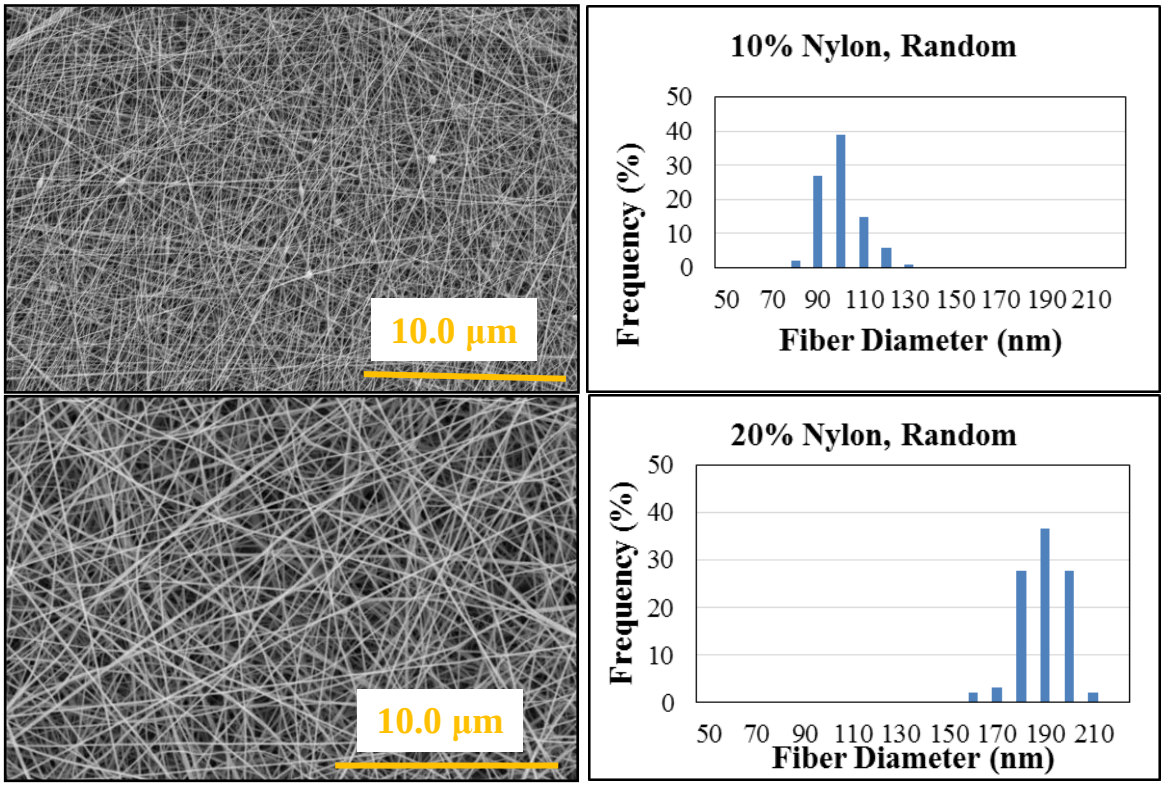

Figure 3.6: SEM images and histograms representing the random Nylon 4,6 fiber diameter distribution.

3.2.3 Fiber beads:

As is shown in the SEM images of Polystyrene and Nylon 4,6, some electrospun fibers contained defects in the form of beads. The formation of beads is based on polymer solution parameters such as concentrations, conductivity, viscosity, and surface tension. Increasing solution concentrations results in an increase of solution viscosity due to the higher polymer chains entanglement. It has been described in detail that increasing the viscosity of electrospun solutions will result in thick fibers with no beads [92]. Also, increasing the electrical conductivity of the electrospinning solutions will reduce the

formation of beads and favor the formation of smooth fibers. High surface tension of the solutions also can increase the formation of beads by creating enough pressure on the surface of the polymer jet. The formation of beads and the parameters affecting it have been defined in detail in previous studies [30][85][93].

In this study, the formation of beads was eliminated by increasing the electrical conductivity of solutions, as well as increasing the solution concentrations. In order to make Polystyrene solutions, a 7:3 ratio of Toluene to THF was used as the solvent due to the solubility parameters and dielectric constants which are described in chapter 2. For this study, the appropriate solution concentrations, 25% and 30% Polystyrene by weight, were selected to result in smooth electrospun fibers.

For Nylon 4, 6, the beads formed on random fibers made with a 10% solution concentration. Figure 3.7 shows changes is solution surface tension and electrical conductivity with different Nylon 4,6 content. The electrical conductivity for 10% Nylon 4,6 is lower compared to the higher solution concentrations. Therefore, the electrical conductivity of the 10% Nylon 4,6 solution was increased by adding 0.2 wt. % Pyridine. Figure 3.8 a and b, show the SEM images of electrospun fibers using 10% Nylon 4,6 with and without adding Pyridine, respectively.

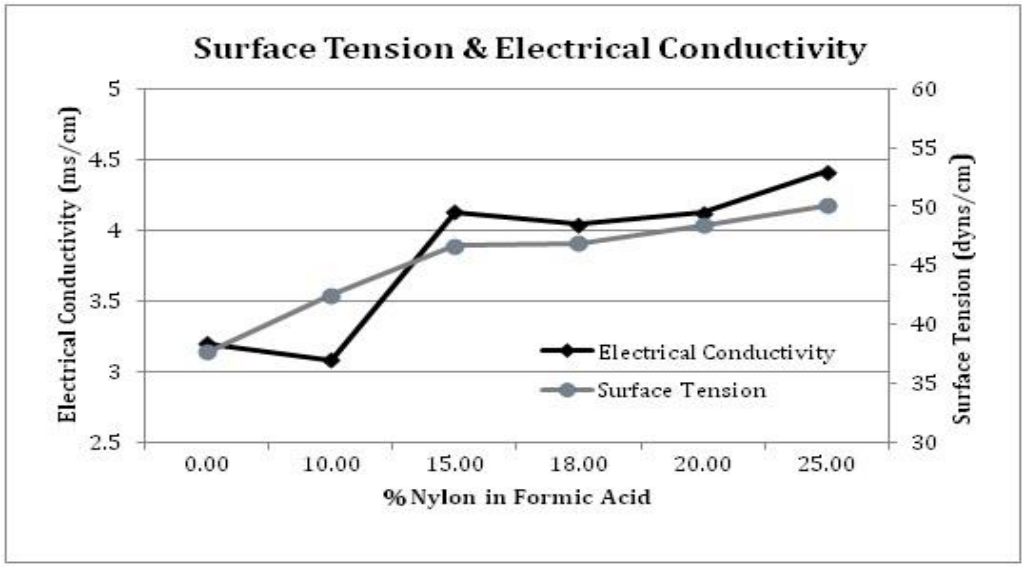

Figure 3.7: Changes in solution surface tension and electrical conductivity with different Nylon 4,6 content.

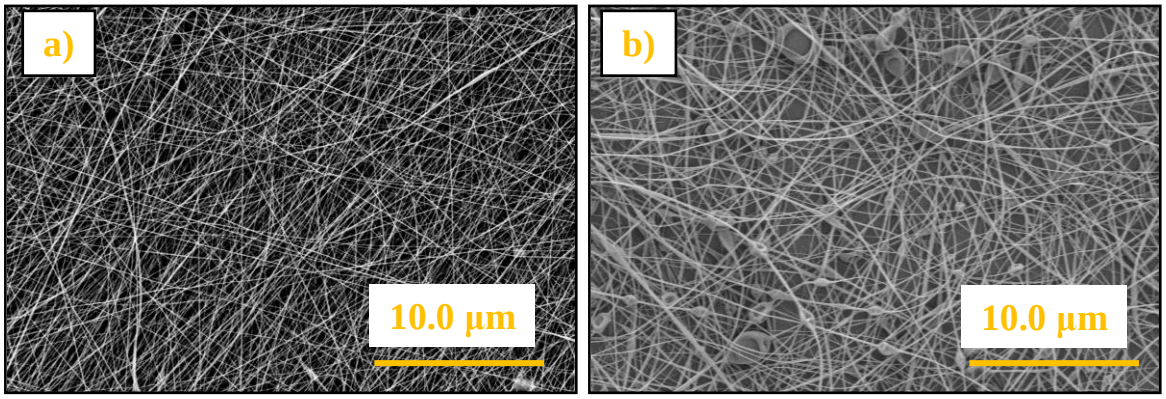

Figure 3.8: SEM images of electrospun fibers using 10% Nylon 4,6 a) with and b) without adding Pyridine.

3.2.4 Nanoweb formation:

It was observed that nanometer electrospun fibers appeared to branch from primary deposited fibers, which results in forming the nanoweb areas. These nanowebs will affect the filtration performance as a secondary effect to the particle capturing. Researchers have shown that the formation of nanowebs is due to solvent degradation, adding TiO_2

nanoparticles, and increasing the applied voltage, and also defined nanowebs as nonwoven webs consisting of nanoscale secondary fibers formed between the larger primary fibers in an electrospun mat [94-96]. For example, Nam et al. showed that the diameter of electrospun Nylon 6 fibers decreases with the standing time of solution which results in the formation of nanoweb areas.

In this study, random fibers collected on a high-speed rotating cylinder (rotation method) showed limited secondary fiber formation, while aligned fibers collected on a stationary collector between two conducting strips (gap method) showed extensive secondary fiber formation. It was observed not only the solution degradation will affect the nanowebs formation but also the spinning method will affect it. In this section, the influence of different electrospinning parameters on the formation of secondary nanofiber webs, such as distance between the needle and drum, solution concentration, solution viscosity, and solution degradation, are investigated.

Figure 3.9 a and b represent the SEM images of mats made with rotation and gap methods, respectively. The formation of nanowebs is more evident in the gap method compare to the rotation method. This can be explained by the speed of solvent evaporation. In the rotation method, the primary fibers dry quickly limiting secondary fiber formation, whereas the primary fibers still contain solvent when deposited using the gap method allowing for the formation of secondary nanofiber webs.

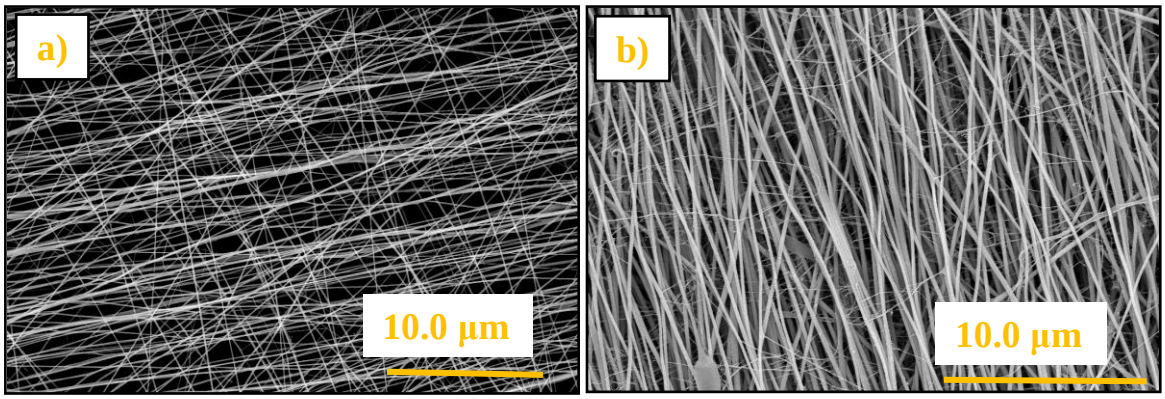

Figure 3.9: SEM images of 15 Wt.% Nylon 4,6 a) high speed rotation method without formation of nanowebs b) gap method with formation of nanowebs.

According to Figure 3.10 high-resolution SEM image, the diameter of these nanofibers ranges from 15 to 60 nm. Also included is the fiber diameter distribution of the nanowebs.

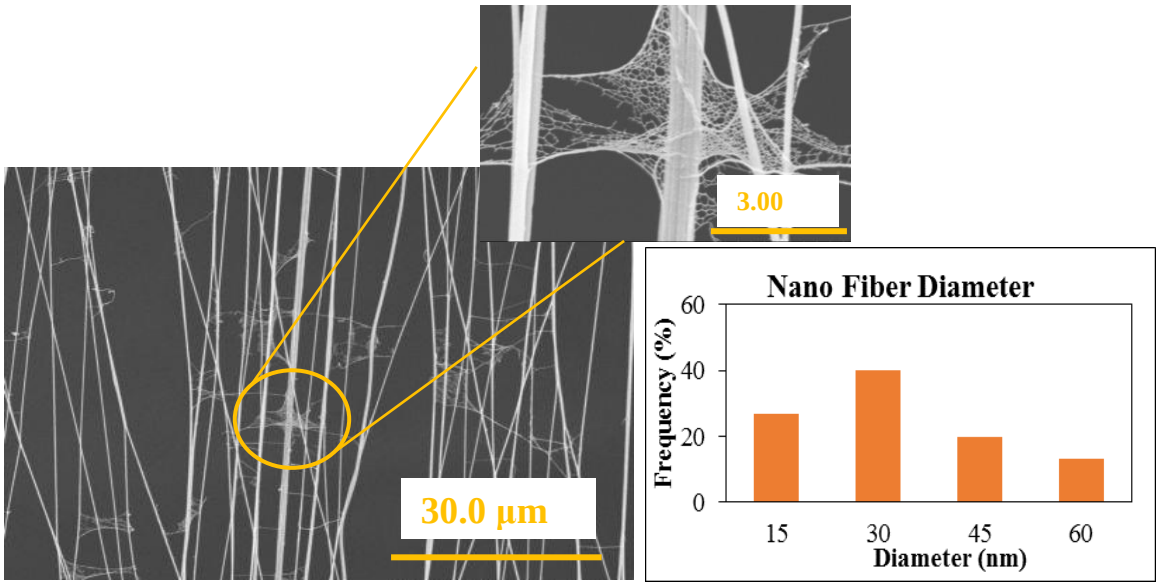

Figure 3.10: SEM image of Nylon 4, 6, 20% concentrations (gap method) with 7 cm needle to drum distance and secondary fiber diameter distribution.

Furthermore, the effect of solution concentration and needle-to-drum distance on the formation of nanowebs in the gap method was investigated. SEM images of fibers electrospun from solutions with varied Nylon 4,6 concentrations were studied and

discussed therein. Images suggest that by using 18% and 20% Nylon concentrations, the extent of nanowebs will increase compared to the 15% nylon concentrations as seen in Figures 3.11, a-c. This is caused by the difference in surface tension and fiber inertia between different solutions, which will affect the secondary fiber formation. Surface tension and electrical conductivity of solutions are shown in the previous section (Figure 3.7).

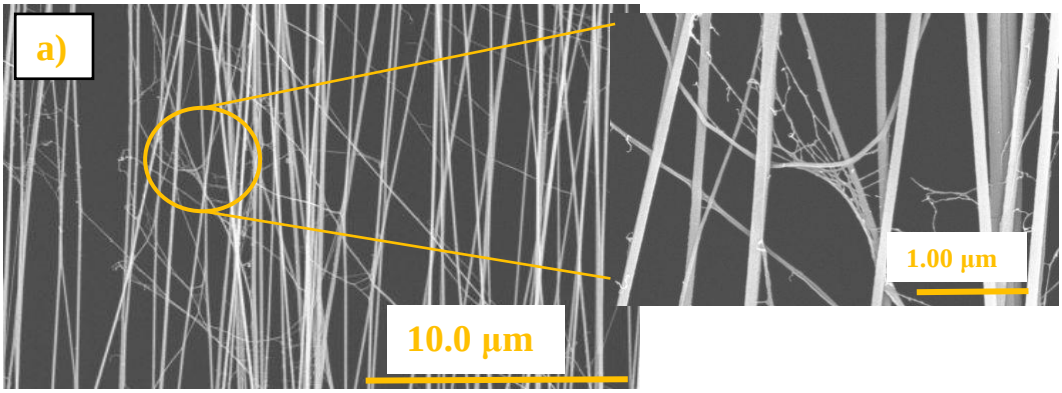

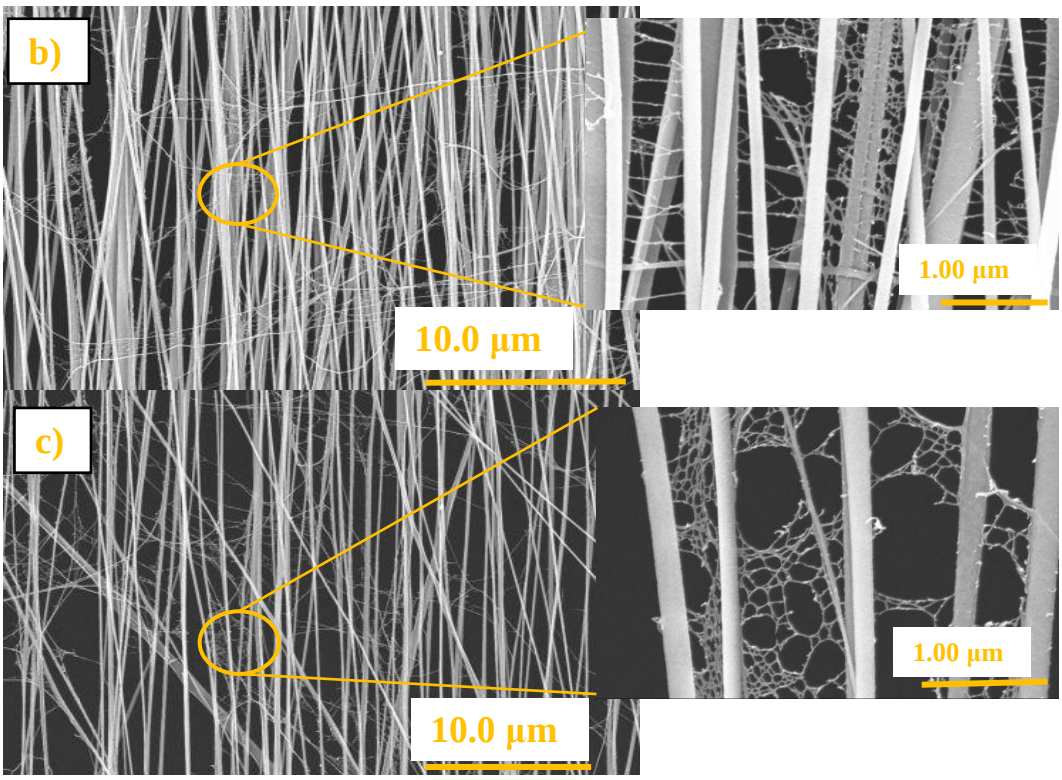

Figure 3.11: SEM images of a) 15% Wt., b) 18% Wt., c) 20% Wt. Nylon 4,6.

For the study of needle-to-drum distance, the distance from needle to drum was varied at 4 cm, 7 cm, and 10 cm, while the other parameters such as concentrations, voltage, and width of the gap were kept constant. SEM images, shown in Figure 3.12, suggest that variations in distance between the needle tip and collector have an effect on the formation of nanowebs. It was observed that fibers collected further away seemed to generate fewer nanowebs than those collected from a shorter distance with the same deposition time. Longer distance also results in less deposition of fibers. These fibers have longer travel time before being collected at the drum and are therefore drier than those collected from a shorter distance.

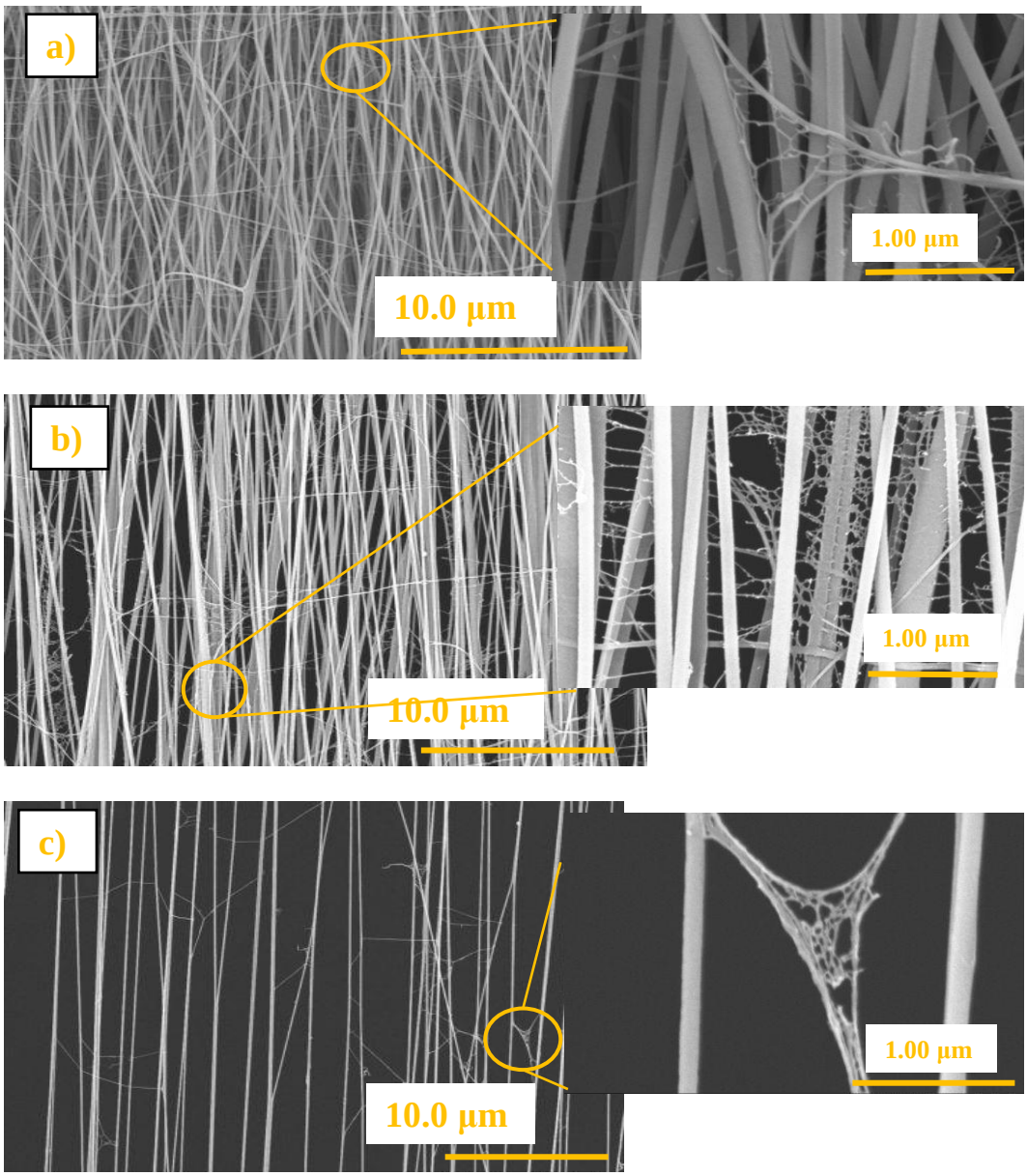

Figure 3.12: SEM images of 18% Wt. Nylon 4,6 fibers show the effect of needle to drum distance on the formation of nanoweb a) 4 cm, b) 7 cm, c) 10cm.

The above study was done using a solution that was 1 up to 14 days old. It was also worth studying the effect of solution degradation on the formation of nanowebs. Following are the results of the formation of nanowebs with different aged solutions using the electrospinning gap method. The fiber mats were made with solutions aged from 1 to 50

days. The mats were tested based on their pressure drops. The results are shown in Figure 3.13. It is observed that the pressure drop is divided into three portions based on solution degradation, 1 up to 20 days old with high pressure drop, 20 up to 33 days old with low pressure drop, and 33 days and older with high pressure drop. The SEM images in Figure 3.14 also indicate that the amount of formed nanowebs changed based on the age of solutions. Figure 3.15 shows the viscosity of the solutions based on their age. The solution viscosity decreases as the solutions degrade. As the solution viscosity decreases, the polymer molecular weight also decreases, which results in more secondary fiber formation. SEM images indicate that mats made of a solution 49 days old has a lot of nanowebs with unclear alignment, whereas mats made of a solution 4 days old has fewer nanowebs with the alignment of primary fibers still evident. Therefore, the pressure drops for mats in these two regions are high. The pressure drop goes down for mats made from solutions 20 up to 33 days old. This can be due to the loss of their uniformity, which can be seen in SEM images, Figure 3.16.

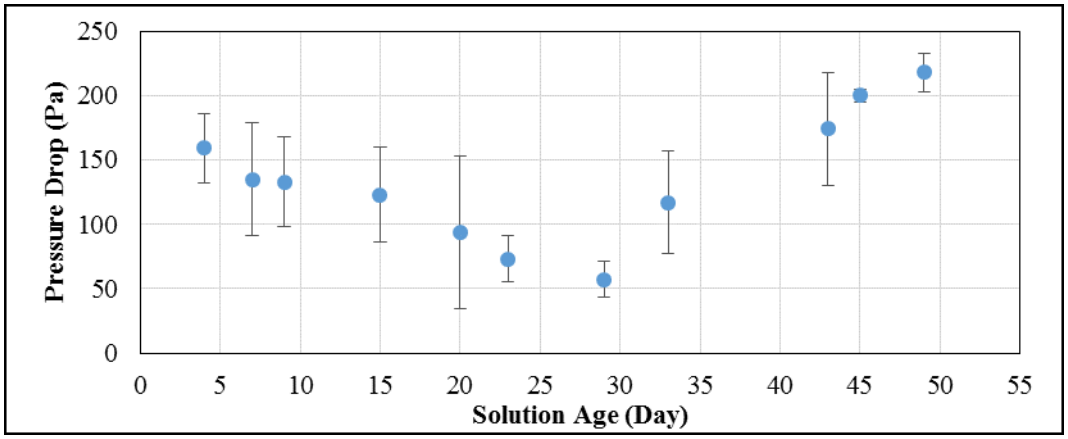

Figure 3.13: Pressure drop based on the solution age for fiber mats made of electrospun aligned 15% wt. Nylon using gap method.

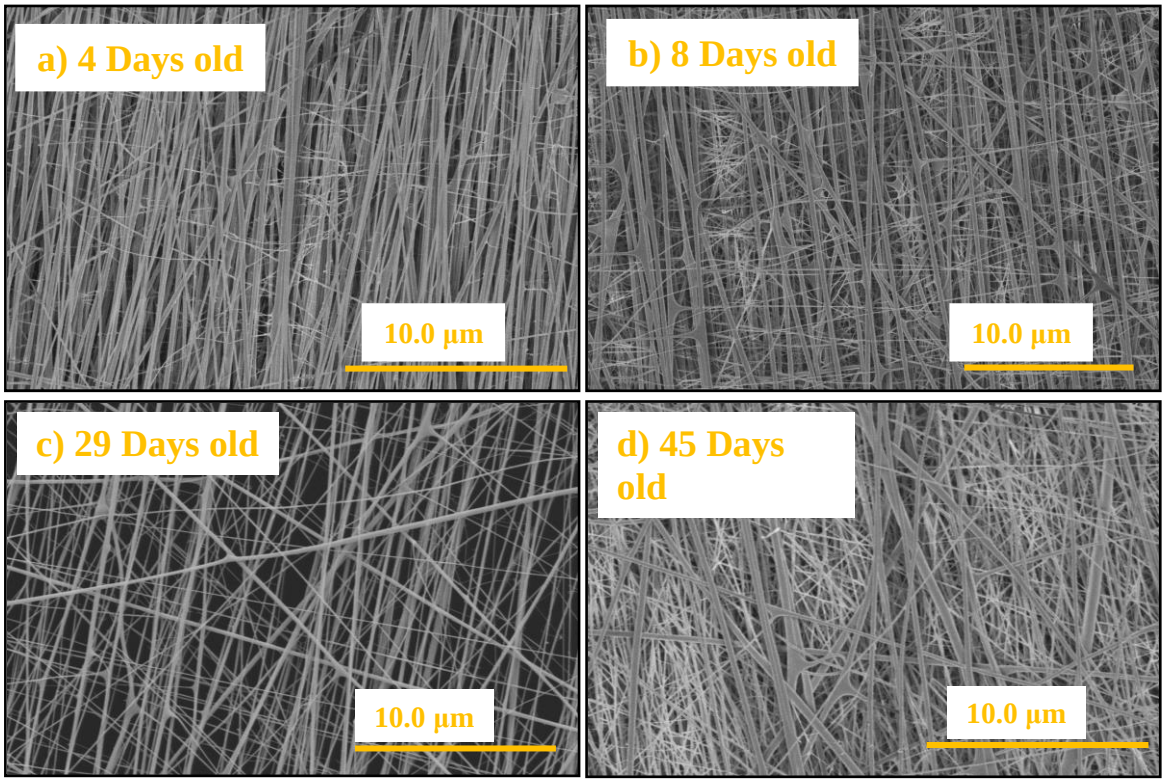

Figure 3.14: SEM images of 15 wt. % Nylon 4,6 made of a) 4 days old, b) 8 days old, c) 29 days old, and c) 45 days old solutions.

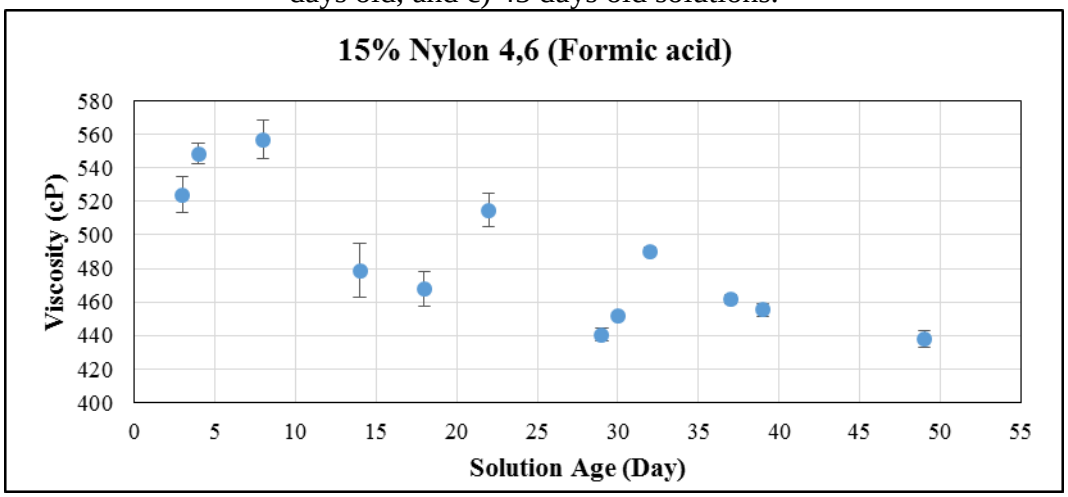

Figure 3.15: Solution viscosity based on the solution age for 15% wt. Nylon 4,6 in Formic acid.

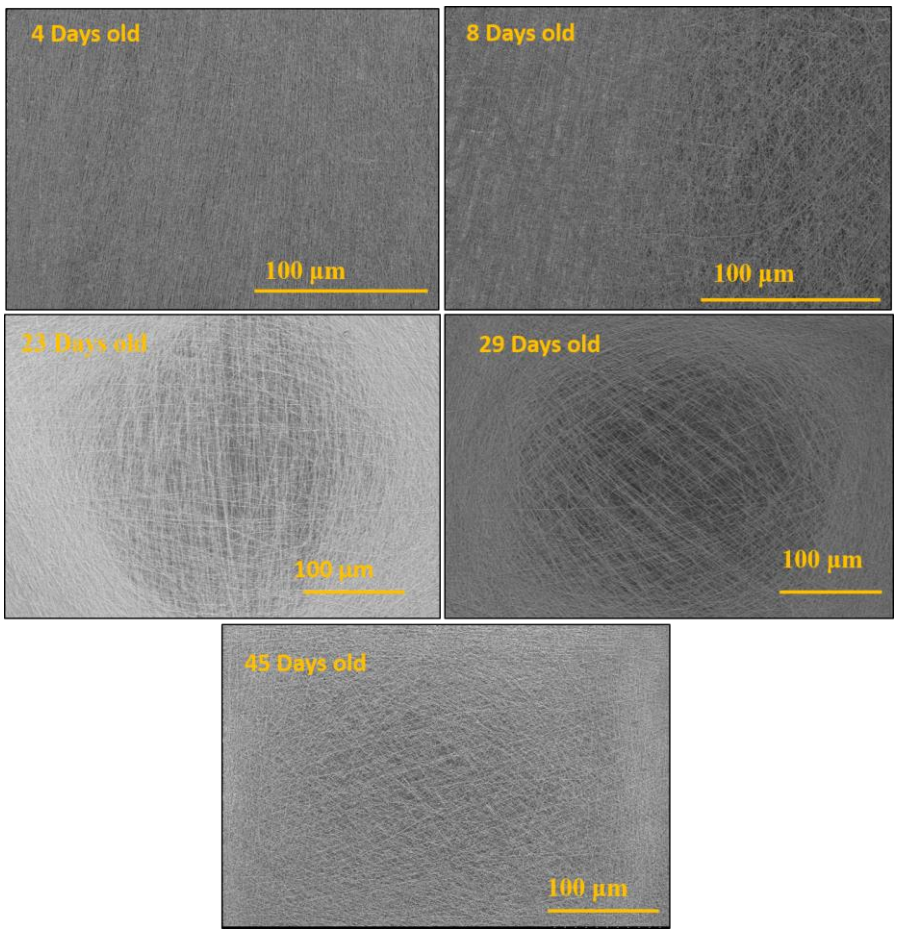

Figure 3.16: Low magnification of SEM images of 15 wt. % Nylon 4,6 made of 4, 8, 23, 29 and 45 days old solutions.

As a summery, in the gap method, the fibers were still wet when deposited on the stationary substrate and still possessed a high charge density. Thus, to get rid of these charges, they produce secondary nanofibers. The production of the nanowebs from wet collected fibers also depends on the viscosity of the solutions, which varies as the solutions degrade. Also, the space between two electrospun fibers acts as a gap to facilitate the formation of secondary nanofibers. Repetitions of forming secondary nanofibers could occur to form nanowebs. However, this explanation is a hypothesis and needs further investigation.

3.3 Fiber Mat Morphology:

The morphology of the micrometer and nanometer fiber mats were investigated using electrospun Polystyrene and Nylon 4,6 fibers, respectively. Different morphologies were considered in this study, which are described below:

- unimodal random fiber mats referred to randomly deposited fibers with only one fiber diameter distribution,
- bimodal random fiber mats referred to randomly deposited fibers with a binary blend of fine and coarse fibers,
- unimodal orthogonal fiber mats referred to orthogonally layered aligned fibers with only one fiber diameter distribution, and
- bimodal orthogonal fiber mats referred to orthogonally layered aligned fibers with a binary blend of fine and coarse fibers.

Figure 3.17 shows an SEM picture of unimodal and bimodal forms of random and orthogonal fibers. The filtration performance of these morphologies was tested based on their basis weight, ratio of coarse to fine fibers, solid volume fraction, and fiber spacing. Different approaches were used to reach the highest possible amount of uniformity of mats.

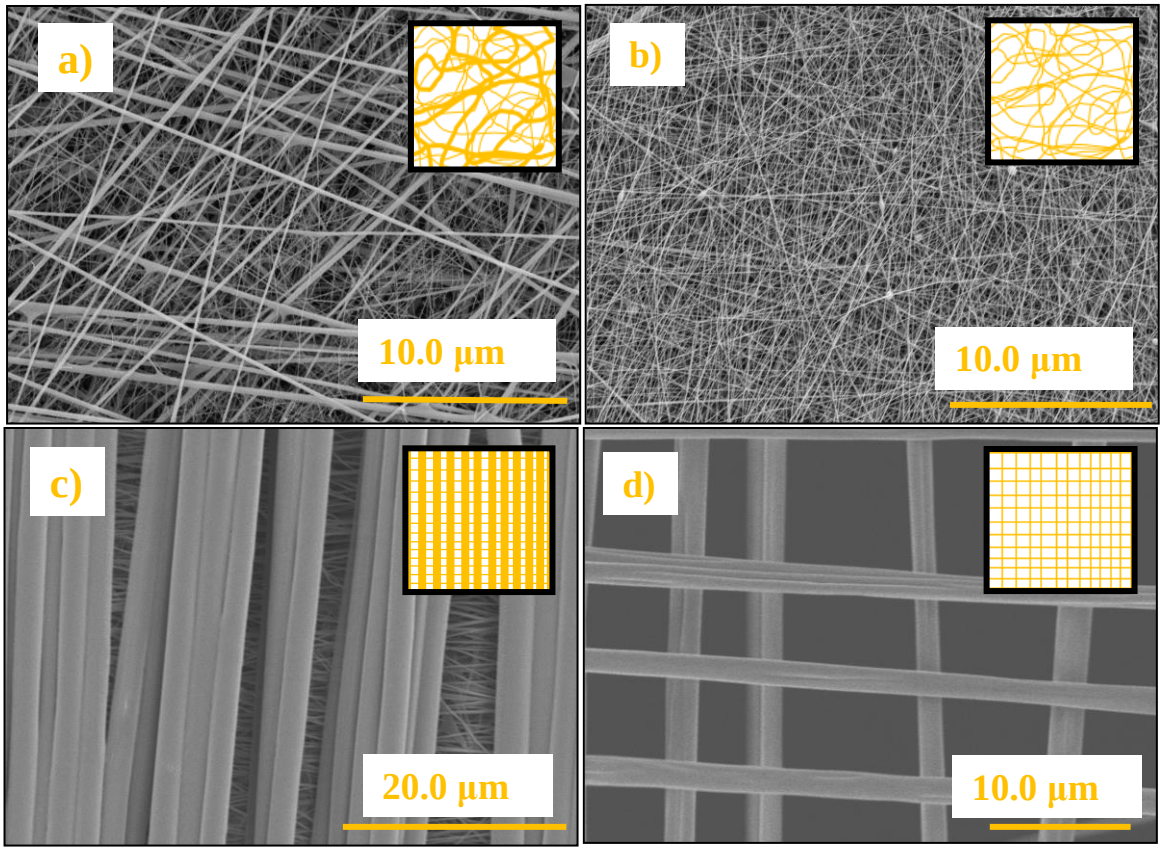

Figure 3.17: SEM pictures of a) bimodal random fibers, b) unimodal random fibers, c) bimodal aligned orthogonal fibers, d) unimodal aligned orthogonal fibers.

3.3.1 Uniformity of fiber mats:

In fibrous filtration, it is important to deposit the fibers uniformly across the surface of the substrate. However, using electrospinning to produce fibers usually resulted in an uneven distribution of fibers. Therefore, some extra efforts will be needed to distribute the fibers uniformly across the substrate. The following are considerations that were used in this study to produce uniform micrometer and nanometer fiber mats.

3.3.1.1 Micrometer fiber mats:

Mats were fabricated using micrometer and nanometer fibers. In micrometer fiber mats, due to the high inertia of micrometer fibers, fiber deposition on the collector is easier to

control than nanometer fibers. Therefore, the effort that achieved the highest degree of uniformity while also controlling the fiber spacing was a collector that used back and forth motion during the electrospinning. The speed of the back and forth motion was selected based on the desired fiber spacing.

3.3.1.2 Nanometer fiber mats:

For fiber mats made of nanometer fibers, controlling uniformity is not as simple as with micrometer fibers. The deposition of nanometer fibers on the substrate, attached to the grounded drum, did not produce a uniform layer even by using back and forth motion for the collector or extended deposition times. This uneven distribution of nanometer fiber mats can be attributed to the effect of charge dissipation of deposited fibers. It is hypothesized that fibers collected on the open regions of the substrate retains their charge and the fibers which are collected on the physical threads lose charge. Although the substrate is a polymer, it cannot act as a perfect insulator and there is a chance for charges to be neutralized. Therefore, there are more fibers deposited on the threads than on the open region of the substrate, which results in an electrostatic imbalance between the open and solid area of the substrates.

To eliminate this effect, ways to neutralize the charges built up on the fiber mats are needed. For the rotational collector, the substrate was electrically neutralized by the corona, which is a high voltage placed on a sharp point. The type of corona used in this study has been explained in previous studies [82]. For the stationary collector, using two

conductive electrodes placed on an insulated substrate as a collector (void gap) helped to neutralize the substrate and resulted in increased fiber collection.

Two experiments were performed to study the relationship between different electrospinning techniques and resultant morphology. The first experiment indicates that between two series of nanometer fiber mats, both collected on a rotational collector, the one with ion deposition will have more uniform coverage than the one without. The second experiment was to create nanofiber mats, one on a conductive stationary substrate and one between two conductive points. In order to better understand the uniformity of mats made of nanometer fibers, the mats were evaluated based on the filtration performance and their SEM pictures. All the mats were made using 15% Wt. Nylon 4,6 as the electrospinning solution.

- Corona assisted deposition and corresponding filter performance:

Table 3.3 summarizes the electrospinning methods and their corresponding filter performance. The first set shows filters that were made without ion deposition (without corona, Figure 2.3A) while the second set comprises filters electrospun with neutralization by negative voltage (with corona, Figure 2.3 B).

Table 3.3: comparing the filter performance of electrospun fiber mats with the rotational collector, with and without corona.

Filter Mats	**A) Without Corona**		**B) With Corona**	
Basis Weight (g/m^2)	1.3	2.4	1.3	2.4
Pressure Drop at 5 cm/s (Pa)	72	162.6	104	211.5
Filtration Efficiency (%)	65.7	85.7	91.0	96.4
Figure of Merit (FOM)	0.015	0.012	0.023	0.016

Time of Electrospinning (min)	40	60	5	10

For each set, data was obtained for two different filter masses. The fibers collected on the substrate are positively charged. When a small layer of fibers is deposited on the substrate, the rate of charge dissipation decreases, hence further deposition slows down and the coverage is no longer uniform. Using negative ion deposition helps to neutralize this electrostatic positive charge on the substrate [83][97]. Figure 3.18 shows the SEM picture of the mats with and without ion deposition. The efficiency and pressure drop of these two test samples were measured and displayed in Figure 3.19.

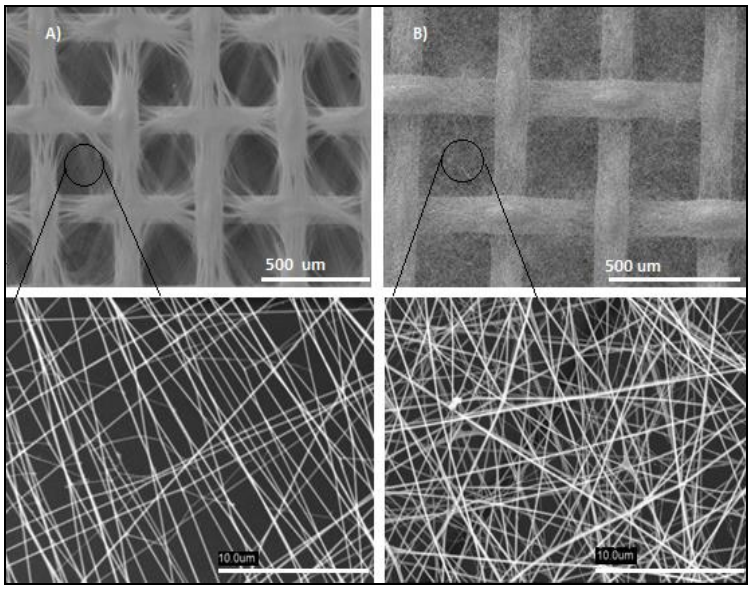

Figure 3.18: SEM images of filter coverage with same basis mass A) without and B) with corona (using rotational collector).

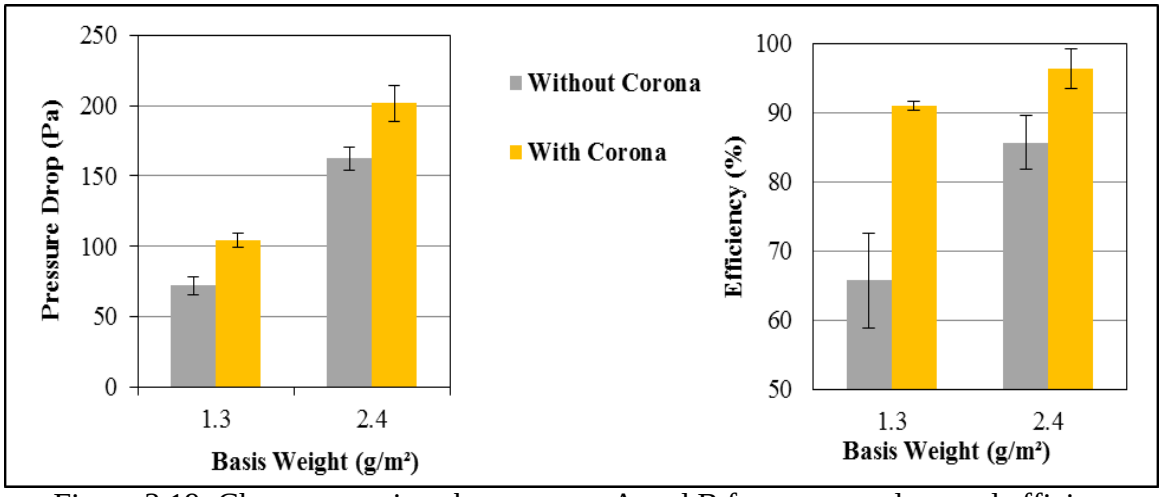

Figure 3.19: Chart comparison between set A and B for pressure drop and efficiency.

As is shown in figure 3.19, non-uniformity still occurs even by increasing the electrospinning time. The test samples with negative ion deposition provide relatively uniform coverage for the filter mat, such that fibers cover even the holes on the substrate, whereas those without ion deposition have very poor coverage on the holes (mesh spaces). Comparing samples with dissimilar masses proved that mass does not play a major role in influencing uniformity. However, deposition of ions using a corona was found to have significant influence. In addition, uniformly distributed fibers had higher efficiency. In spite of approximate values for the FOM, uniform mats still had higher efficiency.

By considering filtration parameters, such as particle size and face velocity, and filter description, including the type of polymer, basis weight and fiber diameter, the pressure drop values are comparable with previous studies for both stationary and rotating collectors using traditional electrospinning methods [80, 98, 99].

- Void Gap collector and corresponding filter performance:

In this part we compare the coverage uniformity and filter performance of mats electrospun with a stationary drum and those produced from a setup with a void gap. It was show that the gap method of collecting nanometer fibers has a very high collection efficiency relative to the stationary conductive collector. Figure 3.20 shows the SEM picture of mats with and without the gap method. Collection efficiency and pressure drop are displayed in Figure 3.21.

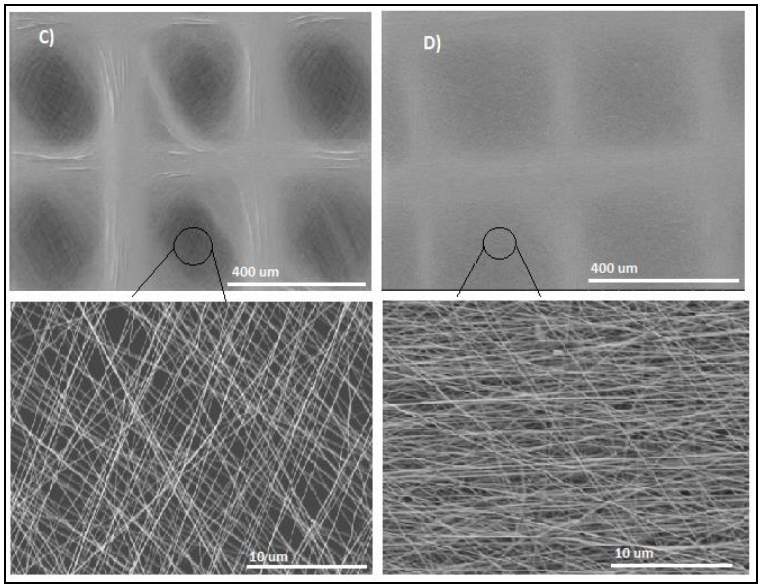

Figure 3.20: SEM images of filter coverage with same basis mass C) without and D) with Gap (using stationary collector).

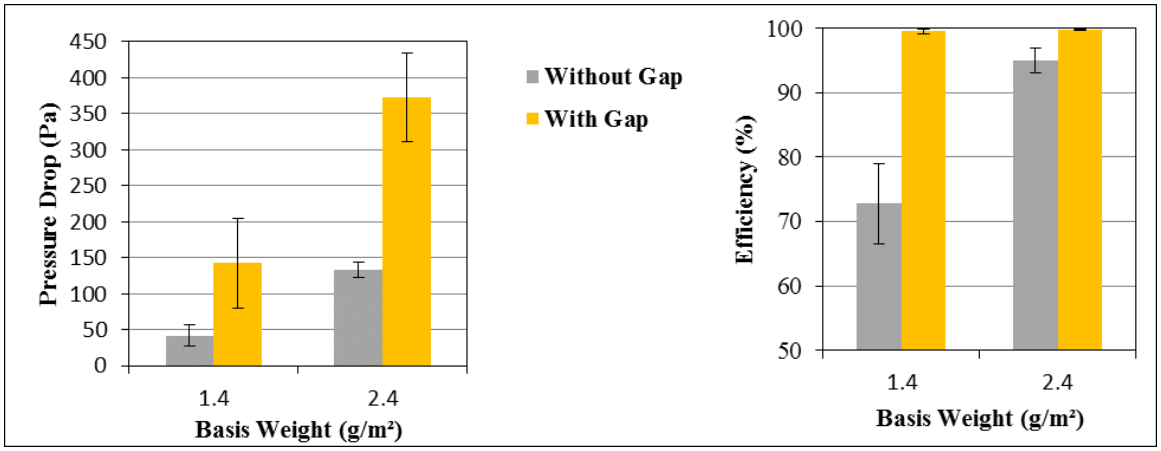

Figure 3.21: Chart comparison between set C and D for pressure drop and efficiency.

The results showed that using the gap method to collect the fibers increases the uniformity of the fiber mats, which will result in better filtration performance. Also, it should be mentioned that increasing the mass in these methods will improve the uniformity. As is shown in Table 3.4, using the gap method is only efficient for the low mass filters, since for the mats with basis mass of 2.4 (g/m^2) the efficiency increases only 5% while the pressure drop increases by 58%. This will cause around a 20% decrease in FOM. Therefore, using the gap method is only efficient for the low mass filters.

Table 3.4: comparing the filter performance of electrospun fiber mats with the stationary collector, with and without Gap method.

Filter Mats	**C) Without Gap**		**D) With Gap**	
Basis Weight (g/m^2)	1.3	2.4	1.3	2.4
Pressure Drop at 5 cm/s (Pa)	42.2	133.1	142.4	320.6
Filtration Efficiency (%)	72.8	95.1	99.5	99.8
Figure of Merit (FOM)	0.031	0.023	0.038	0.019
Time of Electrospinning (min)	10	20	60	120

3.3.2 Ratio of Coarse to Fine Fibers:

As it was mentioned, unimodal fiber mats were made by spinning one fiber diameter distribution while bimodal fiber mats consist of binary blend of fine and coarse electrospun fibers. In this study, the performance of the filter mats were evaluated using the number fraction of each components, fine and/or coarse fibers. The deposition time of the fibers was considered in such a way that different ratios of coarse to fine fibers (N_c/N_f) were achieved. The N_c/N_f is the total number of coarse fibers to the number of fine fibers existing in a fiber mats, which were calculated using the mass fraction and fiber diameter corresponding to each component. By knowing the density and the mass of each

component, the volume can be calculated. Assuming the fiber length is the same as the filter mat's diameter, the volume of each fiber can be calculated using their fiber diameter. Finally, the number of fibers in each component were calculated by dividing the volume of the component by the volume of each fiber, which gives the number of coarse or fine fibers.

3.3.3 Fiber spacing:

In this research, the filtration performance was studied based on the fiber spacing as well as other traditional methods, such as filter mass and thickness. Using the electrospinning method to produce aligned fibers makes it possible to control the fiber spacing. In electrospinning, increasing the deposition time will produce fibers that are more packed. Also, decreasing the speed of back and forth motion of the collector will decrease the fiber spacing. For micrometer fibers, the number of fibers per centimeter of length of the filter was controlled and fiber mats using a different configuration of number of fibers in the x- and y-directions were fabricated. Figure 3.22 and 3.23 show the SEM images of the micrometer aligned fibers, which used to indicate the number of aligned fibers per length of the filter for different times and speed of the back and forth motion of the collector. The fiber spacing is the inverse of the fiber counts per length. Table 3.5 indicate the corresponding fiber counts per length for each fiber deposition using SEM images.

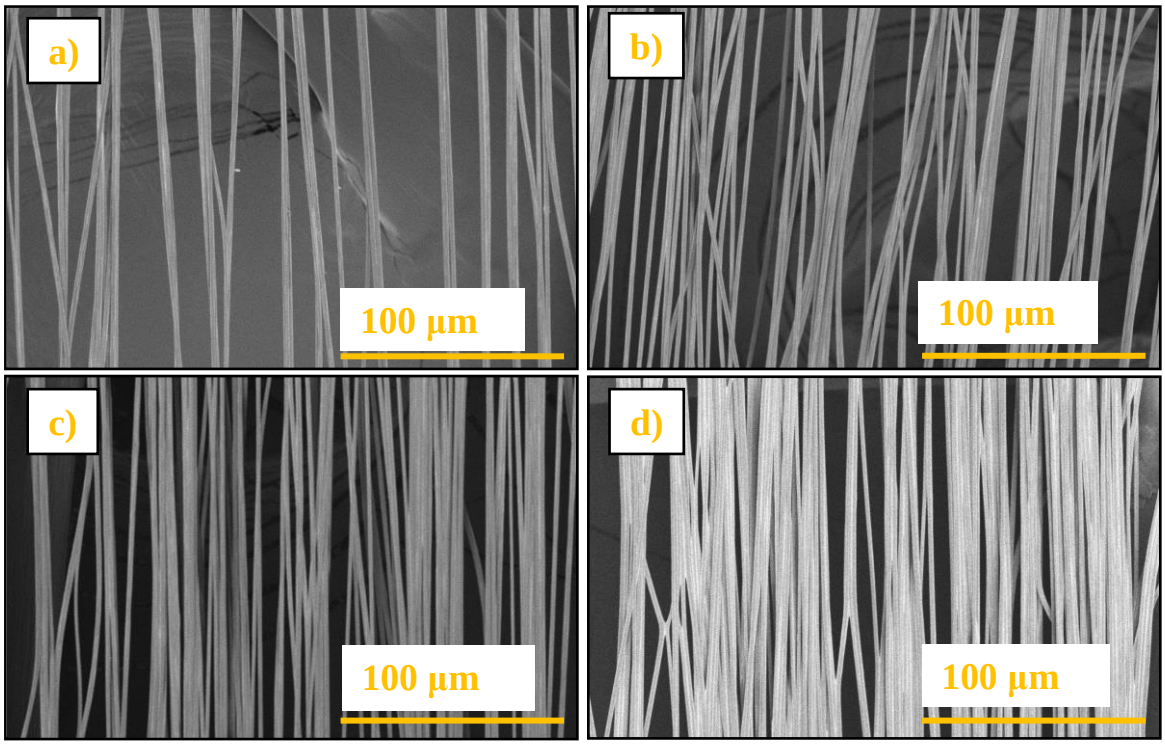

Figure 3.22: SEM images of aligned 25% wt. Polystyrene used to characterize the fiber count, with a-d increasing the fiber counts.

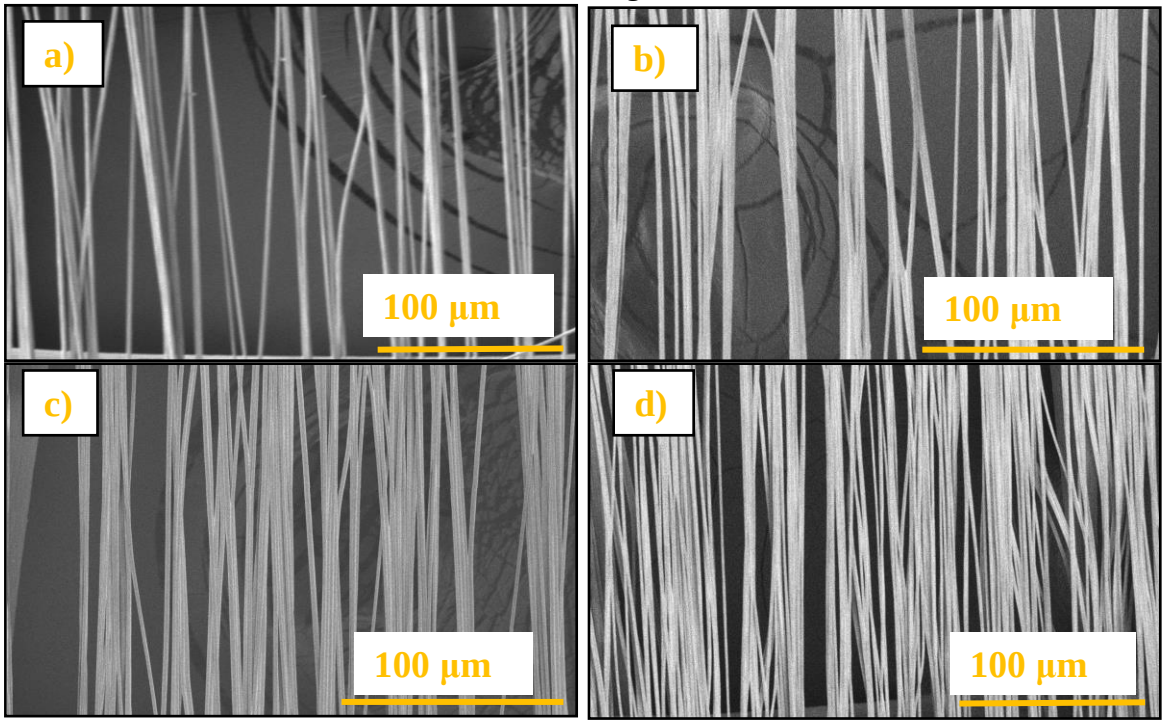

Figure 3.23: SEM images of aligned 30% wt. Polystyrene used to characterize the fiber count, with a-d increasing the fiber counts.

Table 3.5: Corresponding fiber counts per length for each fiber deposition using SEM images.

Spinning Solution	Corresponding SEM image	Spinning Time (min)	Collector speed for back and forth motion (cm/s)	Fiber Count (Fibers/mm)	Fiber Spacing (μm)
25% Wt. Polystyrene	Figure 3.20, a	5	1.5	154±14	~6.5
	Figure 3.20, b	10	1	225±12	~4.5
	Figure 3.20, c	15	1	284±1	~3.5
	Figure 3.20, d	20	0.5	341±9	~3
30% Wt. Polystyrene	Figure 3.21, a	2.5	1.5	122±2	~8.2
	Figure 3.21, b	7.5	1	210±17	~4.8
	Figure 3.21, c	12.5	1	272±6	~3.7
	Figure 3.21, d	17.5	0.5	310±8	~3.2

3.3.4 Filter mats clogging:

Filtration performance test which were explained in chapter 2 section 2.7, were carried out all for the clean filters. The test duration was very low (maximum of 3 minutes), where there is no concern for the effects of filter clogging or particle loading on the fibers. Figure 3.24 are the SEM pictures which were taken before and after filtration performance test. The SEM pictures show the no or very few particles captured on the fibers.

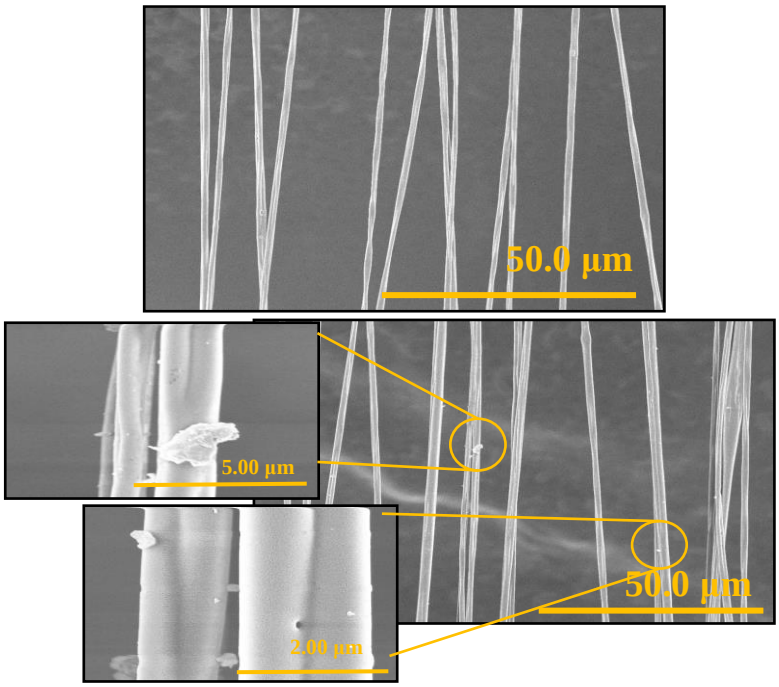

Figure 3.24: SEM pictures indicate very few particles capture on the fibers top) before and bottoms) after filtration performance test.

3.4 Conclusion:

Electrospun fibers were produced with different fiber diameters and orientations using different solution concentrations. Micrometer and nanometer fiber mats were fabricated in a random or an aligned fashioned using Polystyrene and Nylon 4, 6. Fiber mats were created using smooth fibers with no defects and a minimum amount of nanowebs formation. Different morphologies were fabricated using a single fiber diameter for unimodal and a blend of fine and coarse fibers for bimodal fiber mats. Fibers were coated uniformly on the substrate using back and forth motion in the collector, ion charge deposition (corona) for the rotational collector, and the gap method in the stationary collector. The ratio of coarse to fine fibers and fiber spacing were defined for randomly and orthogonally fashioned fiber mats.

The filtration performance of micrometer and nanometer fiber mats with selected morphology, coarse to fine fiber ratio, fiber spacing, and basis weight will be covered in chapter 4. The performance will be evaluated based on the filtration efficiency, pressure drop, and FOM. The experimental values will also be compared with the empirical and theoretical calculations.

CHAPTER 4 Filtration Performance Testing

4.1 Introduction:

The filtration performance of the filter mats with different morphologies were studied based on the pressure drop and particle capture efficiency. The FOM of corresponding filter mats were also calculated using pressure drop and particle penetrations through the filters. The electrospun fiber mats were also evaluated based on empirical equations. The results in this chapter are categorized into three sections. The first section is an evaluation of the performance, based on the basis weight and fiber spacing, of filters made of micrometer fibers. The second section is an evaluation of filter mats, made of random nanometer fibers, in unimodal and bimodal configurations. Finally, the third section discusses the performance of filters made of the mixture of aligned micrometer and nanometer fibers in an orthogonal bimodal fashion.

4.2 Mats with Micrometer Fiber Size:

A series of experimental investigations were done to further examine the effects of unimodal and bimodal micrometer fiber mats as well as the orientation (randomly fashioned verses orthogonally layered) of the micrometer fibers on the filtration performance. The micrometer fiber layers were produced by electrospinning, using

Polystyrene as the polymer. Samples in various fiber orientations were produced by controlling electrospinning parameters. SEM images of Polystyrene unimodal and bimodal fiber mats with random and orthogonal configurations are shown in the Figure 4.1.

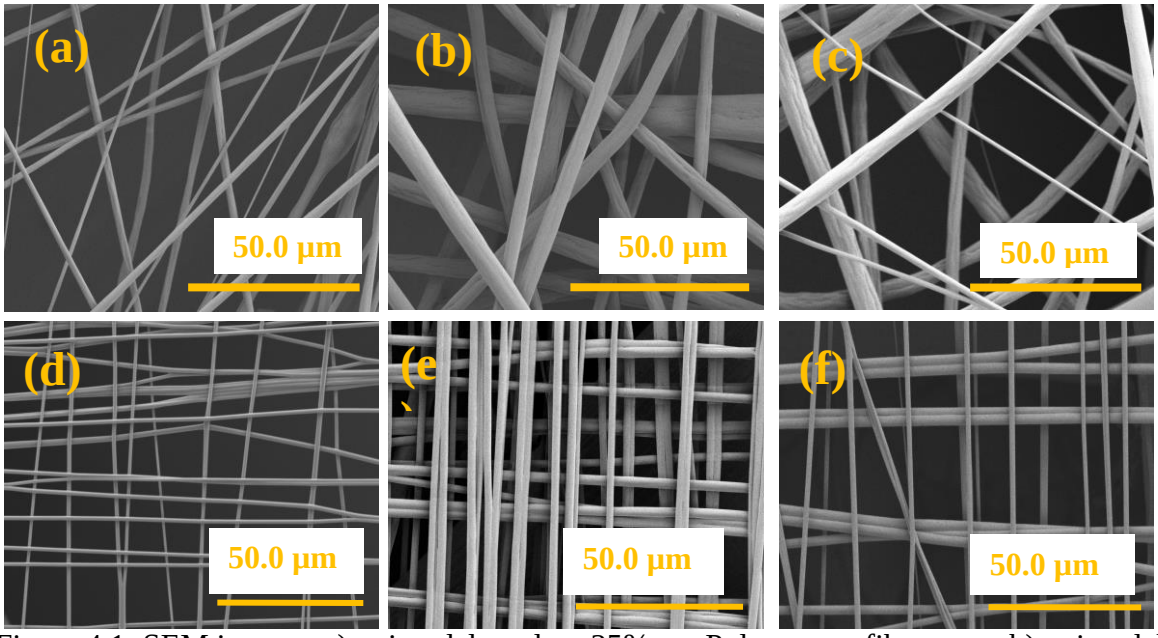

Figure 4.1: SEM images, a) unimodal random 25% wt. Polystyrene fiber mats, b) unimodal random 30% wt. Polystyrene fiber mats, c) bimodal random 25% wt. and 30% wt. Polystyrene fiber mats, d) unimodal aligned 25% wt. Polystyrene fiber mats, e) unimodal aligned 30% wt. Polystyrene fiber mats and f) bimodal aligned 25% wt. and 30% wt. Polystyrene fiber mats.

Based on this study, orthogonally oriented fiber mats can contribute to better filtration performance when compare to the randomly oriented fiber mats with the same basis weight. Also having bimodal fiber mats, regardless of fiber orientation, can improve the filtration performance. Predictions from classical filtration theories were also checked against experimental results.

The study of filtration performance was done by also using fiber spacing. Due to difficulties with thickness and weight measurements of the filter mats, the performance of

the fiber mats can be evaluated using the fiber spacing. By using new technologies, such as electrospinning, controlling fiber spacing is a new window to evaluate the filter performance rather than using conventional method of evaluations. This study is the first experimental study on the performance of micrometer orthogonal fiber mats based on the fiber spacing.

4.2.1 Orthogonal and Random Fiber Mats:

A series of unimodal random and orthogonal fiber mats were made using electrospun Polystyrene fibers (Figure 4.1 (a) and (e)). Fiber diameters and basis weights were kept the same in order to study the effect of the fiber orientation on the filter performance. Table 4.1 is the summary of the mats' specifications with random fibers and aligned fibers. Figure 4.2 indicates the comparison between the random and aligned fiber mats. It was observed that both the pressure drop and efficiency increase when increasing the basis weights for each deposition type.

Table 4.1: Random and orthogonal fiber mat specifications.

Sample	Fiber Diameter (μm)	Basis Weight (g/m^2)	Fiber mats thickness (μm)
Unimodal random Figure 4.1 (a)	2.5±0.7	2.7	55.4±11
		5.4	81.8±9.8
Unimodal Orthogonal Figure 4.1 (e)	2.5±0.4	2.7	44.1±5.1
		5.4	72.3±5.8

As it is shown in Figure 4.2, mats with aligned fibers have a pressure drop and efficiency higher than the mats with random fibers, for both basis weights. The Table 4.1 also indicates that arranging the fibers in aligned format will decrease the thickness compare to

the random orientation for the same basis weight and fiber diameter. For samples with aligned fibers, the FOM increases by almost 61% for basis weight of 2.7 g/m^2 and 96% for 5.4 g/m^2 compared to the random fiber samples. This is as a result of the efficiency being significantly greater than the pressure drop for these samples. The data in this section specifies that for a given filter of known basis weight and fiber diameter, arranging fibers in the aligned orthogonal method, instead of the random method, will increase the performance of filtration.

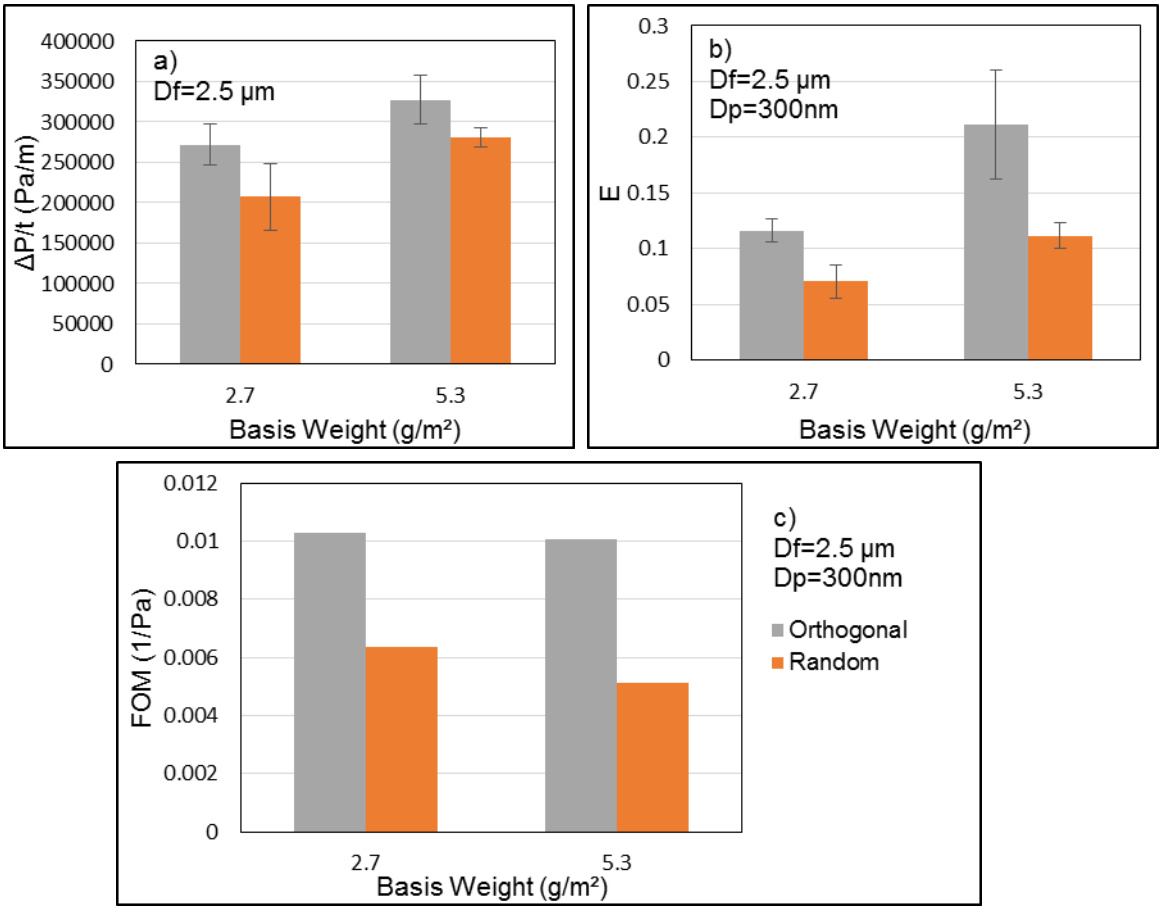

Figure 4.2: Chart comparison between aligned and random fiber mats with the same fiber diameter a) pressure drop per unit thickness, b) efficiency and c) FOM.

4.2.2 Unimodal and Bimodal Random Fiber Mats:

Fiber mats were made with a deposition of random electrospun polystyrene fibers (Figure 4.1 (a), (b), and (c)) with 4 different ratios of coarse to fine fibers (Nc/N_f), which were 0, 0.4, 0.8, and 1. The ratio of 0 and 1 correspond to the unimodal with only fine and only coarse fibers, respectively. The fiber diameter ratios (D_c/D_f) were arranged to be ~1.4. Table 4.2 is the summary of the mats' specifications with random fibers.

Table 4.2: the summary of the random fiber mat specifications.

Sample	N_c/N_f	D_c/D_f	Basis Weight (g/m^2)	Fiber mats thickness (μm)
Unimodal random (fine fibers)	0	—	2.7	55.4±11
			5.4	81.8±9.8
Bimodal random	0.4	1.4	2.7	53.4±13
			5.4	74.6±10.6
Bimodal random	0.8	1.4	2.7	52.0±10.4
			5.4	76.4±11.7
Unimodal random (coarse fibers)	1	—	2.7	53.4±10.7
			5.4	78.8±9.8

The filter mats were tested for pressure drop and efficiency. Figures 4.3 (a) and (b) display these values for unimodal and bimodal random fiber mats with 2.8 and 5.6 g/m^2 basis weights. As was expected, the filtration efficiency decreases as the fiber diameter increases. It is also shown that the bimodal mats of coarse and fine fibers have lower pressure drops compared to the unimodal mats of fine fibers. When comparing bimodal mats to unimodal mats of coarse fibers, it was shown that the larger diameter fibers produced a lower efficiency and pressure drop. It is shown that by using the bimodal form, the filtration efficiency will decrease while the pressure drop decreases more rapidly. This

results in an increase in FOM. Figure 4.3 (c) shows the FOM for unimodal and bimodal random fiber mats. In comparing the FOM of the fiber mats with the same basis weights, bimodal fiber mats provide a higher FOM than unimodal mats. The fine fibers will attribute to filtration efficiency while coarse fibers help decrease pressure drop. Therefore, having a mixture of fine and coarse fibers will optimize the filtration performance in both efficiency and pressure drop.

4.2.3 Unimodal and Bimodal Orthogonal Fiber Mats:

Fiber mats were made with a deposition of electrospun Polystyrene fibers (Figure 4.1 (d), (e), and (f)) with 4 different ratios of coarse to fine fibers (Nc/N_f) which were the same as the previous study, 0, 0.4, 0.8, and 1.The fiber diameter ratios (D_c/D_f) were arranged to be the same in both random and orthogonal cases, which is ~1.4. Table 4.3 is the summary of the mats' specifications with orthogonal fibers.

Table 4.3: the summary of the orthogonal fiber mat specifications.

Sample	N_c/N_f	D_c/D_f	Basis Weight (g/m^2)	Fiber mats thickness (μm)
Unimodal aligned (fine fibers)	0	—	2.7	44.9±3
			5.4	69.7±6.2
Bimodal aligned	0.4	1.4	2.7	42.9±6.7
			5.4	69.8±5
Bimodal aligned	0.8	1.4	2.7	45.2±4.6
			5.4	66.8±4.3
Unimodal aligned (coarse fibers)	1	—	2.7	44.1±5.1
			5.4	72.3±5.8

The filter mats were tested for pressure drop and efficiency. Figures 4.3 (a) and (b) display these values for unimodal and bimodal orthogonal fiber mats with 2.8 and 5.6 g/m^2 basis weights. As was expected, the filtration efficiency decreased as the fiber diameter increase.

It is also shown that the bimodal mats of coarse and fine fibers have lower pressure drops compared to the unimodal mats of fine fibers. Comparison to unimodal mats of coarse fibers still showed that the larger diameter fibers produced a lower efficiency and pressure drop. It is shown that by using the bimodal form, the filtration efficiency will decrease while the pressure drop will decrease more rapidly. This results in an increase in FOM.

Figure 4.3 (c) shows the FOM for unimodal and bimodal orthogonal and random fiber mats. In comparing the FOM of fiber mats with the same basis weights, bimodal fiber mats provide a higher FOM than unimodal mats. This is the case in both random and orthogonal configurations. It is also shown that the performance of orthogonal fiber mats, regardless of the coarse to fine fiber ratio, is always greater than the random mats.

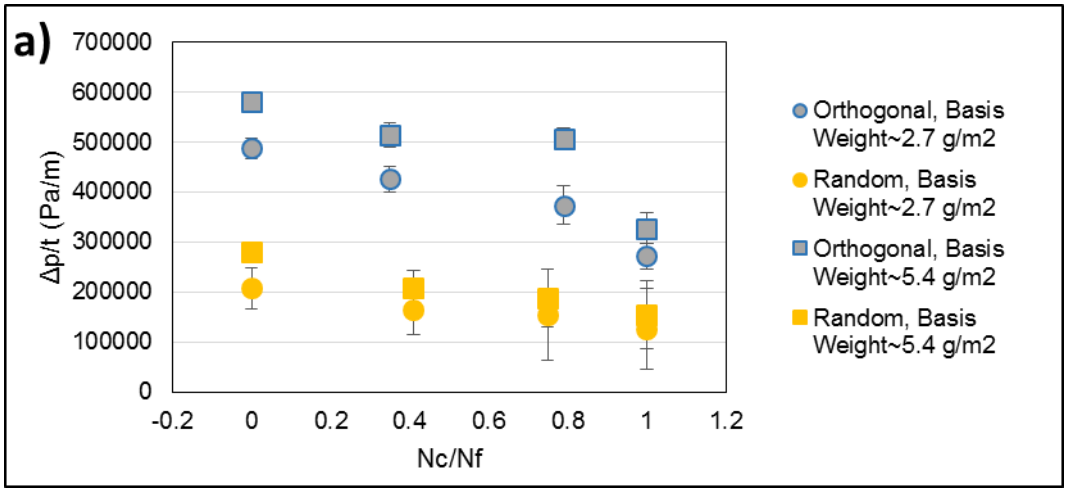

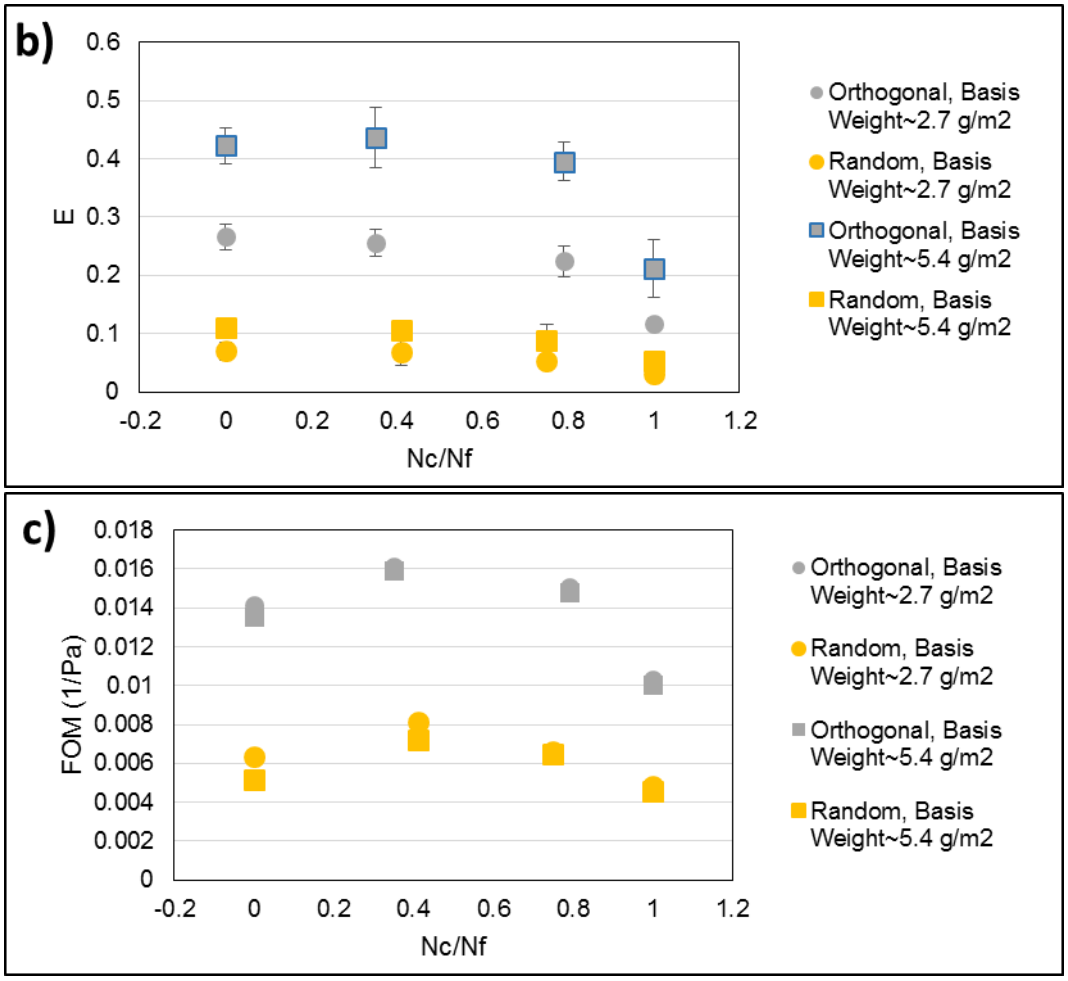

Figure 4.3: Chart comparison between aligned and random fiber mats with different coarse to fine fiber ratios to a) pressure drop per unit thickness, b) efficiency and c) FOM.

4.2.4 Comparing the experimental results with empirical correlations:

In this section, the filtration efficiency and pressure drop of these fiber mats were compared with predictions from analytical models. The empirical correlation of Davies for pressure drop was used. Fiber diameters for bimodal fiber mats were also calculated with three previously stated equations (1.2), (1.3), and (1.4) to find the average fiber diameter. Figure 4.4 shows a comparison between the experimental and theoretical model of pressure

drop per unit thickness versus coarse to fine fiber ratios (Nc/Nf). Prediction of unimodal equivalent fiber diameters was considered using area-weighted average diameter, volume-weighted resistivity model, and the cube root formula. The results for the small basis weight are in relatively good agreement with theoretical calculations, whereas the experimental values for the higher basis weight are lower than what was calculated. This discrepancy can be explained by the effect of the spun fibers being bundled together in the experiment. To obtain a higher basis weight, more time could be considered for electrospinning. This will cause a higher chance for fibers to get bundled together, and will result in bigger fiber diameters and lower pressure drops. Figure 4.5 indicate a SEM picture of fibers that get bundle together.

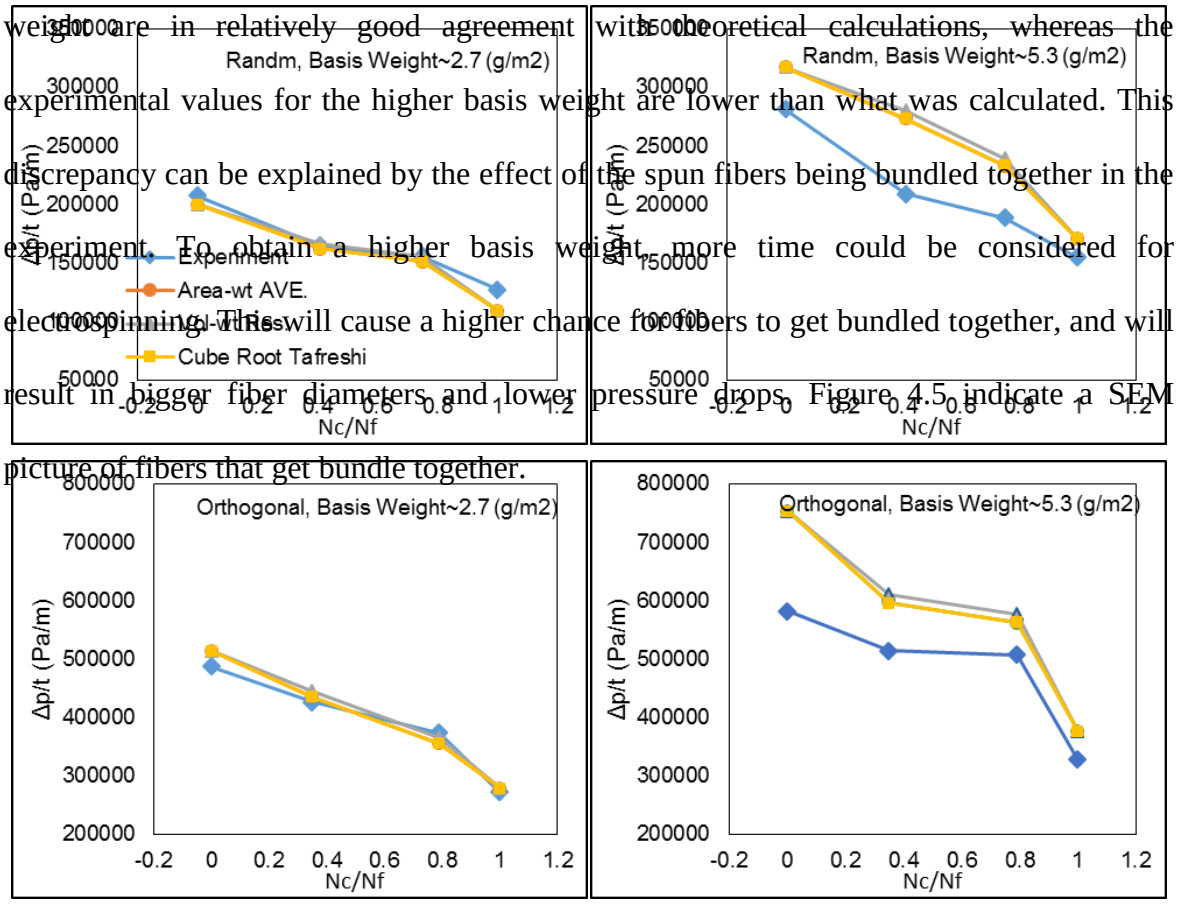

Figure 4.4: Chart comparison between the experimental and theoretical model for pressure drop.

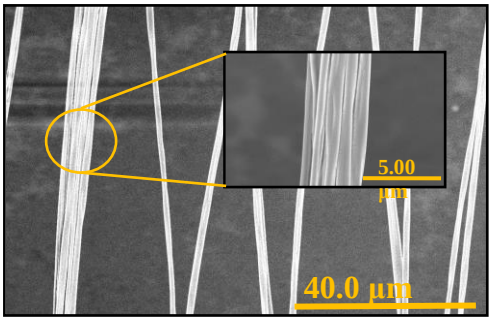

Figure 4.5: SEM images of fiber bundling.

To investigate the accuracy of experimental filtration efficiency for each filter mat, the Pich model was considered. The filtration efficiency obtained for unimodal random and unimodal orthogonal was compared with the computed filtration efficiency with the Pich equation by measuring filter mat thicknesses. The results are plotted in Figure 4.6 for different particle diameters. It shows that the values between experimental results and calculated theoretical predictions closely match.

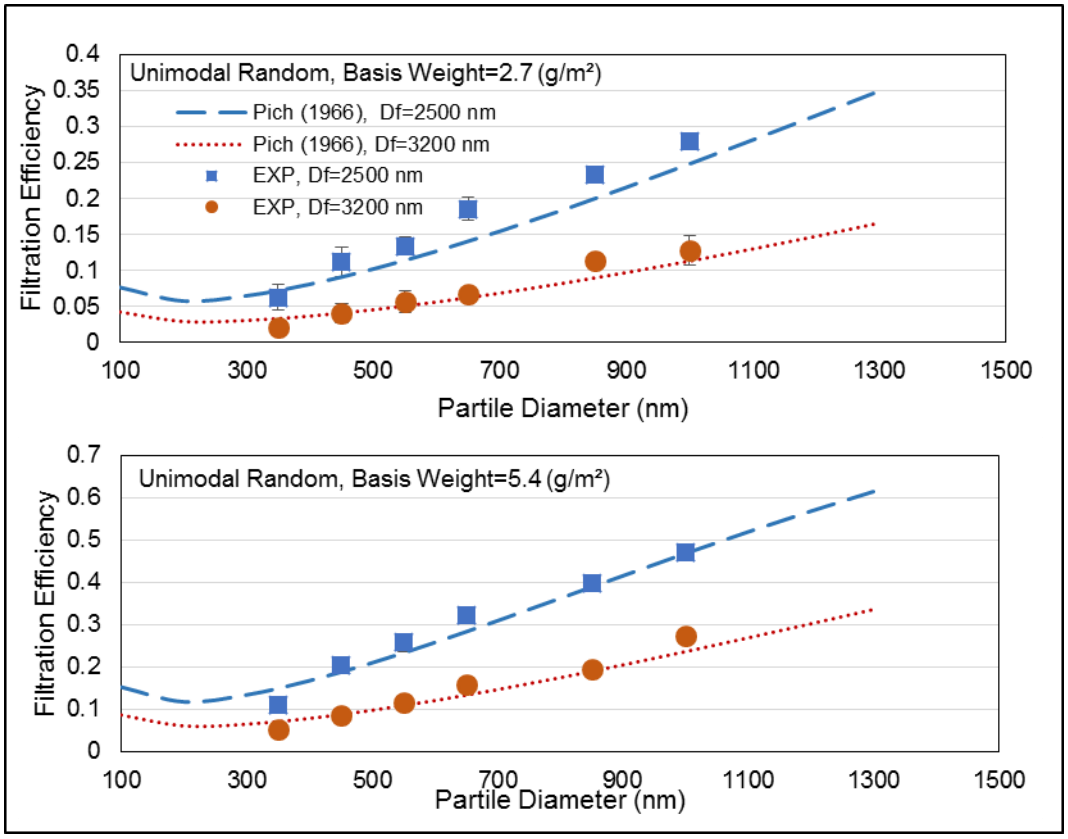
Unimodal Random, Basis Weight=2.7 (g/m²)
Pich (1966), Df=2500 nm
Pich (1966), Df=3200 nm
EXP, Df=2500 nm
EXP, Df=3200 nm
Filtration Efficiency
0.4
0.35
0.3
0.25
0.2
0.15
0.1
0.05
0
100
300
500
700
900
1100
1300
1500
Partile Diameter (nm)
Unimodal Random, Basis Weight=5.4 (g/m²)
Filtration Efficiency
0.7
0.6
0.5
0.4
0.3
0.2
0.1
0
100
300
500
700
900
1100
1300
1500
Partile Diameter (nm)

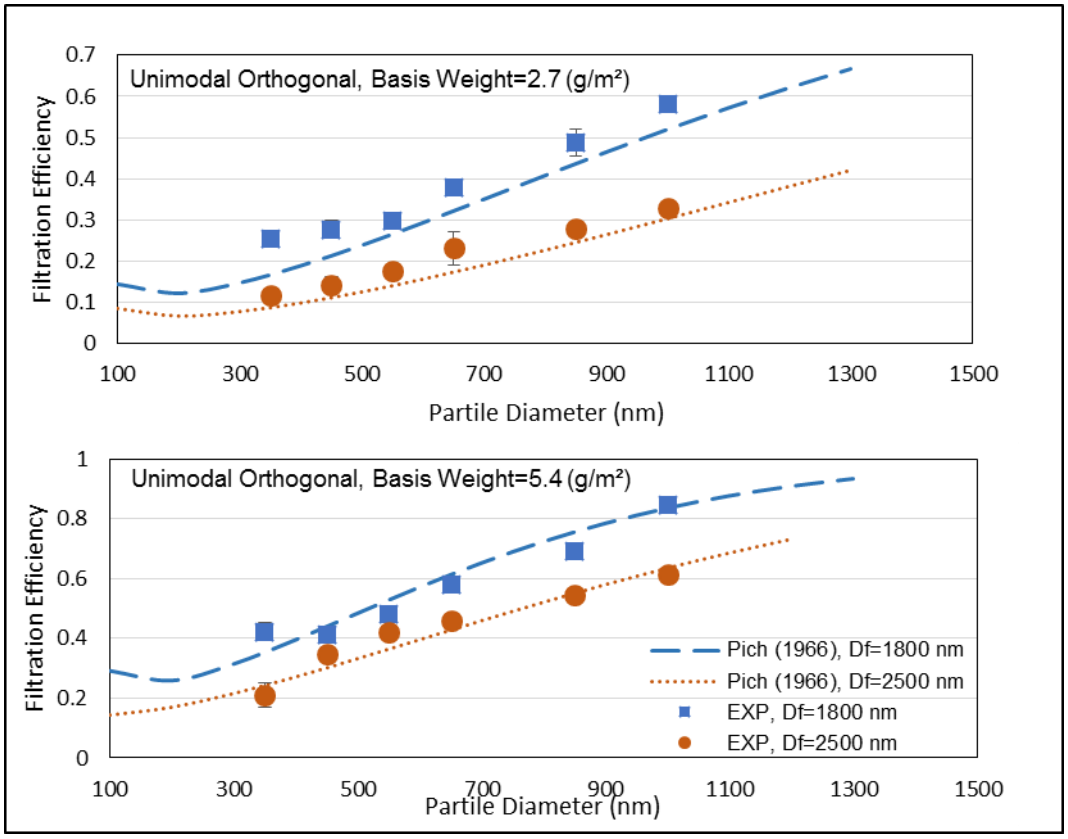

Figure 4.6: Chart comparison between the experimental results and theoretical model for filtration efficiency.

4.2.5 Fiber Spacing for Orthogonal Fiber Mats:

This section presents experimental results of filtration performance of orthogonal fiber mats based on their fiber-to-fiber spacing. The performance of the fiber mats were evaluated based on the fiber distribution across the orthogonal layers. Almost all of the study on the filtration performance are based on the filter mass and thickness, there are only a few studies on the filtration performance based on the fiber distributions. To our knowledge, there is only a study on modeling performance of orthogonally layered fiber mats based on fiber-to-fiber spacing [100].

In this section, the fiber mats were characterized based on their fiber count in the x and y directions. Using SEM images to measure the fiber count per length is more accurate and reliable than measuring thickness and weight (refer to Chapter 3, Section 3.3.3). The results are described in three subsections. The first subsection shows results from studying the effect of varying the fiber counts in fiber mats with a constant fiber diameter. The second subsection discusses results from studying the effect of differing the number of fibers in each direction (x or y). The third subsection presents the results from the effects of layering. In all of these experimental studies, the fiber mats were made of orthogonal layers of aligned Polystyrene fibers with the same fiber diameter, which are considered as unimodal orthogonal fiber mats.

4.2.5.1 Fiber Counts:

Two series of unimodal orthogonal fiber mats were made of micrometer fibers with diameters of 1.8 μm and 2.5 μm, respectively. For each set, the fiber mats were made with different fiber counts. Table 3.5 (in Chapter 3) indicates the corresponding fiber counts for each fiber deposition. The fiber mats were tested based on the particle range from 300 nm to 1 μm and above. There are 6 particle beans, as mentioned in Chapter 2 Section 2.8.2.

As it is shown in Figure 4.7, the pressure drop and filtration efficiency increases when increasing the fiber counts. Figure 4.8 also summarized the results of FOM based on the fiber counts. The filtration efficiency and FOM in these graphs are for particles with a bean size of 300-400 nm.

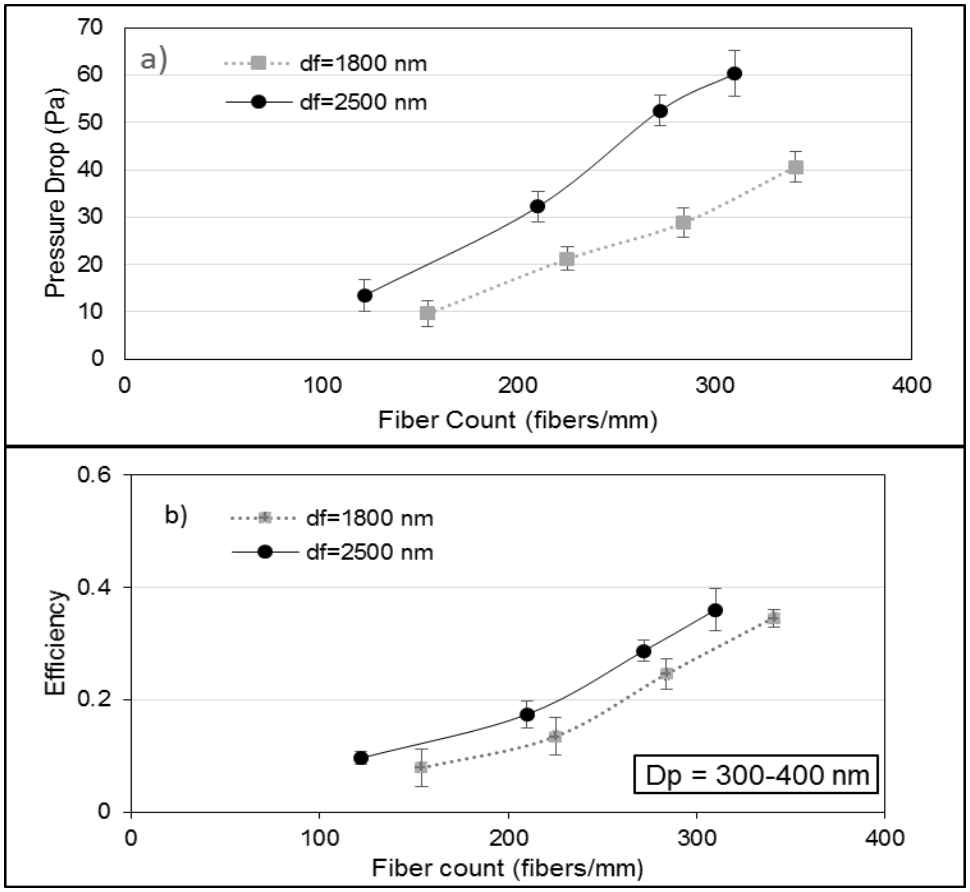

Figure 4.7: shows a) pressure drop and b) filtration efficiency as a function of fiber counts for fiber mats with equal fiber counts in the x and y directions.

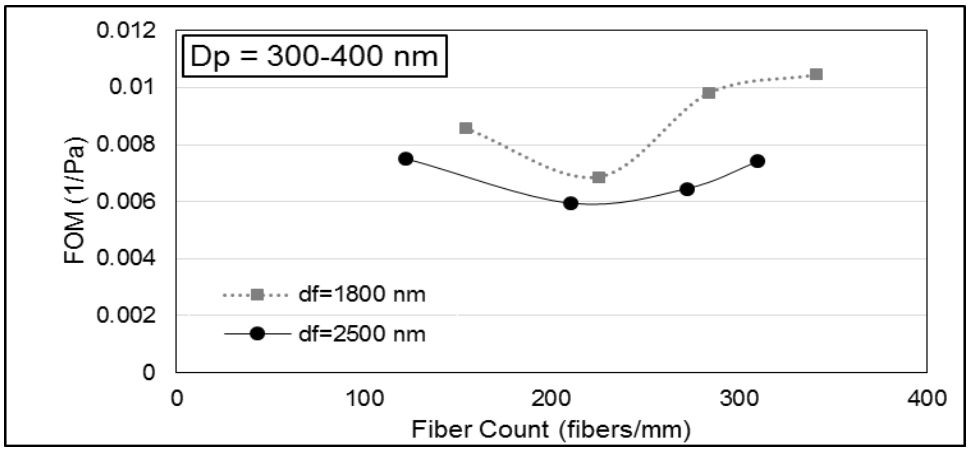

Figure 4.8: shows the FOM as a function of fiber counts for mats with equal fiber counts in the x and y directions and particle size from 300 to 400 nm.

Figure 4.9 and 4.10 indicate the particle capturing efficiency and FOM based on the fiber counts for filter mats with fiber diameters of 1.8 µm and 2.5 µm, respectively, for different particle bean sizes. It is shown that for fiber mats with diameters of 1.8 µm and 2.5 µm, FOM is independent of fiber spacing for bean size of 600 -700 nm and above 700 nm, respectively. It was first documented by Bucher et al. that for certain particle-fiber diameter combinations the quality factor is independent of fiber count in a layer of fiber coating. They stablish a relationship via modeling between fiber diameter and particle diameter for which the quality factor is independent of fiber counts [100]. This experimental study is agreement with the results of independence of the FOM with fiber counts for a specific fiber diameter and particle diameter. This property will confirm that the performance of the fiber mats is independent of fiber spacing for the specific particle diameter regarding the fiber diameter of filter mats.

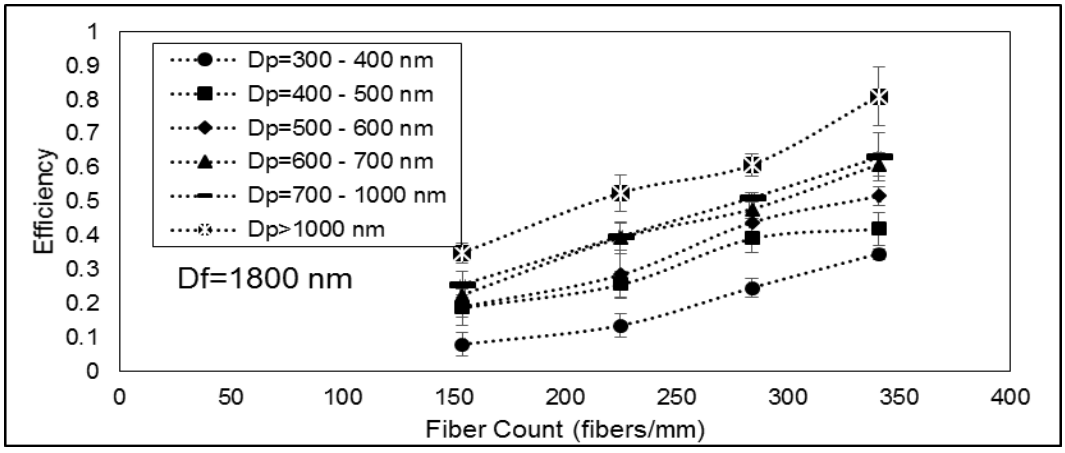

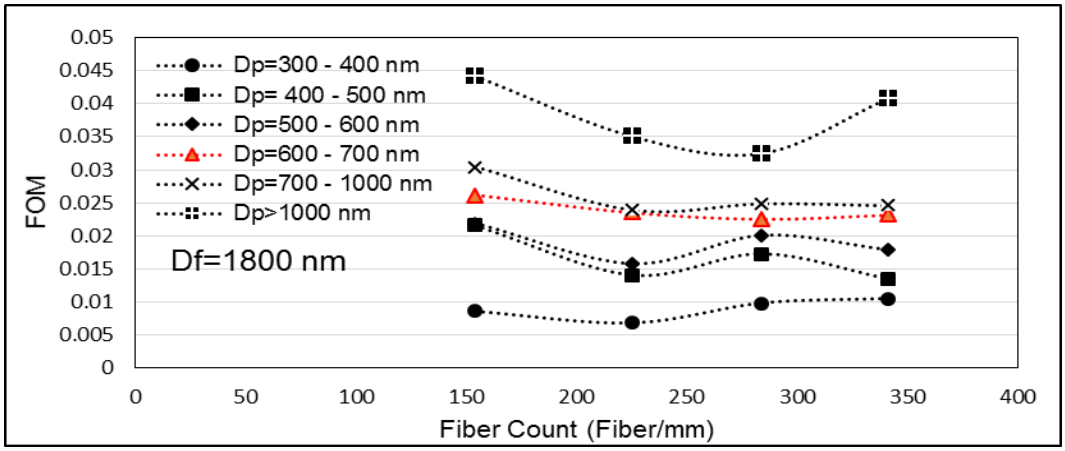

Figure 4.9: filtration efficiency and FOM as a function of fiber counts for fiber diameter 1.8 µm for different particles diameter beans.

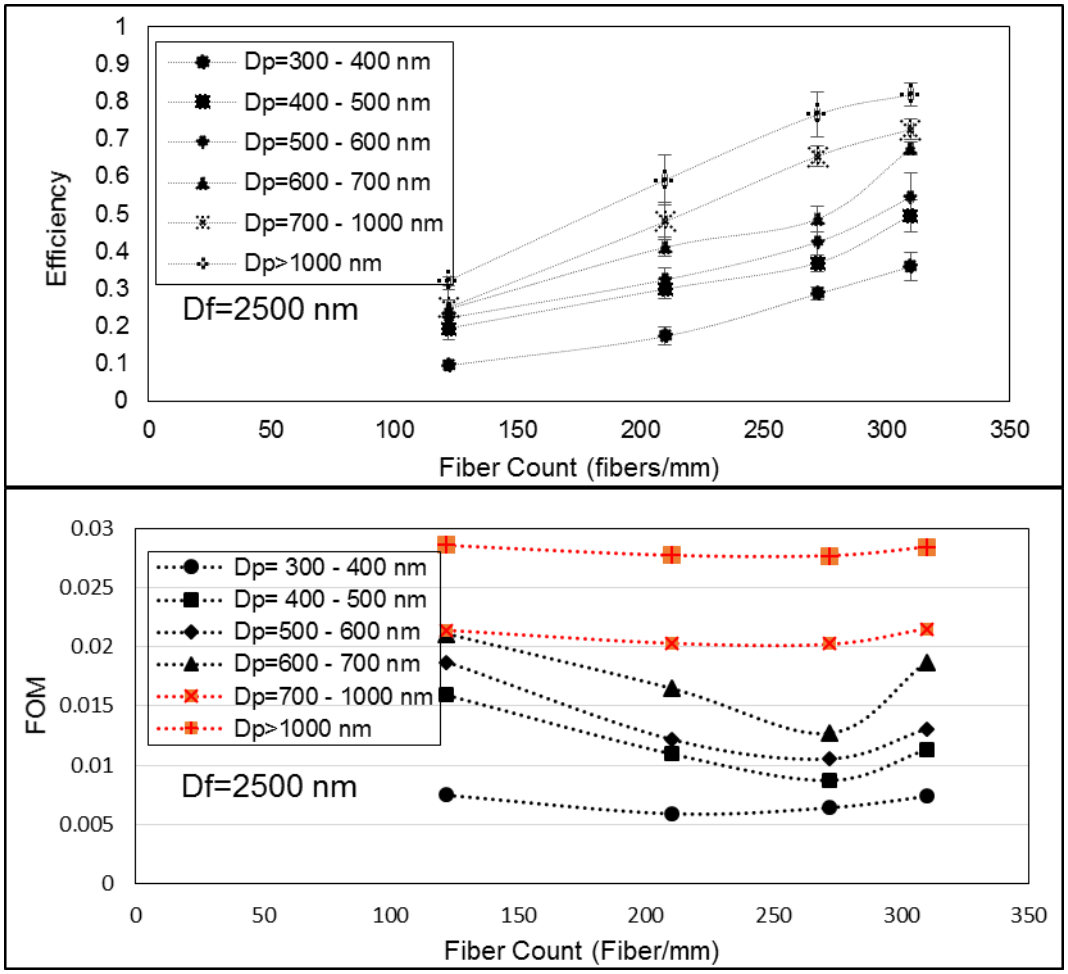

Figure 4.10: filtration efficiency and FOM as a function of fiber counts for fiber diameter 2.5 µm for different particles diameter beans.

4.2.5.2 Fiber counts differing in the x and y directions:

The fiber mats were made and tested based on different numbers of fibers in the x and y directions by keeping the number of fibers in the x direction (f_c^x) constant and changing the number of fibers in y direction (f_c^y). In this case, the openings between fibers are not square. The filtration performance of the fiber mats with different number of fibers in the x and y directions ($f_c^x \neq f_c^y$) were tested and compared with the fiber mats performance with the same number of fibers in the x and y directions($f_c^x = f_c^y$). Figure 4.11 a and b, show SEM images of mats with ($f_c^x \neq f_c^y$) and($f_c^x = f_c^y$), respectively.

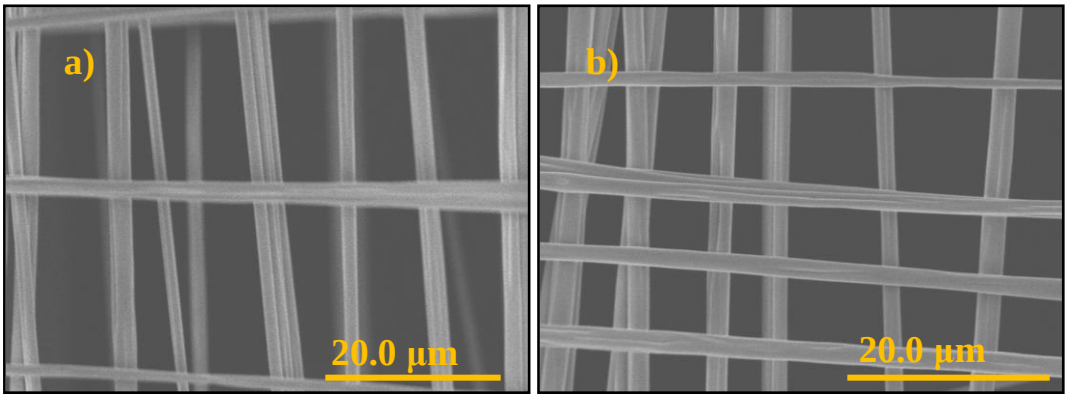

Figure 4.11: SEM images of fiber mats with a) different fiber count in the x and y directions ($f_c^x \neq f_c^y$), and b) equal fiber count in the x and y directions ($f_c^x = f_c^y$).

Figure 4.12 a and b show the pressure drop and filtration efficiency for the fiber mats made with the fiber diameter of 1.8 µm. The filtration efficiency is for the capturing of particles with a bean size of 300-400 nm. As it is seen in the figures, the pressure drop and filtration efficiency both decreases for the case with different fiber counts in the x and y direction. FOM is also calculated and plotted in Figure 4.13.

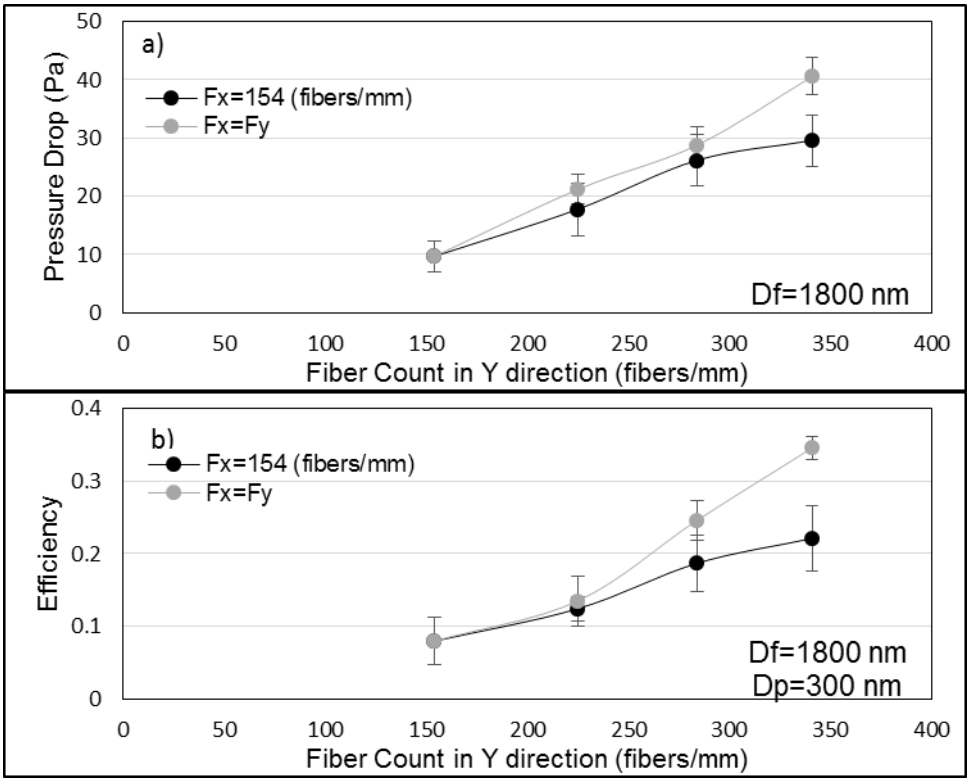

Figure 4.12: shows a) pressure drop and b) filtration efficiency as a function of fiber counts for mats with and without equal fiber counts in the x and y directions.

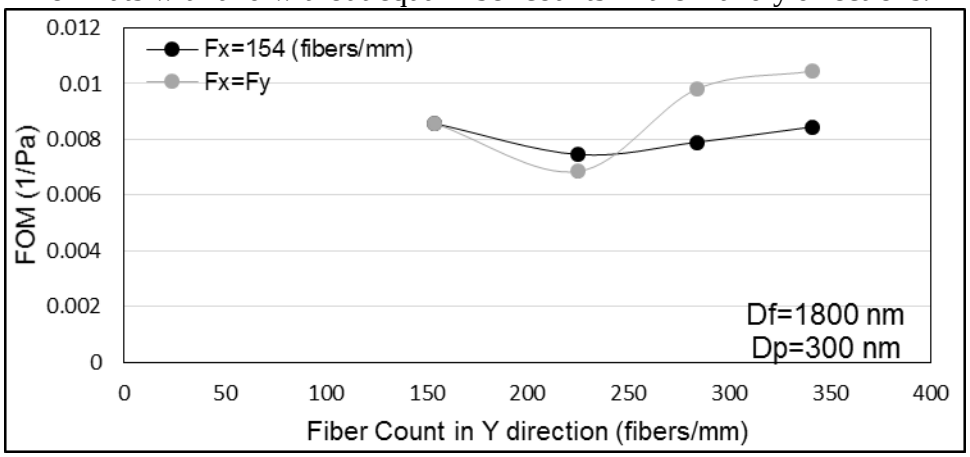

Figure 4.13: shows FOM as a function of fiber counts for mats with and without equal fiber counts in the x and y directions.

This experiment was conducted again for filter mats made of fibers 2.5 µm in diameter.

Figure 4.14 a and b show the pressure drop and filtration efficiency, respectively. FOM is

plotted in Figure 4.15 as well. The results indicate the same trend as previously discovered. There is no obvious trend for changing in FOM as a function of fiber counts for these cases.

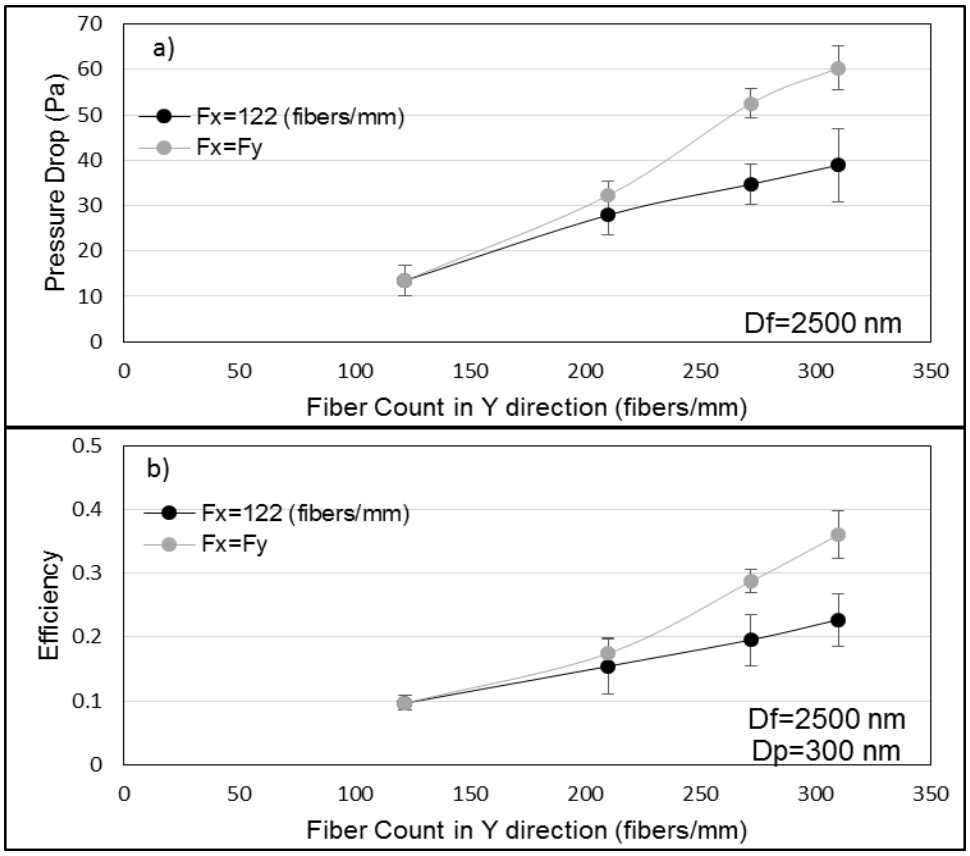

Figure 4.14: shows a) pressure drop and b) filtration efficiency as a function of fiber counts for mats with and without equal fiber counts in the x and y directions.

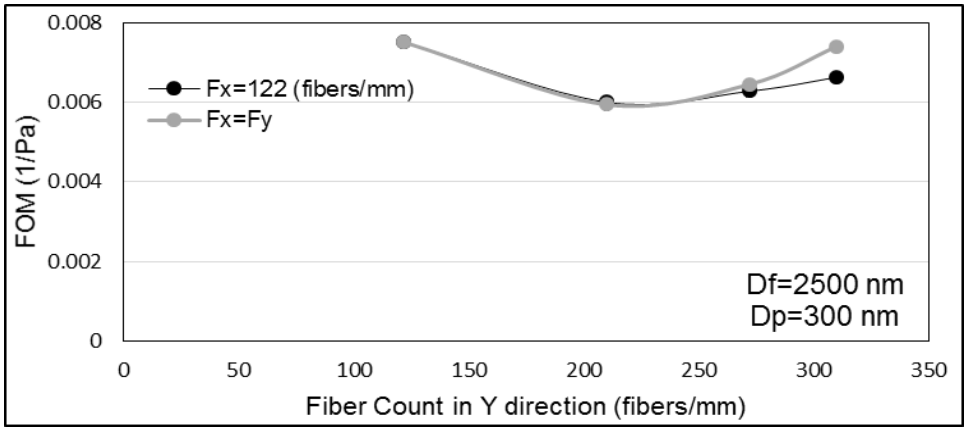

Figure 4.15: shows FOM as a function of fiber counts for mats with and without equal fiber counts in x and y direction.

4.2.5.3 Effect of Layering:

In this section, the effect of layering on the filtration performance is experimentally studied. Two sets were compared with each other. The first set was made of two orthogonal layers of aligned fibers and the second set was made of four layers of aligned fibers perpendicular to each other. The filter mats in both cases were kept at the same basis weight and made of Polystyrene fibers with a diameter of 1.8 μm. In other words, the same number of fibers were distributed in one pair of orthogonal layers for the first case and in two pairs for the second case. Figure 4.16 a and b are the pressure drop and filtration efficiency, respectively. Pressure drop and filtration efficiency increases as the fiber counts increases in each layer. The filtration efficiency is not changing a lot by distributing the mass in more layers. However, the pressure drop for the filter mats consisting of four orthogonal layers is reduced a lot compared to the fiber mats with two orthogonal layers. This results in a higher FOM for the case of using a higher number of layers. Therefore,

the results indicate that spreading the fibers in several layers will improve the filtration performance. Figure 4.17 indicates the FOM for both cases.

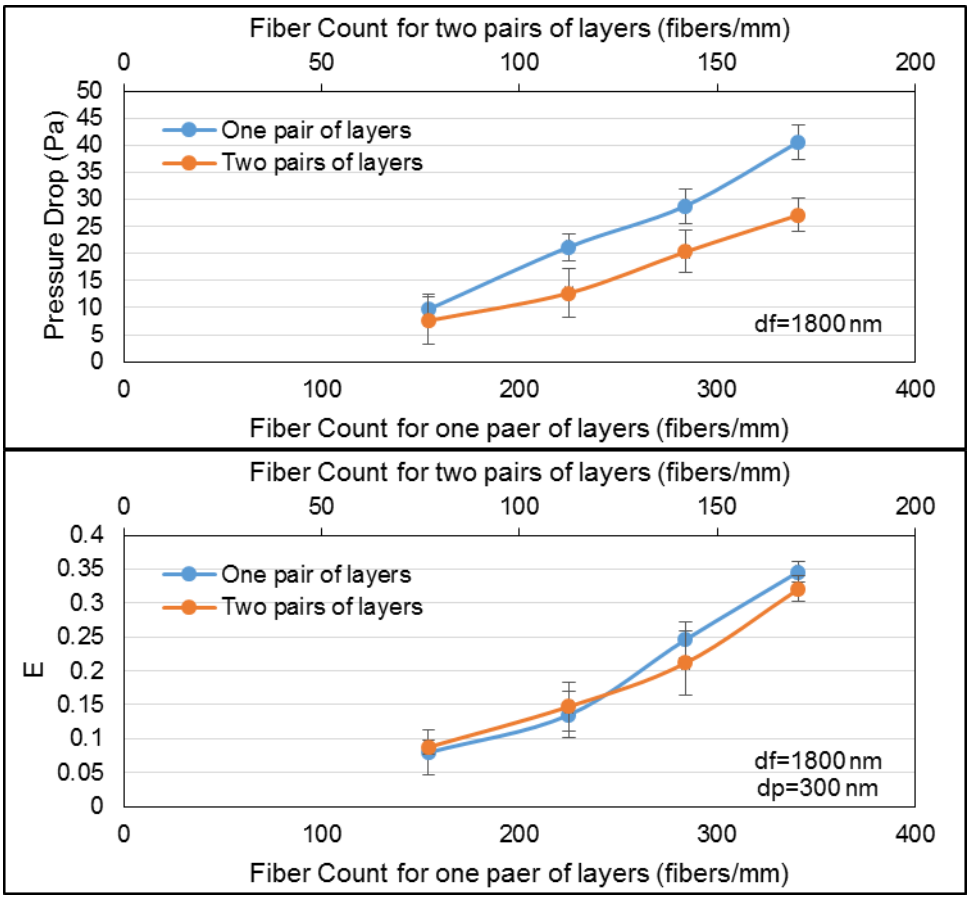

Figure 4.16: shows a) pressure drop and b) filtration efficiency as a function of fiber counts per length for mats with one pair of layers and two pairs of layers.

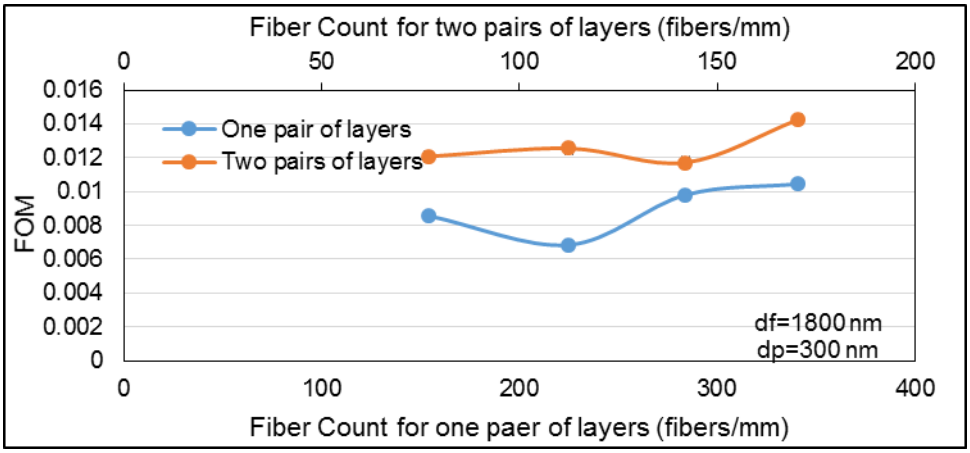

Figure 4.17: shows FOM as a function of fiber counts per length for mats with one pair of layers and two pairs of layers.

4.3 Mats with Nanometer Fiber Size:

In this section, the aim is to study the performance of filter mats made of nanometer fibers. The nanometer fibers were made in random and aligned configurations, explained in detail in chapter 2 and 3. The bimodal and unimodal arrangements of random fiber mats were produced and compared. Due to the narrow range of fiber diameters of aligned nanometer fibers, the orthogonal nanometer fiber mats were not investigated. Therefore, this study was limited to only making bimodal and unimodal random configurations for nanometer fibers. By controlling the spinning time, different basis weights are achievable. Spinning time for nanometer fiber deposition was indicated to achieve a basis weight around 2.7 (g/m^2). Since Nylon fibers are too thin, higher basis weights will cause a pressure drop that was too high to be considered valid.

A Nylon 4,6 solution in Formic Acid with 10% and 20% weight concentration were used to electrospin nanofibers. Deposition of fibers on the substrate was done using the process parameters as described in Chapter 2. Figure 4.18 shows SEM images of unimodal and

bimodal random nanometer fiber mats. Filtration performance for these fiber mats were measured. The results indicate that for nanometer fibers, having bimodal fiber mats will improve the filtration performance. Predictions from classical filtration theories were also checked against experimental results.

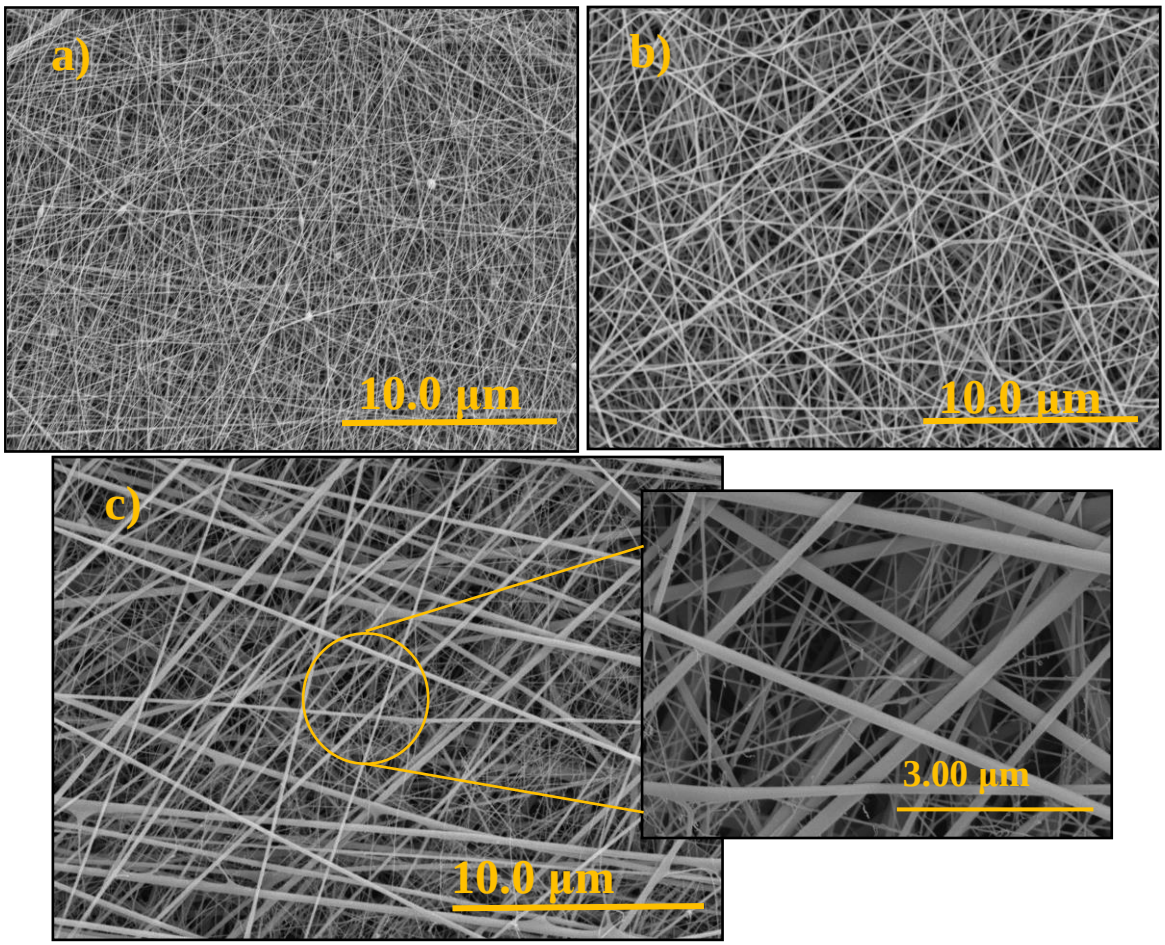

Figure 4.18: SEM images, a) unimodal random 10% Nylon 4,6 fiber mats, b) unimodal random 20% Nylon 4,6 fiber mats, and c) bimodal random 10% and 20% Nylon 4,6 fiber mats.

4.3.1 Unimodal and Bimodal Random Fiber Mats:

The experimental results from unimodal and bimodal nanometer random fiber mats were discussed based on their ratio of coarse to fine fibers (N_c/N_f). Table 4.4 is the summary of

the mats' specifications. The filtration performance results are charted in Figure 4.19 a and b for pressure drop and filtration efficiency, respectively.

Table 4.4: summary of the random nanometer fiber mat specifications.

Sample	N_c/N_f	D_c/D_f	Basis Weight (g/m^2)	Fiber mats thickness (µm)
Unimodal random (fine fibers)	0	—	2.7	93.7±4.2
Bimodal random	0.4	~2	2.7	72.5±5.3
Unimodal random (coarse fibers)	1	—	2.7	63.7±3.1

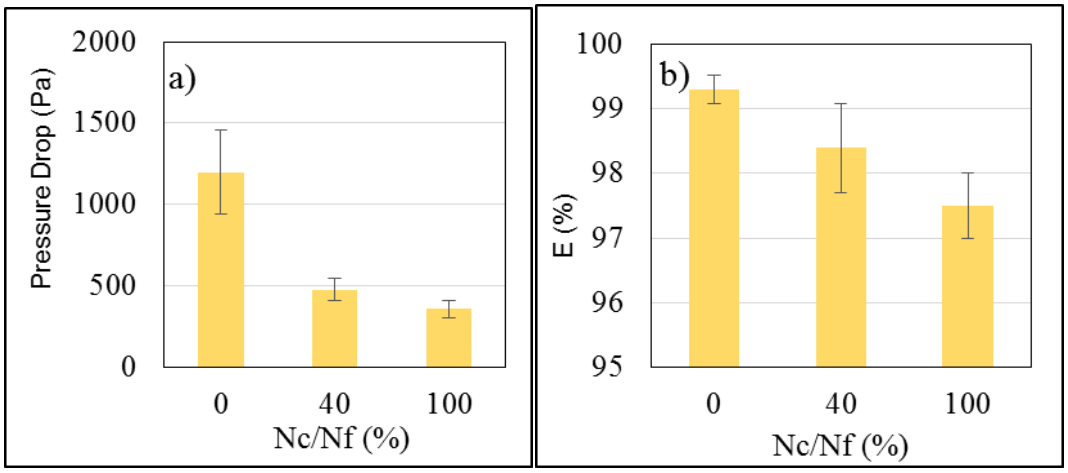

Figure 4.19: Chart comparison of nanometer fibers between unimodal mats with fine fibers (N_c/N_f = 0%), unimodal mats with coarse fibers (N_c/N_f = 100%), and bimodal mats (N_c/N_f = 40%) for a) efficiency, b) pressure drop.

As it shows in the previous Figures, the filtration efficiency for unimodal mats with fine fibers is slightly higher than bimodal mats with the same basis weight. Also, for the same basis weight, pressure drop is lower for bimodal filter mats compared to the unimodal mats with fine fibers, regardless of their fiber diameter. The FOM was calculated based on the equation given in Chapter 1. Figure 4.20 shows the results for FOM. It is shown that FOM for bimodal is higher than unimodal filter mats with fine fibers with the same basis weight.

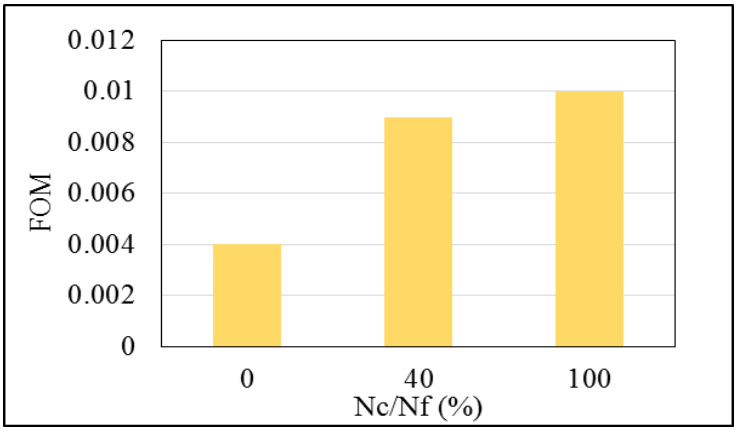

Figure 4.20: Chart comparison of nanometer fibers between unimodal mats with fine fibers ($N_c/N_f = 0\%$), bimodal mats ($N_c/N_f = 40\%$), and unimodal mats with coarse fibers ($N_c/N_f = 100\%$), for FOM.

4.3.2 Comparing the experimental results with empirical correlations:

In this section, filtration performance of the unimodal and bimodal random nanometer fiber mats were compared with the theoretical values. The pressure drop values were obtained from Davies' equation, and filter collection efficiency was calculated from semi-empirical correlations of Liu and Rubow. These equations are explained in Chapter 1.

The calculations for pressure drop and efficiency for bimodal fiber mats were done in two different ways. The first way is to consider the mats as a blend of fine and coarse fibers, and then use the average fiber diameter of fine and coarse fibers. The average fiber diameter was found by using the cube root equation of Tafreshi, which is explained in Chapter 1. The second way is to consider the fiber layers as separate (5 layers total) and then solve the theoretical equations for individual layers in pressure drop and efficiency. The layer values were added for calculation of the pressure drop and multiplied to determine efficiency. The thickness and weight of each layer was approximately determined by knowing the mass fraction of fine to coarse fibers, and the total weight and

thickness of the fiber mats, which are summarized in table 4.4. For unimodal fiber mats, the second method was also used, however both way of calculations will give the same numbers.

The results for pressure drop and filtration efficiency for calculated and experimental values are compared in Figure 4.21 a and b, respectively.

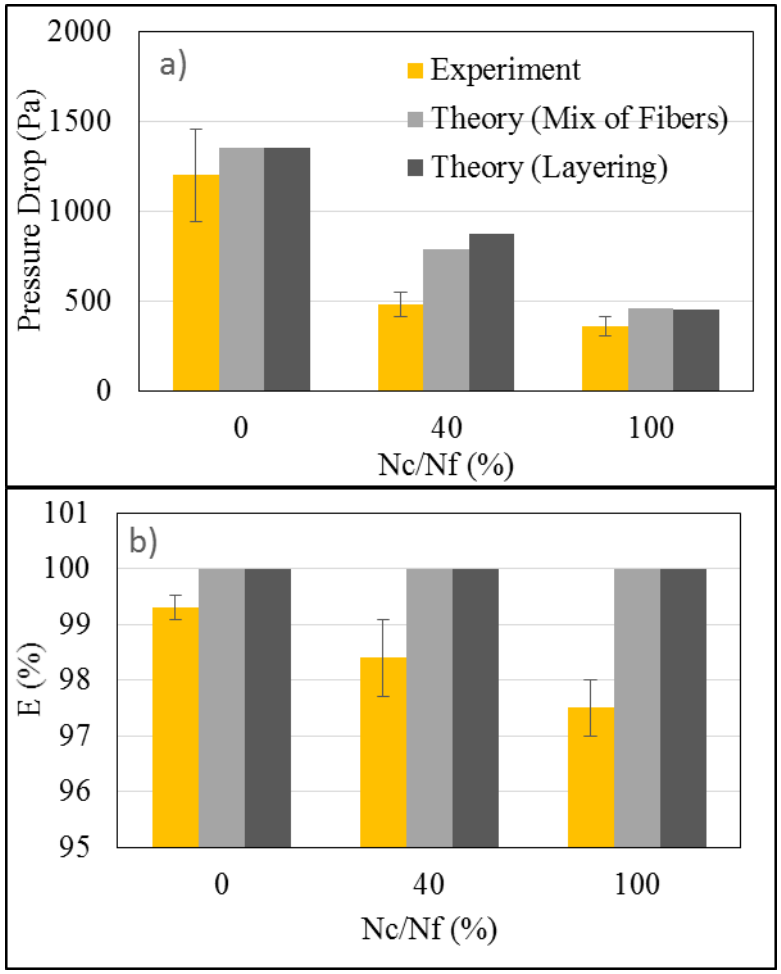

Figure 4.21: Chart comparison between the experimental results and theoretical model for a) pressure drop, and b) filtration efficiency.

4.4 Mats with Micrometer and Nanometer Fiber Size:

This section discusses the filtration performance of the unimodal orthogonal micrometer filter mats with the addition of nanometer layers. The results of adding layers of aligned nanometer fibers to the orthogonal mats indicate improvement in the filtration efficiency. The effects were studied based on the ratio of coarse to fine fibers (Nc/Nf).

4.4.1 Bimodal Orthogonal Fiber Mats:

Bimodal orthogonal fiber mats were prepared by layering electrospun Polystyrene and Nylon 4,6 fibers, each layer with a different fiber diameter, in an orthogonal alignment. 25% wt. Polystyrene and 15% wt. Nylon 4,6 solution concentrations were used to produce coarse and fine fibers, respectively. Therefore, the ratio of coarse to fine fiber diameter (D_c/D_f) is 16 (1.8 μm/0.11 μm). Figure 4.22 shows SEM images of bimodal orthogonal mats made of layering micrometer and nanometer fiber mats. All of the mats were made of 5 layers of alternating fine and coarse fibers, starting with the fine layers.

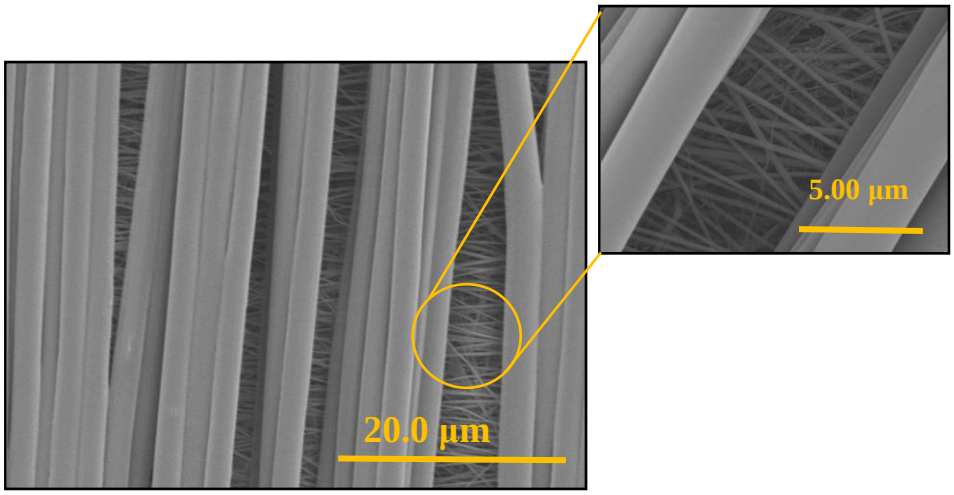

Figure 4.22: SEM image of bimodal orthogonal fiber mats with micrometer 25% Wt. Polystyrene fibers and nanometer 15% Wt. Nylon 4,6 fibers.

4.4.2 Unimodal and Bimodal Orthogonal Fiber Mats:

The electrospinning times were chosen in such a way to have two different basis weights, 2.7 g/m² and 5.4 g/m². Meanwhile, by controlling the basis weights, the ratios of the coarse to fine fibers (N_c/N_f) were kept at 0, 0.006, 0.015, 0.05, 0.15, 0.3, and 1, where 0 indicates mats with only fine orthogonal fibers and 1 indicates mats with only coarse orthogonal fibers. Due to the big difference in fiber diameter of coarse and fine fibers (D_c/D_f ~16), the values between 0.3 and 1 for N_c/N_f were impossible to obtain experimentally. Table 4.5 indicates the summary of mats specifications. In this table, the values for N_c/N_f are expressed as percentages (%). Average fiber diameters were also calculated using the cube root equation of Tafreshi which is explained in Chapter 1.

Table 4.5: summary of the bimodal nanometer and micrometer orthogonal fiber mat specifications.

Sample Description	Basis Weight (g/m^2)	N_c/N_f (%)	Fiber mats thickness (μm)	Average fiber diameter [a] (nm)
Bimodal Orthogonal Fibers **Coarse** fiber diameter: 1.8 μm **Fine** fiber diameter: 0.11 μm	2.7	0	58±2	110
		0.6	65±5	309
		1.5	52±2	400
		5	50±2	586
		15	53±3	870
		30	54±5	1090
		100	45±3	1800
	5.4	0	118±11	110
		0.6	93±8	309
		1.5	80±5	400
		5	79±6	586
		15	84±2	870
		30	95±6	1090
		100	70±6	1800

[a] Average fiber diameter were calculated using the cube root of Tafreshi.

Furthermore, the filtration performance was tested as described in Chapter 2. The performance of the filters were tested with a face velocity of ~5 cm/s. Figure 4.23 a and b indicate the pressure drop and filtration efficiency of these fiber mats, respectively. FOM also was calculated for these fiber mats and the results are shown in Figure 4.23 c.

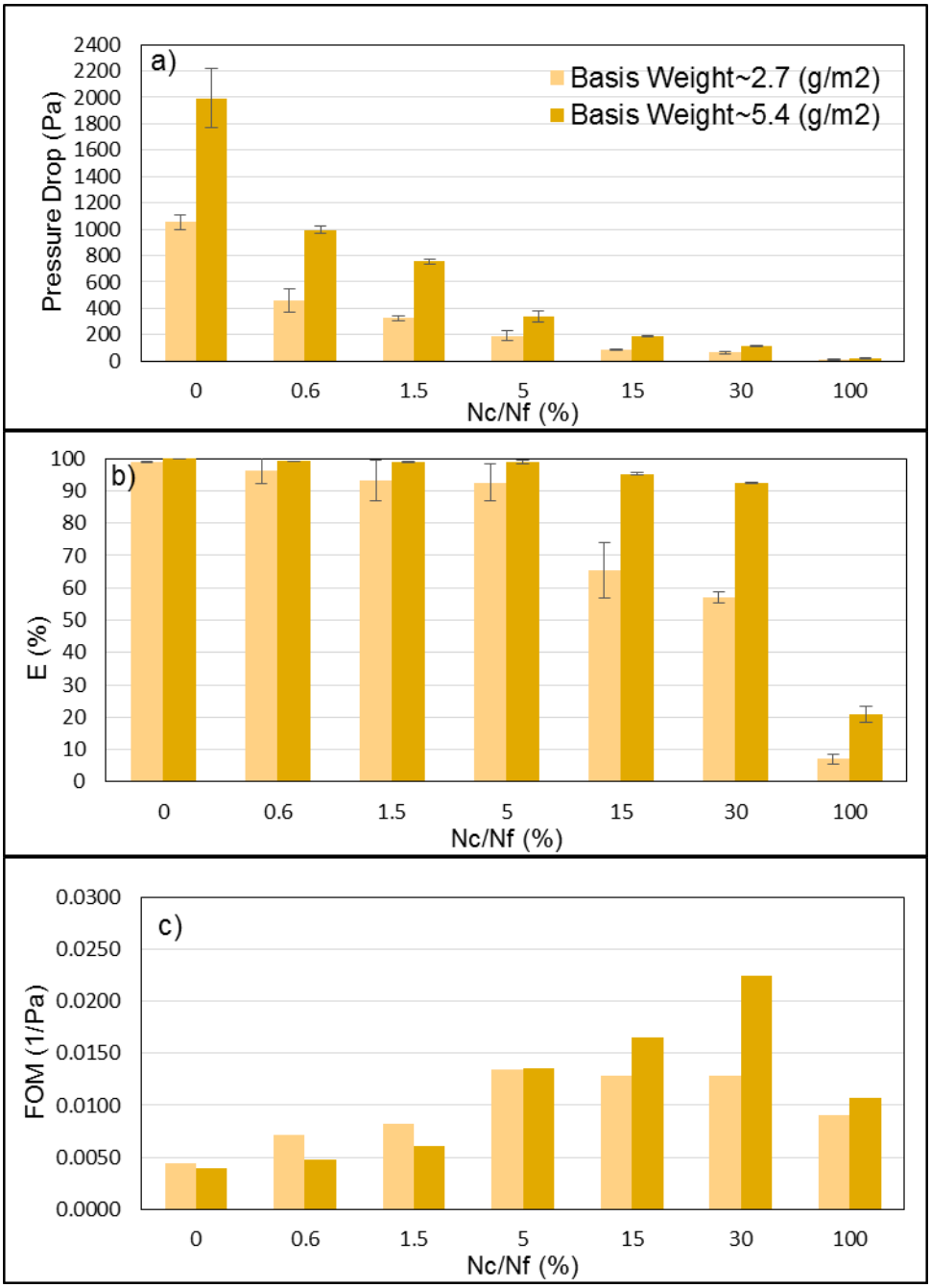

Figure 4.23: Chart comparison of a) pressure drop, b) filtration efficiency, and c) FOM for 5-layerd bimodal orthogonal filter mats consisting of nanometer and micrometer aligned fibers with two basis weights, 2.7 and 5.4 g/m^2.

Figure 4.23 a and b indicate that by increasing the number of coarse fibers to the bimodal orthogonal fiber mats, the pressure drop and filtration efficiency will both decrease. This is the result of adding fibers with a larger diameter, which was expected as well. Also, by considering the basis weights, mats with higher basis weights will results in higher pressure drop and filtration efficiency. Figure 4.23 c compares the quality factor of the mats, which indicates that for both basis weights, the bimodal filter mats have better performance compared to the unimodal case of only fine fibers or only coarse fibers. The fiber mats with N_c/N_f equal to 5, 15, and 30% will result in an FOM greater than 0.01, which indicates filtration improvement.

In this study, for mats with a basis weight of 2.7 g/m^2, the FOM reaches its highest value, 0.0135 by adding 5% coarse fibers. This is almost an increase of 200% FOM compared to the unimodal fine fiber mats (N_c/N_f = 0%) and an increase of 50% FOM compared to the unimodal coarse fiber mats (N_c/N_f = 100%). Whereas for mats with a basis weight of 5.4 g/m^2, adding 30% coarse fibers will results in the highest FOM value, 0.0224. This is almost an increase of 470% FOM compare to the unimodal fine fiber mats (N_c/N_f = 0%) and an increase of 100% FOM compare to the unimodal coarse fiber mats (N_c/N_f = 100%).

4.4.3 Comparing the experimental results with empirical correlations:

The outcome of the filtration performance experiment of the bimodal orthogonal fiber mats (D_c/D_f ~16) are compared with the results from empirical equations. The pressure drop values were obtained from the Davies equation (1.36). The filter collection efficiency values were calculated using equation (1.35), where the semi-empirical correlations of Liu

and Rubow were used for validation. The calculations for pressure drop and filtration efficiency for bimodal fiber mats were done in two different ways, which is explained in Section 4.3.2. Due to the high coarse to fine fiber ratio (D_c/D_f ~16), the average fiber diameter that was calculated for the bimodal mats are not a good assumption for high fiber diameter ratios. Since in the actual experiment the spinning of nanometer and micrometer fibers were done layer by layer, therefore it is more realistic to deal with them as a layered structure rather than as a blend of fine and coarse fibers. Also, the experimental values are match more with the theory that uses the layering of fibers. Therefore, the thickness and weight of each layer was approximately determined by knowing the mass fraction of fine to coarse fibers, and the total weight and thickness of the fiber mats. For unimodal fiber mats the second method was also used, however both ways of calculation will give the same numbers.

Figure 4.24 and 4.25 show a comparison between the experimental results and the calculated values from empirical equations for basis weights of 2.7 g/m^2 and 5.4 g/m^2, respectively.

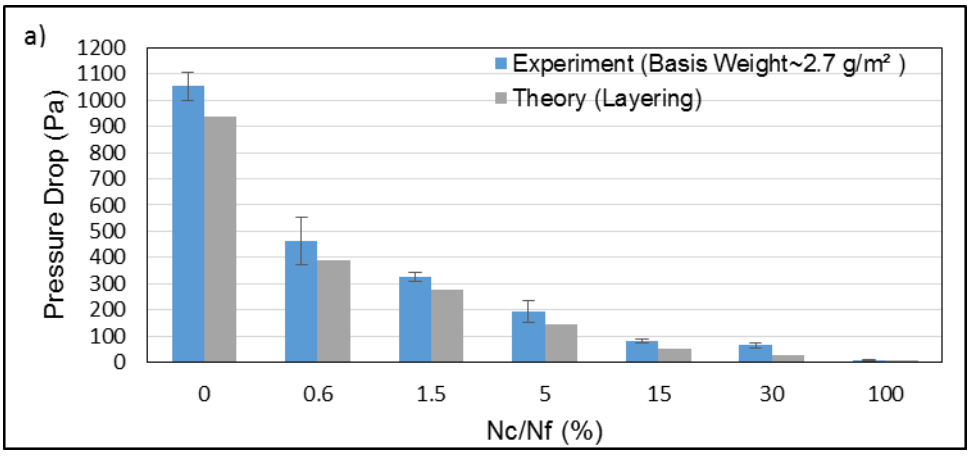

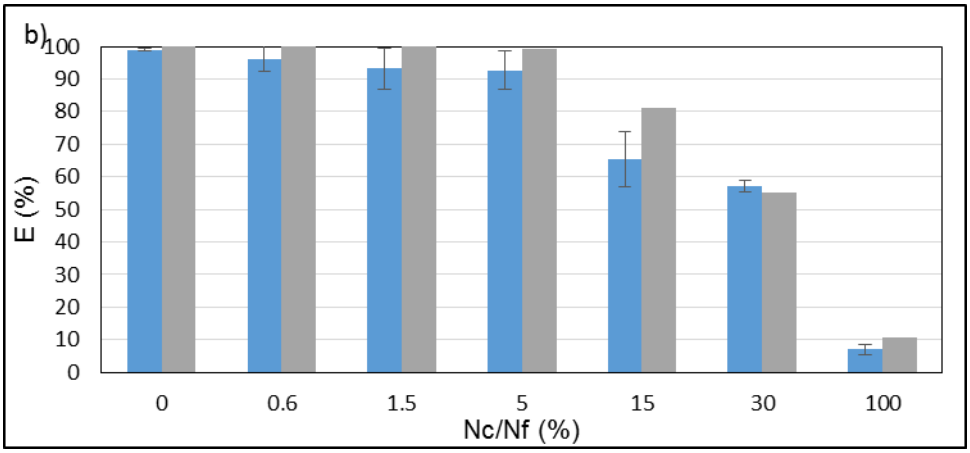

Figure 4.24: Plots showing the comparison between experimental and calculated a) pressure drop and b) filtration efficiency, with respect to N_c/N_f for bimodal orthogonal nanometer and micrometer fiber mats having 2.7 g/m^2 as the basis weight.

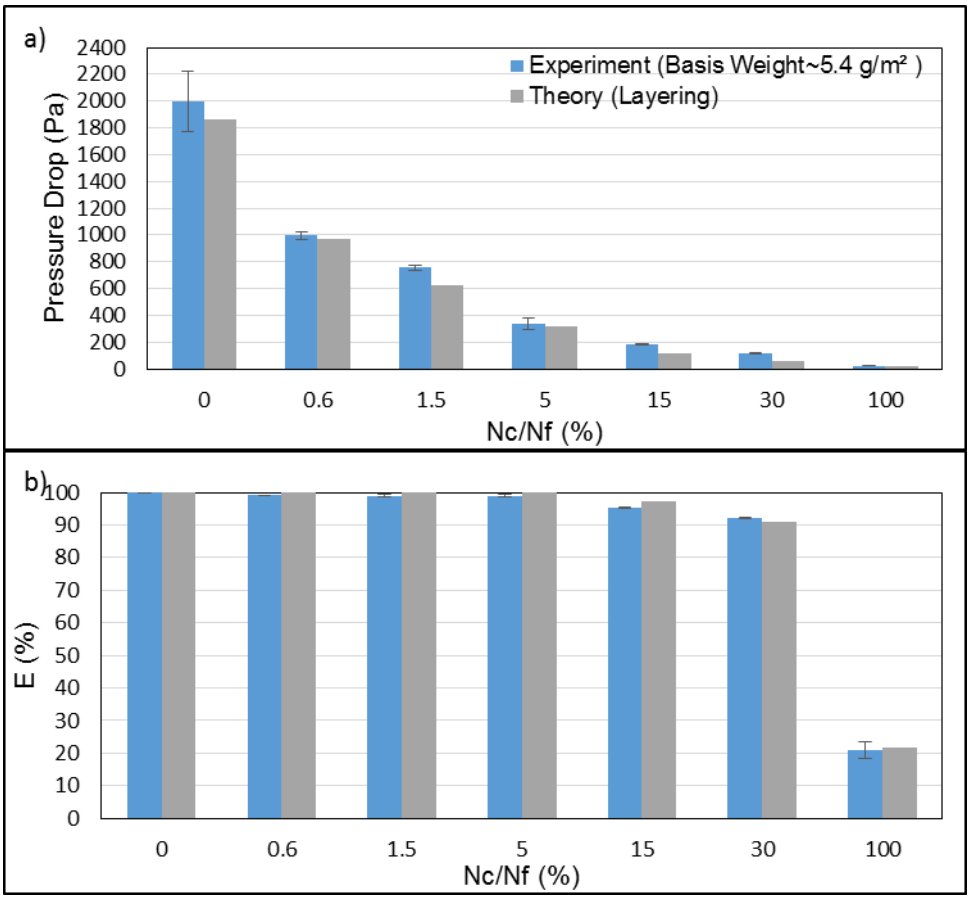

Figure 4.25: Plots showing the comparison between experimental and calculated a) pressure drop and b) filtration efficiency, with respect to N_c/N_f for bimodal orthogonal nanometer and micrometer fiber mats having 5.4 g/m^2 as the basis weight.

As shown above in Figure 4.24 a and Figure 4.25 a, the results for pressure drop indicate that the experimental values are higher than the calculated ones. Due to the experimental errors, such as non-uniformity of filter mats, it was expected to get lower values from experiments compare to the calculated values. But in this case, the experimental values are greater than the calculated ones, and this can be caused by the presence of the nanowebs. As it was mentioned in Chapter 3 Section 3.2.4, nanowebs will form during the production of aligned nanometer fibers using the gap method, and this might be the reason why the experimental values are higher than the calculated ones. Also, high values for filtration efficiency from experiments compare to the theoretical values gives further evidence to the formation of nanowebs in the structure. These nanowebs are not accounted for in the theoretical calculations, and exact number of nanowebs needs to be known in order to include them. Further research needs to be conducted to determine the best way to account for nanowebs in current theoretical calculations.

4.4.4 Effect of Layering:

This section is the second facet of experimental study on the bimodal orthogonal fiber mats with D_c/D_f ~16. In addition to seeing how the filtration performance changes with the ratio of coarse to fine fibers, there are also the effects of the number of layers on the filter performance. In this section, four different sets were made using 1, 2, 3, and 4 pairs of layers. Each pair of layers consisted of a micrometer fiber layer and a nanometer fiber layer, which were placed orthogonally. The mats were made so that they started with a

micrometer layer and ended with a nanometer layer. The basis weight were the same for all of the sets and measured 1.3 g/m^2. In other words, the same number of fibers were distributed in different layers and the effect of layering on the performance was evaluated. The Nc/Nf was kept at 1.2%. The figure below (Figure 4.26) shows pressure drop, filtration efficiency, and FOM based on the number of pairs of layers. The results indicated that by increasing the number of layers, the filtration efficiency and pressure drop decreased, but the reduction in pressure drop was much quicker, which resulted in increasing FOM.

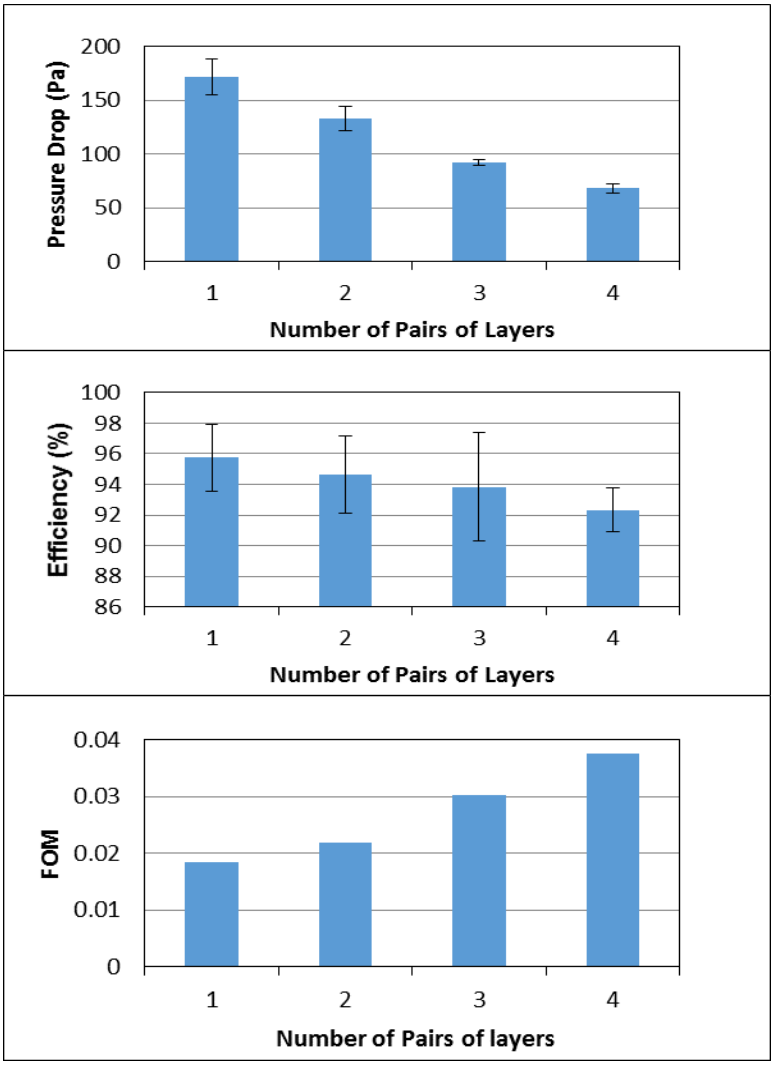

Figure 4.26: plot showing the effect of layering for a) pressure drop, b) filtration efficiency, and c) FOM for orthogonal bimodal fibers (dc/df=16).

4.5 Conclusion:

The performance of electrospun fiber based filters with different morphologies, bimodal vs unimodal and random vs orthogonal configurations, were studied. It was found that the orthogonal micrometer fiber mats will have higher FOM compare to the random micrometer fiber mats, with the same fiber diameter. It is shown that regardless of fiber orientation (random or orthogonal), the filtration performance is improved by having

bimodal fiber mats compared to the unimodal fiber mats. This study was done based on the ratio of coarse to fine fibers.

A performance comparison of bimodal fiber mats and unimodal fiber mats was also investigated using nanometer fibers. It is reported that FOM will increases by 125% with having bimodal random fiber mats (N_c/N_f =40%) compared to the unimodal random fiber mats (N_c/N_f =0%). Furthermore, the performance of filter mats composed of nanometer and micrometer fibers in an orthogonal fashion was studied. It is shown that in bimodal fiber mats, increasing the number of coarse fibers caused decreases in the pressure drop and filtration efficiency. The rate of decrease is higher for pressure drop, which will result in higher values for FOM. The effect of layering was also studied for orthogonal bimodal fibers (dc/df=16).

Also presented is an experimental study on the performance of orthogonally layered micrometer fibers based on fiber spacing. The performance of the filters were optimized by studying the effect of changing fiber-to-fiber spacing for two different fiber diameter. It is shown that for a specific fiber diameter and particle size, the FOM is independent of fiber counts per layer. Moreover, the effect of spreading the fibers with an increasing number of layers was studied for orthogonal unimodal micrometer fibers.

Finally, from this study, due to the higher performance of layers composed of orthogonal bimodal arranged mats, they can be considered for use in future HEPA filters. Also, the orthogonally layered fiber mats can be a good candidate for application to commercial filters to improve their filtration performance.

CHAPTER 5 Overall Research Observations

This dissertation is designed to revise the performance of the fibrous filters based on their microstructure. While analytical and modeling studies are available for unimodal and bimodal random fiber configuration, there are few studies on unimodal and bimodal orthogonal fiber configurations. Also, there is need for experimental studies to confirm and support these models and calculations.

Different morphologies, including bimodal and unimodal with random and orthogonal fiber orientations, were made using different fiber sizes. Electrospinning was used as the main method to produce fibers while controlling their orientations. There are some studies on making aligned fibers using different electrospinning setups. However, only a few of these studies are applicable to collecting aligned fibers in a way to completely coat mats for various applications. Different polymers with different electrospinning parameters and setups were used to successfully make unimodal and bimodal random and orthogonal fashioned fiber media.

After making a filter with a known microstructure, the weight, thickness, pressure drop, efficiency and FOM were measured. The theoretical calculation for each sample was used to confirm the experimental observation. The results were explained for micrometer and/or nanometer fiber mats.

For micrometer fibers, the random and orthogonal fiber mats were made and tested using one fiber size, or unimodal fibers. The results indicate that for random and orthogonal fiber mats with the same fiber diameter and basis weight, the orthogonal orientation will increase the filtration performance. Also, the performance of unimodal mats were

compared with bimodal mats based on the ratio of coarse to fine fibers. The results indicate that using a mixture of fine and coarse fibers will improve the performance by decreasing the pressure drop faster than decreasing filtration efficiency. This study was also conducted to understand the fibrous mats' performance based on the fiber spacing.

The nanometer fibers were examined to better understand their influence on the performance of fibrous media. Our results indicate that bimodal random fiber mats with a 0.4 ratio of coarse to fine fibers has better performance compare to the unimodal random fiber mats with only fine fibers. Adding some number of coarse fibers will improve the performance through a significant reduction in the pressure drop and very small reduction in filtration efficiency.

As mentioned, no experimental studies have yet been done to evaluate the performance of bimodal orthogonal fiber mats. In this study, the bimodal orthogonal fiber mats were made of micrometer and nanometer aligned fibers as the coarse and fine fibers, respectively. The fibers were placed layer by layer orthogonally on top of each other. Different ratios of coarse to fine fibers were made and tested. The results indicate that bimodal fiber mats, with ratios of coarse to fine fibers of 0.15 and 0.3, have high FOM, and can thereby be used in existing commercial filters.

Comparing unimodal orthogonal fiber mats, having only fine or only coarse fibers, with bimodal orthogonal fiber mats, having a mix of fine and coarse fibers, indicate the advantage of adding coarse to fine fibers, as this decreases the pressure drop at a faster rate than it decreases the filtration efficiency, which results in higher FOM.

More interestingly, the existence of nanowebs in producing aligned nanometer fibers can attribute to higher particle collection efficiency. This research study encountered and then investigated the physics behind the formation of nanowebs during electrospinning. However, further investigation is needed for a more complete understanding.

In addition to comparing the mats microstructure, the uniformity of filters made with electrospun fibers was also tested. Analyses showed that using negative ions to discharge the samples during the electrospinning process and using two conductive strips to collect the fibers will enhance filter uniformity. In this study, these two methods were used independently to eliminate the effects of non-uniformity of the electrospun fibrous mats.

Finally, the effect of layering for the orthogonal bimodal samples and unimodal orthogonal micrometer fibrous mats was tested. The results indicate that samples with more layers will give higher FOM in comparison to those with a lower number of layers.

This research provides facts about the performance of unimodal and bimodal filters in random and orthogonal fiber configurations, which can be used as evidence for their potential use in commercial filters. Further research can be done based on this work to explore and confirm these filters' viability as up-stream, down-stream, in between, and/or mechanical support components of commercial filters.

Literature Cited

Literature Cited

[1] D. B. Purchas and K. Sutherland, Handbook of Filter Media. Elsevier, 2001, pp. 529–549.

[2] K. Sutherland, Filters and Filtration Handbook, Fifth edit. Oxford, UK: Elsevier Ltd, 2008.

[3] A. Boni and M. Clark, "Filter media: Improving filter media to achieve cleaner air," Filtr. Sep., vol. 45, no. 9, pp. 20–23, Nov. 2008.

[4] R. Barhate and S. Ramakrishna, "Nanofibrous filtering media: Filtration problems and solutions from tiny materials," J. Memb. Sci., vol. 296, no. 1–2, pp. 1–8, Jun. 2007.

[5] P. Tronville and R. D. Rivers, "International standards: filters for buildings and gas turbines," Filtr. Sep., vol. 42, no. 7, pp. 39–43, 2005.

[6] C. Davies, Air Filtration. New York: Academic Press INC., 1973.

[7] T. Ondarçuhu and C. Joachim, "Drawing a single nanofibre over hundreds of microns," EPL Europhysics Lett., vol. 42, no. 2, p. 215, 1998.

[8] G. M. Whitesides and B. Grzybowski, "Self-assembly at all scales", Science, vol. 295, no. 5564, pp. 2418–21, Mar. 2002.

[9] P. X. Ma and R. Zhang, "Synthetic nano-scale fibrous extracellular matrix," no. June, pp. 27–30, 1998.

[10] C. R. Martin, "Membrane-Based Synthesis of Nanomaterials," vol. 20, no. 23, pp. 1739–1746, 1996.

[11] Z.-M. Huang, Y.-Z. Zhang, M. Kotaki, and S. Ramakrishna, "A review on polymer nanofibers by electrospinning and their applications in nanocomposites," Compos. Sci. Technol., vol. 63, no. 15, pp. 2223–2253, Nov. 2003.

[12] V. Thavasi, G. Singh, and S. Ramakrishna, "Electrospun nanofibers in energy and environmental applications," Energy Environ. Sci., vol. 1, no. 2, p. 205, 2008.

[13] T. Ho, N. Ghochaghi, and G. Tepper, "Development of magnetic fabrics with tunable hydrophobicity," J. Appl. Polym. Sci., vol. 130, no. 4, pp. 2352–2358, Nov. 2013.

[14] D. C. Aduba, J. a Hammer, Q. Yuan, W. A. Yeudall, G. L. Bowlin, and H. Yang, "Semi-interpenetrating network (sIPN) gelatin nanofiber scaffolds for oral mucosal drug delivery.," Acta Biomater., vol. 9, no. 5, pp. 6576–84, May 2013.

[15] C. Huang, S. Chen, C. Lai, D. H. Reneker, H. Qiu, Y. Ye, and H. Hou, "Electrospun polymer nanofibres with small diameters," vol. 1558, 2006.

[16] A. Formhals, "Electrical spinning of fibers from solutions," 2123992, 1934.

[17] N. Bhardwaj and S. C. Kundu, “Electrospinning: a fascinating fiber fabrication technique,” Biotechnol. Adv., vol. 28, no. 3, pp. 325–347, 2010.
[18] G. M. Bose, “Recheres sur la cause et sur la varitable theorie del’electricite: Wittenberg,” 1745.
[19] H. L. Simons, “Process and apparatus for producing patterned non-woven fabrics,” US3280229, 1966.
[20] A. Formhals, “Artificial threads,” US2187306, 1940.
[21] G. Taylor, “Electrically driven jets,” vol. 313, no. 1515, pp. 453–475, 1969.
[22] a. L. Yarin, S. Koombhongse, and D. H. Reneker, “Taylor cone and jetting from liquid droplets in electrospinning of nanofibers,” J. Appl. Phys., vol. 90, no. 9, p. 4836, 2001.
[23] C. Guignard, “Process for the manufacture of a plurality of filaments,” US4230650, 1980.
[24] C. Guignard, “Device for forming a nonwoven product from a fluid dielectric substance and process,” US4287139, 1981.
[25] A. Bornat, “Electrostatic spinning of tubular products,” US4323525, 1982.
[26] J. Doshi and D. H. Reneker, “Electrospinning Process and Application of Electrospun Fibers,” vol. 35, pp. 151–160, 1995.
[27] N. Vitchuli, Q. Shi, J. Nowak, M. Mccord, and M. Bourham, “Electrospun Ultrathin Nylon Fibers for Protective Applications,” vol. 116, pp. 2181–2187, 2010.
[28] T. Subbiah, G. S. Bhat, R. W. Tock, S. Parameswaran, and S. S. Ramkumar, “Electrospinning of nanofibers,” J. Appl. Polym. Sci., vol. 96, no. 2, pp. 557–569, Apr. 2005.
[29] D. H. Reneker, A. L. Yarin, H. Fong, and S. Koombhongse, “Bending instability of electrically charged liquid jets of polymer solutions in electrospinning,” J. Appl. Phys., vol. 87, no. 9, p. 4531, 2000.
[30] D. H. Reneker and A. L. Yarin, “Electrospinning jets and polymer nanofibers,” vol. 49, pp. 2387–2425, 2008.
[31] Y. M. Shin, M. M. Hohman, M. P. Brenner, and G. C. Rutledge, “Electrospinning: A whipping fluid jet generates submicron polymer fibers,” Appl. Phys. Lett., vol. 78, no. 8, pp. 1149–1151, 2001.
[32] D. H. Reneker, W. Kataphinan, a Theron, E. Zussman, and A. L. Yarin, “Nanofiber garlands of polycaprolactone by electrospinning,” Polymer (Guildf)., vol. 43, no. 25, pp. 6785–6794, Jan. 2002.
[33] Y. M. Shin, M. M. Hohman, M. P. Brenner, and G. C. Rutledge, “Experimental characterization of electrospinning: the electrically forced jet and instabilities,” Polymer (Guildf)., vol. 42, no. 25, pp. 09955–09967, Dec. 2001.
[34] I. Chun, “Fine fibers spun by electrospinning process from polymer solutions and polymer melts in air and vacuum: characterization of structure and morphology on electrospun fibers and developing a new process model,” University of Akron, OH, 1995.

[35] M. M. Hohman, M. Shin, G. Rutledge, and M. P. Brenner, “Electrospinning and electrically forced jets. II. Applications,” Phys. Fluids, vol. 13, no. 8, p. 2221, 2001.
[36] J. D. Schiffman and C. L. Schauer, “A Review: Electrospinning of Biopolymer Nanofibers and their Applications,” Polym. Rev., vol. 48, no. 2, pp. 317–352, May 2008.
[37] D. Li and Y. Xia, “Electrospinning of Nanofibers: Reinventing the Wheel?” Adv. Mater., vol. 16, no. 14, pp. 1151–1170, Jul. 2004.
[38] Y. Liu, Z.-F. Ren, and J.-H. He, “Bubble electrospinning method for preparation of aligned nanofibre mat,” Mater. Sci. Technol., vol. 26, no. 11, pp. 1309–1312, Nov. 2010.
[39] P. Katta, M. Alessandro, R. D. Ramsier, and G. G. Chase, “Continuous Electrospinning of Aligned Polymer Nanofibers onto a Wire Drum Collector,” Nano Lett., vol. 4, no. 11, pp. 2215–2218, Nov. 2004.
[40] K. L. Ou, C. S. Chen, L. H. Lin, J. C. Lu, Y. C. Shu, W. C. Tseng, J. C. Yang, S. Y. Lee, and C. C. Chen, “Membranes of epitaxial-like packed, super aligned electrospun micron hollow poly(l-lactic acid) (PLLA) fibers,” Eur. Polym. J., vol. 47, no. 5, pp. 882–892, May 2011.
[41] S. Sarkar, S. Deevi, and G. Tepper, “Biased AC Electrospinning of Aligned Polymer Nanofibers,” Macromol. Rapid Commun., vol. 28, no. 9, pp. 1034–1039, May 2007.
[42] Y. Ishii, H. Sakai, and H. Murata, “A new electrospinning method to control the number and a diameter of uniaxially aligned polymer fibers,” Mater. Lett., vol. 62, no. 19, pp. 3370–3372, Jul. 2008.
[43] N. Chanunpanich and H. Byun, “Alignment of electrospun polystyrene with an electric field,” J. Appl. Polym. Sci., 2007.
[44] H. Pan, L. Li, L. Hu, and X. Cui, “Continuous aligned polymer fibers produced by a modified electrospinning method,” Polymer (Guildf)., vol. 47, no. 14, pp. 4901–4904, Jun. 2006.
[45] J. M. Deitzel, J. D. Kleinmeyer, J. K. Hirvonen, and N. C. B. Tan, “Controlled deposition of electrospun poly (ethylene oxide) fibers,” vol. 42, pp. 8163–8170, 2001.
[46] D. Li, Y. Wang, and Y. Xia, “Electrospinning of polymeric and ceramic nanofibers as uniaxially aligned arrays,” Nano Lett., vol. 3, no. 8, pp. 1167–1171, 2003.
[47] D. Li, Y. Wang, and Y. Xia, “Electrospinning Nanofibers as Uniaxially Aligned Arrays and Layer-by-Layer Stacked Films,” Adv. Mater., vol. 16, no. 4, pp. 361–366, Feb. 2004.
[48] D. Thomas, R. P. Contal, V. Renaudin, P. Penicot, D. Leclerc, J. S. Vendel, and H. Poincare, “Modelling Pressure Drop in HEPA Filters During Dynamic Filtration,” vol. 30, no. 2, pp. 235–246, 1999.
[49] R. C. Brown, Air Filtration An Integrated Approach to the Theory and Applications of Fibrous Filters, First. New York: Pergamon Press, 1993.

[50] R. Brown and A. Thorpe, “Glass-fibre filters with bimodal fibre size distributions,” Powder Technol., vol. 118, no. 1–2, pp. 3–9, Aug. 2001.
[51] D. S. Clague and R. J. Phillips, “A numerical calculation of the hydraulic permeability of three-dimensional disordered fibrous media,” Phys. Fluids, vol. 9, no. 6, 1997.
[52] H. Vahedi Tafreshi, M. S. A Rahman, S. Jaganathan, Q. Wang, and B. Pourdeyhimi, “Analytical expressions for predicting permeability of bimodal fibrous porous media,” Chem. Eng. Sci., vol. 64, no. 6, pp. 1154–1159, Mar. 2009.
[53] S. Fotovati, H. Vahedi Tafreshi, A. Ashari, S. A. Hosseini, and B. Pourdeyhimi, “Analytical expressions for predicting capture efficiency of bimodal fibrous filters,” J. Aerosol Sci., vol. 41, no. 3, pp. 295–305, Mar. 2010.
[54] S. A. Hosseini and H. V. Tafreshi, “Modeling permeability of 3-D nanofiber media in slip flow regime,” Chem. Eng. Sci., vol. 65, no. 6, pp. 2249–2254, Mar. 2010.
[55] R. K. Duggirala, C. J. Roy, S. M. Saeidi, J. M. Khodadadi, D. R. Cahela, and B. J. Tatarchuk, “Pressure Drop Predictions in Microfibrous Materials Using Computational Fluid Dynamics,” J. Fluids Eng., vol. 130, no. 7, p. 071302, 2008.
[56] S. A. Hosseini and H. V. Tafreshi, “3-D simulation of particle filtration in electrospun nanofibrous filters,” Powder Technol., vol. 201, no. 2, pp. 153–160, Jul. 2010.
[57] S. Fotovati, H. Vahedi Tafreshi, and B. Pourdeyhimi, “Influence of fiber orientation distribution on performance of aerosol filtration media,” Chem. Eng. Sci., vol. 65, no. 18, pp. 5285–5293, Sep. 2010.
[58] M. D. Maroto, “Filtration Efficiency of Intermediate Ventilation Air filters on Ultrafine and Submicron Particles A laboratory test on new full-scale filter modules,” Chalmers University of Technology Göteborg, 2011.
[59] S. S. Kulkarni, “Performance Comparison of Layered Composite Bimodal Fiber Mats,” Virginia Commonwealth University, 2011.
[60] H.-C. YEH and B. Y. H. Liu, “Aerosol Filtration by Fibrous Filters-I. Theoretical,” Aerosol Sci., vol. 5, pp. 191–204, 1974.
[61] H.-C. YEH and B. Y. H. Liu, “Aerosol Filtration by Fibrous Filters-II. Experimental,” Aerosol Sci., vol. 5, pp. 205–2017, 1974.
[62] W. C. Hinds, Aerosol Technology PROPERTIES, BEHAVIOR, AND MEASUREMENT OF AIRBORNE PARTICLES. New York: Wiley Interscience, 1982.
[63] W. W.-F. Leung, C.-H. Hung, and P.-T. Yuen, “Effect of face velocity, nanofiber packing density and thickness on filtration performance of filters with nanofibers coated on a substrate,” Sep. Purif. Technol., vol. 71, no. 1, pp. 30–37, Jan. 2010.
[64] N. Fuchs, The Mechanics of Aerosols. New York: Dover Publications, Inc., 1989.
[65] Baron, A. Paul, Willeke, and Klaus, Aerosol measurement : principles, techniques, and applications, 2nd ed. New York : Wiley, 2001.
[66] I. B. Tager, “Health Effects of Aerosols,” in *Aerosol Handbook*, .

[67] T. C. Dickenson, FILTERS and FILTRATION HANDBOOK, Fourth. Oxford, UK: Elsevier Advanced Technology, 1997.
[68] M. A. Tahir and H. Vahedi Tafreshi, "Influence of fiber orientation on the transverse permeability of fibrous media," Phys. Fluids, vol. 21, no. 8, p. 083604, 2009.
[69] S. A. Hosseini and H. Vahedi Tafreshi, "Modeling particle-loaded single fiber efficiency and fiber drag using ANSYS–Fluent CFD code," Comput. Fluids, vol. 66, pp. 157–166, Aug. 2012.
[70] J. A. Rosati, K. K. Isaacs, and T. B. Martonen, "Mechanisms of Particle," in Aerosols Handbook, CRC Press, 2012.
[71] S. Datta and S. Deo, "Stokes flow with slip and Kuwabara boundary conditions," Proc. Math. Sci., vol. 112, no. 3, pp. 463–475, Aug. 2002.
[72] S. K. Friedlander, Smoke, Dust and Haze, 1st ed. New York: Wiley-Interscience, 1977.
[73] D. W. VanOsdell, B. Y. H. Liu, K. L. Rubow, and D. Y. H. Pui, "Experimental Study of Submicrometer and Ultrafine Particle Penetration and Pressure Drop for High Efficiency Filters," Aerosol Sci. Technol., vol. 12, no. 4, pp. 911–925, Jan. 1990.
[74] S. Jaganathan, H. Vahedi Tafreshi, and B. Pourdeyhimi, "On the pressure drop prediction of filter media composed of fibers with bimodal diameter distributions," Powder Technol., vol. 181, no. 1, pp. 89–95, Jan. 2008.
[75] B. Maze, H. Vahedi Tafreshi, Q. Wang, and B. Pourdeyhimi, "A simulation of unsteady-state filtration via nanofiber media at reduced operating pressures," J. Aerosol Sci., vol. 38, no. 5, pp. 550–571, May 2007.
[76] M. D. Maroto, "Filtration Efficiency of Intermediate Ventilation Air filters on Ultrafine and Submicron Particles," Chalmers University of Technology, 2011.
[77] A. Boni and M. Clark, "Filter media: Improving filter media to achieve cleaner air," Filtr. Sep., vol. 45, no. 9, pp. 20–23, Nov. 2008.
[78] N. Rao and M. Faghri, "Computer Modeling of Aerosol Filtration by Fibrous Filters," Aerosol Sci. Technol., vol. 8, no. 2, pp. 133–156, Jan. 1988.
[79] K. Spurny, Advances in aerosol filtration. Boca Raton, FL : Lewis, 1998.
[80] Y. C. Ahn, S. K. Park, G. T. Kim, Y. J. Hwang, C. G. Lee, H. S. Shin, and J. K. Lee, "Development of high efficiency nanofilters made of nanofibers," Curr. Appl. Phys., vol. 6, no. 6, pp. 1030–1035, Oct. 2006.
[81] J. Wang, S. C. Kim, and D. Y. H. Pui, "Investigation of the figure of merit for filters with a single nanofiber layer on a substrate," J. Aerosol Sci., vol. 39, no. 4, pp. 323–334, Apr. 2008.
[82] J. C. Uecker, "The production and filtration efficiency testing of nonwoven electrospun mats," Virginia Commonwealth University, 2007.
[83] J. C. Uecker, G. C. Tepper, and J. Rosell-Llompart, "Ion-assisted collection of Nylon-4,6 electrospun nanofibers," Polymer (Guildf)., vol. 51, no. 22, pp. 5221–5228, Oct. 2010.

[84] M. Alger, Polymer Science Dictionary, 2nd ed. London: Chapman & Hall, 1997.
[85] H. Fong, I. Chun, and D. H. Reneker, "Beaded nanofibers formed during electrospinning," Polymer (Guildf), vol. 40, no. 16, pp. 4585–4592, Jul. 1999.
[86] J. Brandrup, E. H. Immergut, and E. A. Grulke, Polymer Handbook, 4th ed. New York: Wiley Interscience, 1999.
[87] A. F. M. Barton, Handbook of Solubility Parameters and Other Cohesion Parameters. CRC Press, 1983.
[88] L. Wannatong, A. Sirivat, and P. Supaphol, "Effects of solvents on electrospun polymeric fibers: preliminary study on polystyrene," Polym. Int., vol. 53, no. 11, pp. 1851–1859, Nov. 2004.
[89] H. Liu and Y.-L. Hsieh, "Ultrafine fibrous cellulose membranes from electrospinning of cellulose acetate," J. Polym. Sci. Part B Polym. Phys., vol. 40, no. 18, pp. 2119–2129, Sep. 2002.
[90] V. K. Rangari, M. Yousuf, S. Jeelani, M. X. Pulikkathara, and V. N. Khabashesku, "Alignment of carbon nanotubes and reinforcing effects in nylon-6 polymer composite fibers.," Nanotechnology, vol. 19, no. 24, p. 245703, Jun. 2008.
[91] R. S. Figliola and D. E. Beasley, Theory and Design for Mechanical Measurements, 3rd ed. NJ: John Wiley & Sons, Inc., 2000.
[92] J. M. Deitzel, W. Kosik, S. H. Mcknight, N. C. B. Tan, J. M. Desimone, and S. Crette, "Electrospinning of polymer nanofibers with specific surface chemistry," Polymer (Guildf)., vol. 43, pp. 1025–1029, 2002.
[93] N. Olaru and L. Olaru, "Electrospinning of Cellulose Acetate Phthalate from Different Solvent Systems," Ind. Eng. Chem. Res., vol. 49, no. 4, pp. 1953–1957, Feb. 2010.
[94] H. R. Pant, M. P. Bajgai, C. Yi, R. Nirmala, K. T. Nam, W. Il Baek, and H. Y. Kim, "Effect of successive electrospinning and the strength of hydrogen bond on the morphology of electrospun nylon-6 nanofibers," Colloids Surfaces A Physicochem. Eng. Asp., vol. 370, no. 1–3, pp. 87–94, Nov. 2010.
[95] H. R. Pant, M. P. Bajgai, K. T. Nam, Y. a Seo, D. R. Pandeya, S. T. Hong, and H. Y. Kim, "Electrospun nylon-6 spider-net like nanofiber mat containing TiO(2) nanoparticles: a multifunctional nanocomposite textile material.," J. Hazard. Mater., vol. 185, no. 1, pp. 124–30, Jan. 2011.
[96] K.-T. Nam, H. R. Pant, J. Jeong, B. Pant, B. Kim, and H.-Y. Kim, "Solvent degradation of nylon-6 and its effect on fiber morphology of electrospun mats," Polym. Degrad. Stab., vol. 96, no. 11, pp. 1984–1988, Nov. 2011.
[97] R. Kessick, J. Fenn, and G. Tepper, "The use of AC potentials in electrospraying and electrospinning processes," Polymer (Guildf)., vol. 45, no. 9, pp. 2981–2984, Apr. 2004.
[98] M. Lackowski, A. Krupa, and A. Jaworek, "Nonwoven filtration mat production by electrospinning method," J. Phys. Conf. Ser., vol. 301, pp. 012–013, Jun. 2011.

[99] S. Zhang, W. Shim, and J. Kim, “Design of ultra-fine nonwovens via electrospinning of Nylon 6: Spinning parameters and filtration efficiency,” Mater. Des., vol. 30, no. 9, pp. 3659–3666, 2009.
[100] T. M. Bucher, H. V. Tafreshi, and G. C. Tepper, “Modeling performance of thin fibrous coatings with orthogonally layered nanofibers for improved aerosol filtration,” Powder Technol., vol. 249, pp. 43–53, Nov. 2013.

VITA

Negar Ghochaghi

Education:

- **Doctor of Philosophy - Engineering**; Graduation: December 2014
  Dissertation Title: Experimental development of advanced air filtration media based on electrospun polymer fibers.
  Virginia Commonwealth University (VCU); Richmond, VA

- **Master of Science – Mechanical Engineering**; Graduation: December 2012
  Virginia Commonwealth University (VCU); Richmond, VA

- **Bachelor of Science – Material Engineering**; Graduation: May 2010
  Isfahan University of technology (IUT); Isfahan, Iran

Publication:

1) T. Ho, N. Ghochaghi, G. Tepper, Development of Magnetic Fabrics with Tunable Hydrophobicity, Journal of Applied Polymer Science, Accepted (06-Feb-2013).

2) N. Ghochaghi, A. Taiwo, B. Dodd, M. Winkel, K. Mossi and G. Tepper, Electrospun Polystyrene Coatings with Tunable Wettability, Journal of Applied Polymer Science, Accepted (02-Oct-2014).

3) N. Ghochaghi and G.C. Tepper, Electrospun Fibers for Air Filtration Applications, The Fiber Society Conference; Geelong Victoria, Australia, May 2013

Skills:

- C++, Solidworks, Matlab, JMP, Mathematica, EndNote, Microsoft Office (Word, Excel, PowerPoint).

- SEM, TEM, EDAX, XRD, Nondestructive Tests (NDT), Electrospinning, Contact Angle Goniometry, Nanoindentation.

- Six Sigma training.

Honors and Awards:

- Reviewer for the Journal of Applied Polymer Science; Since December 2013
- Marine Corps Leadership Workshop; Participate, 2013
- Intercultural Festival, VCU's Persian American Students' dance group; 2012
- American Society of Mechanical Engineering; Since 2012
- Society of Women Engineers; Since 2012
- Phi Kappa Phi National Honor Society; Since 2011
- VCU’s Dean’s Fellowship; 2010-2011
- Valedictorian, Undergraduate; 2009-2010